IONIC MOTION IN SOLID ELECTROLYTES: A SOLID STATE NMR STUDY OF SODIUM AND LITHIUM IN β-ALUMINA

Thesis by

Albert John Highe

In Partial Fulfillment of the Requirements

For the Degree of

Doctor of Philosophy

California Institute of Technology

Pasadena, California 91125

1981

(Submitted November 18, 1980)

This thesis is dedicated to my mother,

LOTTIE M. HIGHE

(September 17, 1921 - February 19, 1980)

ACKNOWLEDGEMENTS

I would like to express my admiration for the late Robert W. Vaughan, my friend and advisor. His tragic death is a great loss to those of us who had the pleasure of knowing him and to the scientific community.

I am greatly indebted to Dr. Terry Cole who introduced me to this fascinating field of solid electrolytes. I have indeed been fortunate to have been able to draw upon his knowledge and I appreciate the keen interest he has always shown in my progress.

To Professor Sunney I. Chan, I owe great thanks for his guidance in the final, difficult year of my graduate studies.

I would like to thank Dr. Micha Polak for his work in developing the interferometric technique and for sharing in the tedium of data taking in Chapter III.

Finally, I thank my dear friend (and typist) Yolande Johnson for her patience during the hectic days in which this thesis was written.

ABSTRACT

Solid state NMR techniques have been used as a microscopic probe of the structural and dynamical properties of the mobile cations in the solid electrolyte β-alumina. The first order quadrupole shifts in the ($\pm 3/2 \longleftrightarrow \pm 1/2$) transitions in the spin 3/2 nuclei sodium and lithium have allowed the electric field gradients (EFG) for the nominal Beevers and Ross (BR) and mid-oxygen (MO) sites to be characterized. The details of the EFG's for and the distribution of cations among BR and MO sites reflect the differences in the potential wells for lithium and sodium in β-alumina. In particular, unlike sodium, the MO site for lithium is lower in energy than the BR site which results in a different structural arrangement of lithium ions. In sodium β-alumina, the equilibrium position for sodium in the BR site is displaced from the three-fold symmetry axis. It is believed that this is due to the presence of nearby MO-MO pairs. Furthermore, an activation energy of 0.04 eV is observed for the motion of sodium ions among the displaced BR sites which is associated with the correlated motion of MO-MO pairs. The effects of a second motional process with an activation energy of 0.08 eV are observed in both lithium and sodium spectra which are associated with the motion of cations among BR and MO sites. The interaction of cations in MO-MO pairs was further investigated by observing the effect of varying the ratio of lithium and sodium in mixed lithium-sodium β-alumina on the distribution of cations

among the available sites. The results were interpreted using a theory previously developed to explain the mixed-alkali effect in glasses and indicate that there is a strong interaction between unlike MO-MO pairs which governs the cation site distribution and raises the activation energy for conduction.

TABLE OF CONTENTS

CHAPTER I: INTRODUCTION

Solid electrolytes are a class of materials which display high ionic mobility well below the melting point of the solid that can be equal to or greater than the ionic mobility of the same ions in molten salts.[1] They are characterized by a large density of current carrying cations loosely bound to a large number of energetically similar sites provided by an essentially rigid framework. Solids with these features are expected to have radically different mechanisms of conduction compared to conventional solids where simple lattice defects, which occur in small numbers, are responsible for ionic conduction.

Solids with high ionic conductivities such as AgI[2] and $RbAg_4I_5$[3] have been known for some time. However, interest in solid electrolytes continued to lay dormant until Yao and Kummer[4] reported in 1967 that the ionic conductivity of sodium ions in β-alumina at room temperature is comparable to the ionic conductivity of sodium ions in aqueous NaCl. Furthermore, Kummer and Weber[5] revealed in 1968 that the β-alumina could be used in a battery in which it plays the role of the electrolyte and the electrodes are molten sodium and sulfur.

The major applications of solid electrolytes have been their use in batteries, fuel cells, and thermoelectric conversion devices. Consequently, understanding the relationship between the physical properties of solid electrolytes and their performance in devices has been of the utmost

technological importance. However, interest in these materials as representatives of another phase of matter has motivated a great number of physical and theoretical investigations[1] which seek to record and explain the characteristics of the unusual transport phenomena.

This work focuses on one of the most studied solid electrolytes: β-alumina. It and its analogs probably hold the greatest promise for use in device applications, combining high ionic conductivity, low electronic conductivity, and good chemical stability.[6] As such, β-alumina represents the "model" solid electrolyte to study since one of the results of the widespread attention, which provides the contributions and expertise of many researchers, should be a rapid growth in our understanding of these materials and subsequent improved performance of devices which incorporate them.

Pioneering x-ray crystallographic work[7,8] identified β-alumina to be a sodium aluminate with the proposed stoichiometry of $Na_2O \cdot 11Al_2O_3$. It was discovered soon thereafter that β-alumina could not be made with this stoichiometry[9], but instead, was always soda-rich, corresponding more closely to the composition, $Na_2O \cdot 8.5Al_2O_3$ with some variation of the excess sodium content ranging from approximately 15 to 30 weight percent.[4] Initially blamed on intergrowth[10] of related phases, it is now recognized that single crystals of β-alumina are inherently non-stoichiometric. Other more sophisticated crystallographic

techniques[9,11] have since been used to refine the structure, and the discussion which follows draws from all of these works.

Consider the spinel structure which can be described by beginning with oxygen atoms stacked in a closest-packing sequence of ABCABC, etc. In this arrangement, charge compensation occurs by placing cations of appropriate charge (+2 and +3, for example, in $MgAl_2O_4$) into some of the available tetrahedral and octahedral holes. In β-alumina, the sequence is somewhat altered and every fifth layer of oxygen atoms (denoted with primes) has three-quarters of its oxygen atoms removed. The arrangement of the oxygen atoms follows the sequence BAC'ABCAB'AC and defines the length of the unit cell in the c direction. Instead of +2 and +3 charges, only aluminum with a charge of +3 occupies sites among the unprimed layers. The primed layers are quite spacious by virtue of the missing oxygen atoms and include the mobile sodium. The projection of the conduction plane in Figure 1 displays the available sites and the honeycomb path about which the sodium atoms may move.

These available sites in β-alumina include:

1. The so-called Beevers and Ross (BR) sites. Sodium can sit in an equilateral triangular prism of oxygen atoms each 2.87 Å away, with three in-plane oxygen atoms 3.23 Å away, related by a 120° rotation.
2. The anti-Beevers and Ross (aBR) site.

Figure 1

Projection of the conduction plane for β-alumina. The raft of large open circles represents the layer of oxygen atoms above and below the conduction plane. The large darkened circles represent the oxygen atoms in the conduction plane. The small darkened circles, the small open circles, and the open squares are the BR, aBR and MO sites, respectively. The occupation of all the small darkened circles by sodium ions constitutes stoichiometric β-alumina.

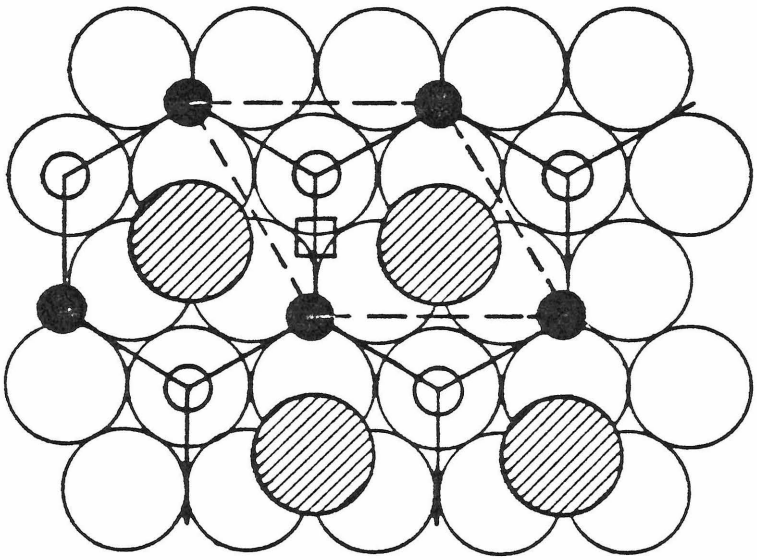

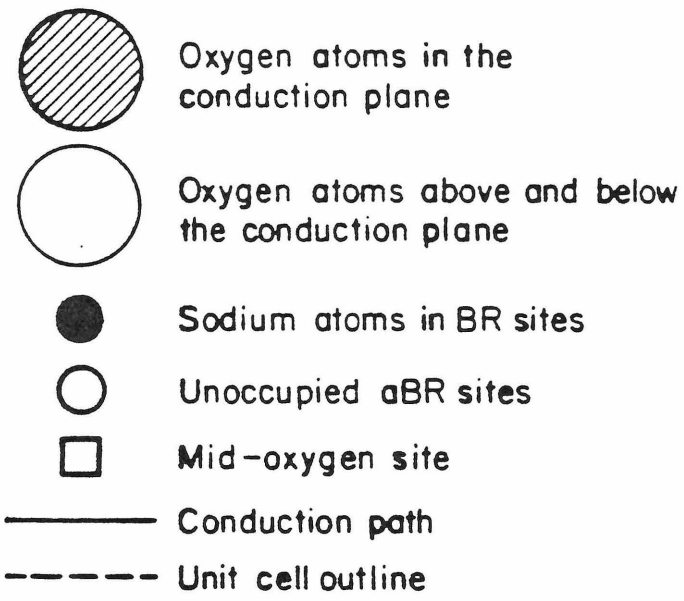
Oxygen atoms in the conduction plane
Oxygen atoms above and below the conduction plane
Sodium atoms in BR sites
Unoccupied aBR sites
Mid-oxygen site
Conduction path
Unit cell outline

A sodium in this site has one oxygen atom above and below it 2.37 Å away and the same arrangement as the BR site of three oxygen atoms in the plane.

3. The mid-oxygen (MO) site is midway between the BR and aBR sites. It is similar to the BR site with the same equilateral triangular prism of oxygen atoms, but it has two-fold symmetry due to the two in-plane oxygen atoms each 1.615 Å away.

The non-stoichiometry plays two important roles in the structure of the β-alumina. First of all, because there are more sodium atoms than preferred BR sites, there must be a distribution of sodium among the other sites. This is shown in Figure 2 where the electron density of sodium in the conduction plane is projected for various temperatures[12]. The site occupation probabilities are given in Table 1.[13] The sodium clearly favors the BR and MO sites at low temperatures, but at higher temperatures, the "liquid-like" behavior of the mobile sodium in the conduction plane is illustrated. Secondly, the presence of excess cations in the conduction plane necessitates the presence of counter-charge ions to preserve charge neutrality. This charge compensation has been shown to be accomplished by oxygen atom interstitials[12] located at the MO site, one for every two excess sodium atoms. Two aluminum atoms, one from above and one from below the conduction plane, are displaced from the spinel blocks as

Figure 2

The projected density of sodium ions in the conduction plane of sodium β-alumina obtained by neutron diffraction at a) -180°C, b) 20°C and c) 600°C.[12] d) Unit cell outline in the conduction plane showing the positions of the BR, MO and aBR sites for comparison to the neutron diffraction data. Large open circle is an oxygen atom in the conduction plane.

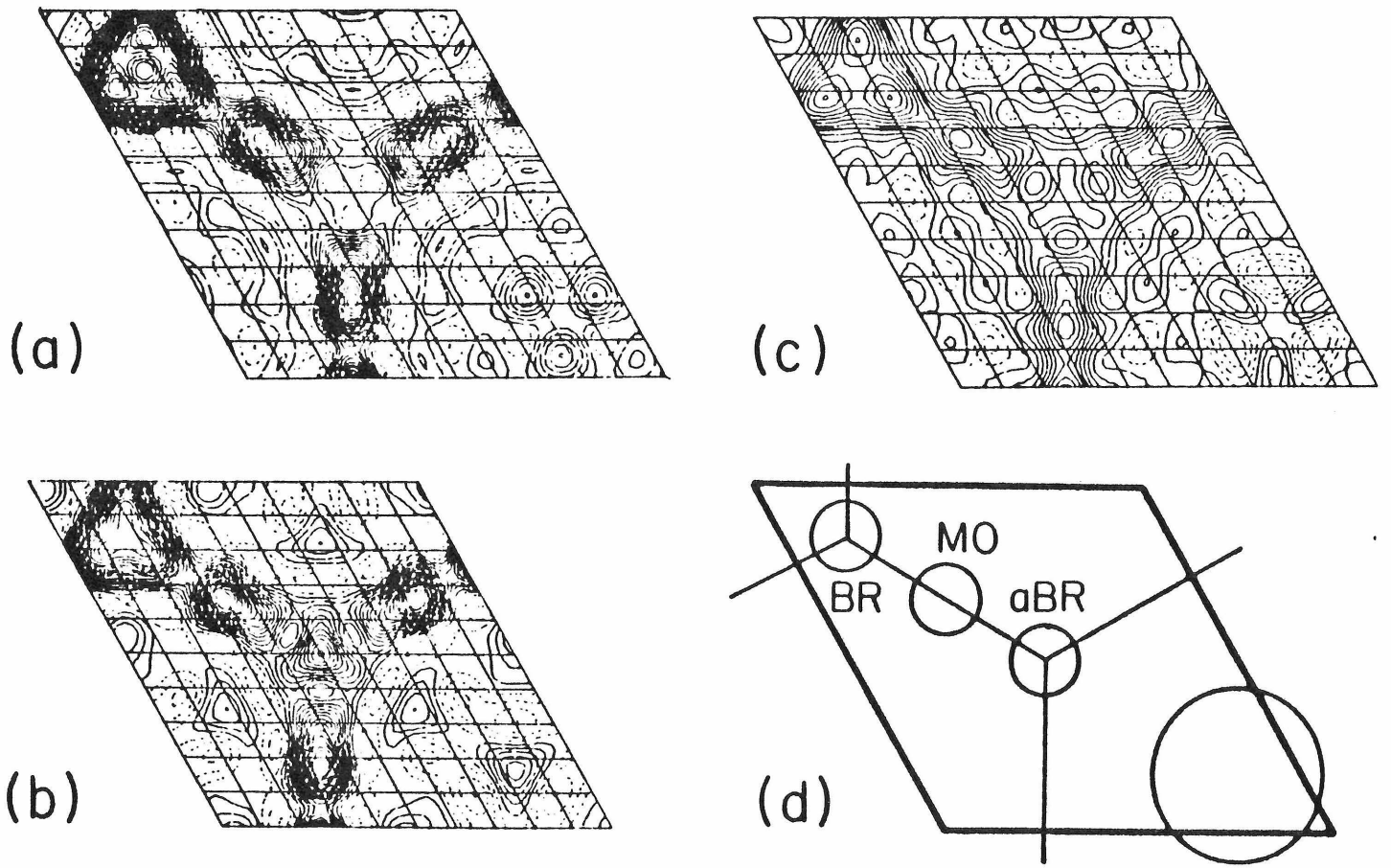
(a)
(c)
(b)
(d)
MO
BR
aBR

Table 1: Site Occupation Probabilities for Sodium in β-alumina from 80 K to 873 K.[13]

T(K)	BR	MO	aBR
80	.63	.36	.01
300	.66	.30	.04
623	.59	.36	.05
873	.61	.31	.08

Frenkel dislocations and coordinate with the interstitial oxygen. However, it should be pointed out that this defect offers a means of blocking the conduction pathway and further contributes to the disorder of the cation.

Structural analysis techniques such as x-ray[9] and neutron scattering[12,13] are able to provide in addition to a description of the solid electrolyte framework, details of mobile cation site character and occupancy. However, a disadvantage of conventional structural analyses is that it is difficult to separate the contributions to the intensity data arising from in-plane defects, static disorder, anharmonic vibrations, and diffusive motion of the cations and an average of these effects is observed. Likewise, information obtained with tracer diffusion,[4,6,14] ionic conductivity,[14-16] and dielectric loss measurements[17,18] reflect an average of the motional properties. On the other hand, spectroscopic results from Raman scattering,[19-21] and Infrared[21-24] techniques are able to probe the small-amplitude vibrations of the mobile cations, but they furnish little information on the long range transport processes.

In contrast to other techniques which are limited by their ability to measure either structural or dynamical properties, Nuclear Magnetic Resonance (NMR) techniques are able to probe both. Consequently, NMR has proven to be a most useful experimental method for supplying details of the relationship between local structure and motion in solids. The ^{23}Na isotope is NMR sensitive and conveniently

100% abundant, a fact which has led many investigators to apply conventional NMR relaxation and line shape analysis techniques to the study of the ($\frac{1}{2} \longleftrightarrow -\frac{1}{2}$) transition of the spin 3/2 sodium nucleus in β-alumina.[25-31] However, despite these studies, certain limitations of conventional NMR techniques have left many issues unresolved.

This work is, in part, an extension of the ^{23}Na NMR line shape analysis in β-alumina. Using a recently developed spin interferometric technique[32] described in Chapter II, the ($\pm 3/2 \longleftrightarrow \pm 1/2$) ^{23}Na transitions are used in Chapter III to i) characterize the individual sites in β-alumina, ii) observe details of motion between these sites, and iii) measure activation energy barriers for motion among these sites.

A major question about the motional process in solid electrolytes is whether correlated or independent particle motion exists. In β-alumina, this correlated motion is believed to result from the interaction of a pair of cations which reside in neighboring mid-oxygen (MO) positions.[33] The possible role of cation-cation interactions in the conduction process is the subject of investigation in Chapter IV. Here, the cation pair interactions are studied by introducing another mobile cation, ^{7}Li, another NMR sensitive nucleus, into the β-alumina structure. The results of these studies indicate that i) the characteristics of the lithium ion sites (potential wells) are different than those of sodium, ii) the distribution of lithium ions (structure) in lithium β-alumina is different than for sodium

β-alumina, iii) there is a strong interaction between pairs of cations, and iv) the interaction can be explained by a theory previously developed for the mixed-alkali effect in glasses.[34]

References

1. For a review of this subject, see, for example: (a) (a) Van Gool, W., Ed. (1973), "Fast Ion Transport in Solids", Plenum Press, New York. (b) Mahan, G.D. and Roth, W.L., Eds. (1976), "Superionic Conductors", Plenum Press, New York. (c) Geller, S., Ed. (1977), "Solid Electrolytes", Top. Appl. Phys., V. 21, Springer-Verlag, Berlin, Heidelberg, New York. (d) Salamon, M.B., Ed. (1979), "Physics of Superionic Conductors", Top. Current Phys., V. 15, Springer-Verlag, Berlin, Heidelberg, New York. (e) Vashista, P., Mundy, J.N. and Shenoy, G.K., Eds. (1979), "Fast Ion Transport in Solids-Electrodes and Electrolytes", North-Holland, New York, Amsterdam, Oxford.

2. Tubandt, C. and Lorenz, E. (1914), Z. Phys. Chem. 87, 513.

3. Bradley, J.N. and Greene, P.D. (1967), Trans. Far. Soc. 63, 424.

4. Yao, Y.-F.Y. and Kummer, J.T. (1967), J. Inorg. Nucl. Chem. 29, 2453.

5. Kummer, J.T. and Weber, N., U.S. Patent 3,404,036, October 1, 1968 and U.S. Patent 3,413,150, November 26, 1968.

6. Kummer, J.T. (1972), Progr. Solid State Chem. 7, 141.

7. Bragg, W.L., Gottfried, C. and West, J. (1931), Z. Krist. 77, 225.

8. Beevers, C.A. and Ross, M.A. (1937), Z. Krist. 97, 59.

9. Peters, C.R., Bettman, M., Moore, J. and Glick, M. (1971), Acta Cryst. B27, 1826.

10. Bevan, D.J., Hudson, B. and Moseley, P.T. (1974), Mat. Res. Bull. 9, 1073.

11. Yamaguchi, G. and Suzuki, K. (1968), Bull. Chem. Soc. Japan 41, 93.

12. Roth, W.L. (1974), General Electric Report #74CRD054, March.

13. Roth, W.L., Reidinger, F. and LaPlaca, S.L. in ref. 1(b), p. 223.

14. Kim, K.K., Chen, W.K. and Mundy, J.N. (1979), J. Phys. & Chem. Solids (GB) 40, 743.

15. Whittingham, M.S. and Huggins, R.A. (1971), J. Chem. Phys. 54, 414.

16. Whittingham, M.S. and Huggins, R.A. (1971), J. Electrochem. Soc. 118, 1.

17. Radzilowski, R.H., Yao, Y.-F.Y. and Kummer, J.T. (1969), J. Appl. Phys. 40, 4716.

18. Strom, U., von Schickfus, M. and Hunklinger, S. (1978) Phys. Rev. Lett. 41, 910.

19. Chase, L.L., Hao, C.H. and Mahan, G.D. (1976), Solid State Comm. 18, 401.

20. Hao, C.H., Chase, L.L. and Mahan, G.D. (1976), Phys. Rev. B 13, 4306.

21. Klein, P.B., Schafer, D.E. and Strom, U. (1978), Phys. Rev. B 18, 4411.

22. Strom, U., Taylor, P.C., Bishop, S.G., Reinecke, T.L.,

and Nagi, K.L. (1976), Phys. Rev. B 13, 3329.

23. Barker, A.S., Jr., Ditzenberger, J.A. and Remeika, J.P. (1976), Phys. Rev. B 14, 386.

24. Allen, S.J., Jr., Cooper, A.S., DeRosa, F., Remeika, J.P. and Ulasi, S.K. (1978), Phys. Rev. B 17, 4031.

25. Kline, D., Story, H.S. and Roth, W.L. (1972), J. Chem. Phys. 57, 5180.

26. Chung, I., Story, H.S. and Roth, W.L. (1975), J. Chem. Phys. 63, 4903.

27. Boilot, J.P., Zuppiroli, L., Delplanque, G. and Jerome, L. (1975), Philos. Mag. 32, 343.

28. Bailey, W., Glowinkowski, S., Story, H.S. and Roth, W.L. (1976), J. Chem. Phys. 64, 4126.

29. West, L.C., Cole, T. and Vaughan, R.W. (1978), J. Chem. Phys. 68, 2710.

30. Jerome, D. and Boilot, J.P. (1974), J. Phys. Lett. (Paris) 35, L-129.

31. Walstedt, R.E., Dupree, R., Remeika, J.P. and Rodriguez, A. (1977), Phys. Rev. B 15, 3442.

32. Polak, M. and Vaughan, R.W. (1978), J. Chem. Phys. 69, 3232.

33. Wang, J.C., Gaffari, M. and Choi, S. (1975), J. Chem. Phys. 63, 792.

34. a) Hendrickson, J.R. and Bray, P.J. (1972), Phys. and Chem. Glasses 13, 43. b) Hendrickson, J.R. and Bray, P.J. (1972), Phys. and Chem. Glasses 13, 107.

CHAPTER II: MATERIALS AND METHODS

A. MATERIALS

Our single crystal sample of β-alumina originated from the melt-grown boule prepared by the Union Carbide Corporation and provided to us by Dr. Terry Cole while employed at the Ford Motor Company Research Laboratory. Single crystal samples of appropriate size were cut with a diamond saw and oriented with Laue and precession x-ray photographs. These samples were then mounted so as to have either the $(10\bar{1}0)$ or $(11\bar{2}0)$ directions as the axis of rotation.

The Union Carbide sample of β-alumina, as grown, has sodium as the mobile cation. Procedures for exchanging the sodium for other cations exist in the literature.[1] Our procedure is similar and is outlined below.

1. Samples of appropriate dimensions are cut, washed with labtone in water to remove the lubricating oil, rinsed with water, and then dried in air.
2. The sample is further cleaned with conc. HNO_3 warmed in a platinum crucible. The acid is diluted and further heated.
3. Sample is rinsed with water and then heated with water to remove all acid.
4. Final rinse with water and dried in furnace at $550^{o}C$.
5. Sample is weighed.
6. Mixture of $LiNO_3$ and $NaNO_3$ is placed in

platinum crucible with sample and heated to 350°C.

7. Remove excess salt with water. Repeat steps 2-4.

8. Reweigh sample.

Sodium is strongly favored in the β-alumina structure over the melt and trace amounts of sodium in the $LiNO_3$ used in the exchange prevents more than approximately 80% conversion. To obtain higher concentrations of lithium, LiCl is used in step 6 and the furnace temperature is approximately 600°C. The remaining procedure is the same. Samples prepared by this method have less than 0.5% sodium (relative to initial sodium content).

B. INSTRUMENTATION AND EQUIPMENT

1. Description of Pulsed NMR Spectrometer. The NMR apparatus is built around a 63 kilogauss field of a superconducting solenoid. In this field, ^{23}Na and ^{7}Li have resonant frequencies of 71.5 and 105.1 MHz, respectively.

Homebuilt digital timing circuits control the sequence and duration of pulses driving a gating network which produces the radio frequency (rf) pulses. The pulses are amplified with a broadband power amplified before being applied to the probe. A broadband receiver and mixer amplifies and detects the resultant NMR free induction decay (FID) signal which is digitized with an A/D converter and stored in a computer. A schematic is shown in Figure 1.

FIGURE 1

Schematic of NMR spectrometer electronics.

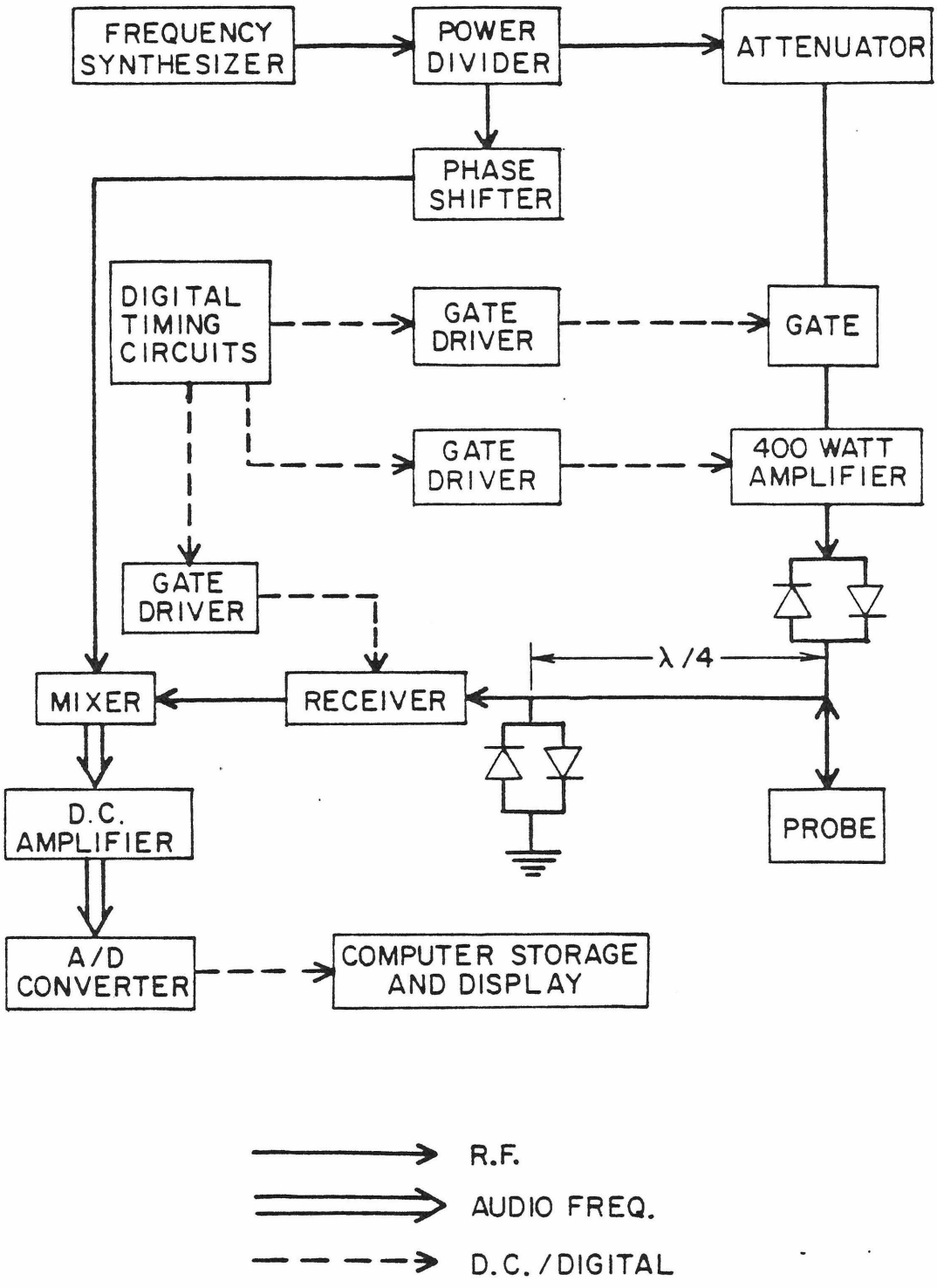
FREQUENCY SYNTHESIZER
POWER DIVIDER
ATTENUATOR
PHASE SHIFTER
DIGITAL TIMING CIRCUITS
GATE DRIVER
GATE
GATE DRIVER
400 WATT AMPLIFIER
GATE DRIVER
λ/4
MIXER
RECEIVER
D.C. AMPLIFIER
PROBE
A/D CONVERTER
COMPUTER STORAGE AND DISPLAY
R.F.
AUDIO FREQ.
D.C./DIGITAL

The standard $\lambda/4$ (where λ is the wavelength corresponding to the resonance frequency) terminated by crossed diodes to ground is used to isolate the receiver input from the output of the power amplifier. In addition, the power amplifier output is gated to reduce noise and the receiver amplifier stages are gated to prevent receiver amplifier overload arising from incomplete receiver isolation.

2. Basic Probe Design and Variable Temperature Gear. The probe design is constrained by the need to fit within the cylindrical bore of the superconducting solenoid, and the desire to have variable temperature capabilities. The design used is shown in Figure 2. The probe body consists of a bottom support, a support shaft (with an inner conductor to make it part of the transmission line) segmented into copper and stainless steel (for reduced thermal conductivity) tubing, and probe head. The probe head is made of copper and removal of a screw-on cap allows access to the flattened copper wire coil and the teflon rotation device mounting for the single crystal samples. The cap is wound with Nichrome wire for heating purposes. Also included in the probe head are thermocouple wires for sensing and regulating the temperature. A styrofoam plug fits over the lower end of the shaft for thermal isolation. The rotation device is essentially a teflon wheel into which a sample holder containing the crystal may be attached. The wheel can be turned via cotton threads which run down the center of the inner conductor of the support shaft and attach to a spring-loaded calibrated rota-

FIGURE 2

Probe and probe dewar design. a) Cutaway view of probe dewar. b) Cutaway view of dewar tail section with probe inserted. c) Probe head with cap removed. Coil dimensions are approximately 7 mm x 16 mm.

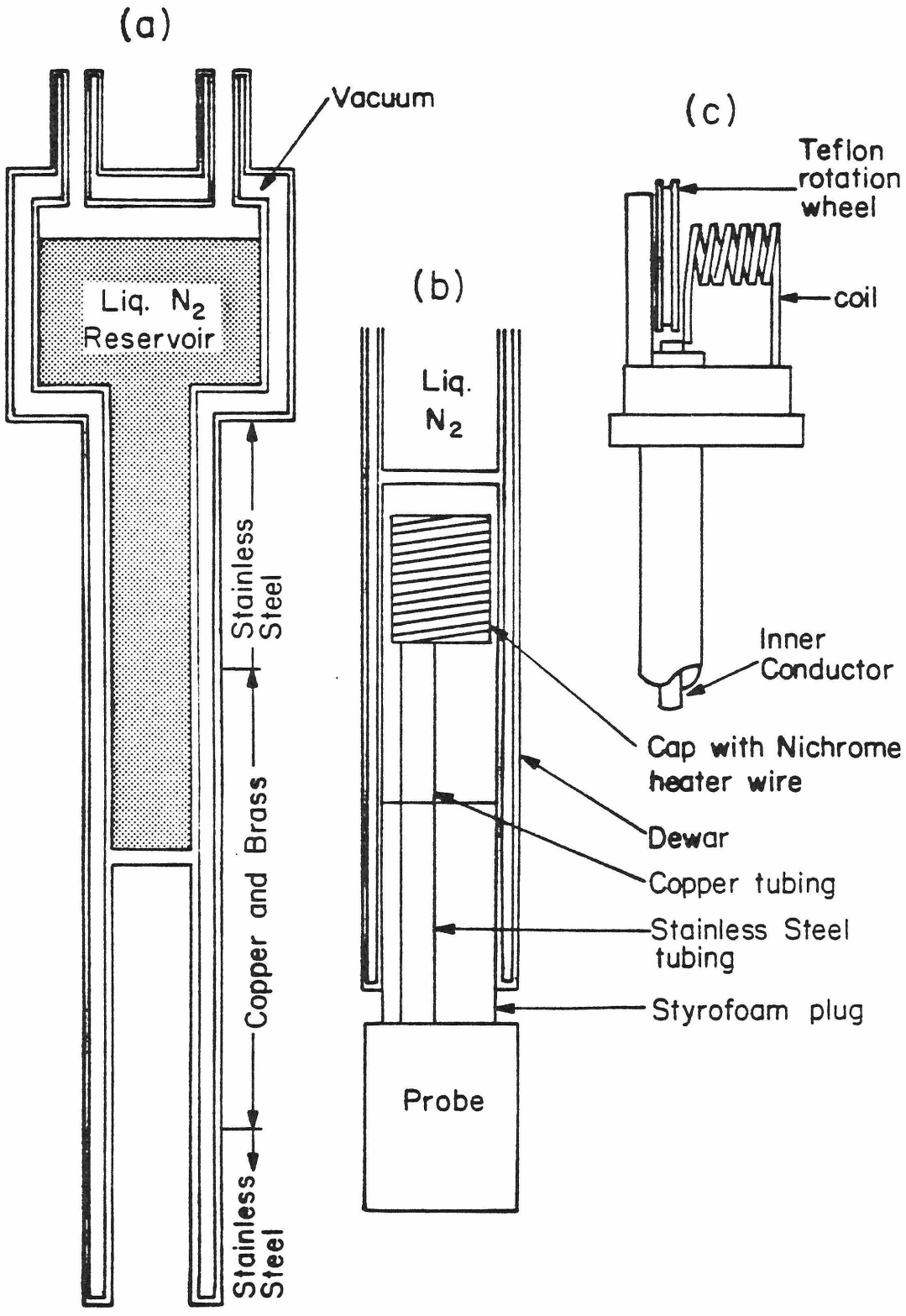
(a)
Vacuum
Liq. N_2 Reservoir
Stainless Steel
Copper and Brass
Stainless Steel
(b)
Liq. N_2
Probe
(c)
Teflon rotation wheel
coil
Inner Conductor
Cap with Nichrome heater wire
Dewar
Copper tubing
Stainless Steel tubing
Styrofoam plug

tion dial anchored to the base of the magnet. Reproducibility for this setup is $\pm 2^{o}$.

The probe is inserted into the magnet and dewar from the bottom and is cooled by conduction through air in contact with the liquid nitrogen-cooled dewar walls. The entire assembly reaches liquid nitrogen temperatures within an hour. For temperatures between that of liquid nitrogen and room temperature, the output of the thermocouple leads is differentially amplified and used to regulate a proportioning rate controller which supplies the current to the heater wires to maintain a preset temperature. Regulation within $\pm 0.3^{o}$ and stability of 0.5^{o}/8 hrs. can be achieved over the temperature range of 77 K to 300 K.

3. Probe Electronics. The tuning circuit is the familiar series-resonant arrangement[2] shown in Figure 3, but the configuration of its elements differs from conventional practice in order that both sodium and lithium resonances can be observed on the same sample without requiring separate probes. The design in Figure 3 utilizes the transformation characteristics of transmission lines to place the tuning circuit far from the probe coil. The external transmission line coaxial cable, equal in length to a multiple of $\lambda/2$, provides exact transformation of the coil impedence to modules pre-tuned for a particular nucleus, both of which may be changed at will without disturbing the probe or sample. In addition, the $\lambda/2$ values for lithium and sodium are 90 cm and 140 cm, respectively, which places the temperature-sensitive tuning capacitors far from the cold source.

FIGURE 3

a) Series resonant probe circuit. L is the probe coil, and C1 and C2 are the tuning and matching capacitors, respectively. b) Diagram illustrating the $\lambda/2$ distance at which the tuned probe modules occur from the probe coil. Values for $\lambda/2$ for lithium and sodium are 90 cm and 140 cm, respectively.

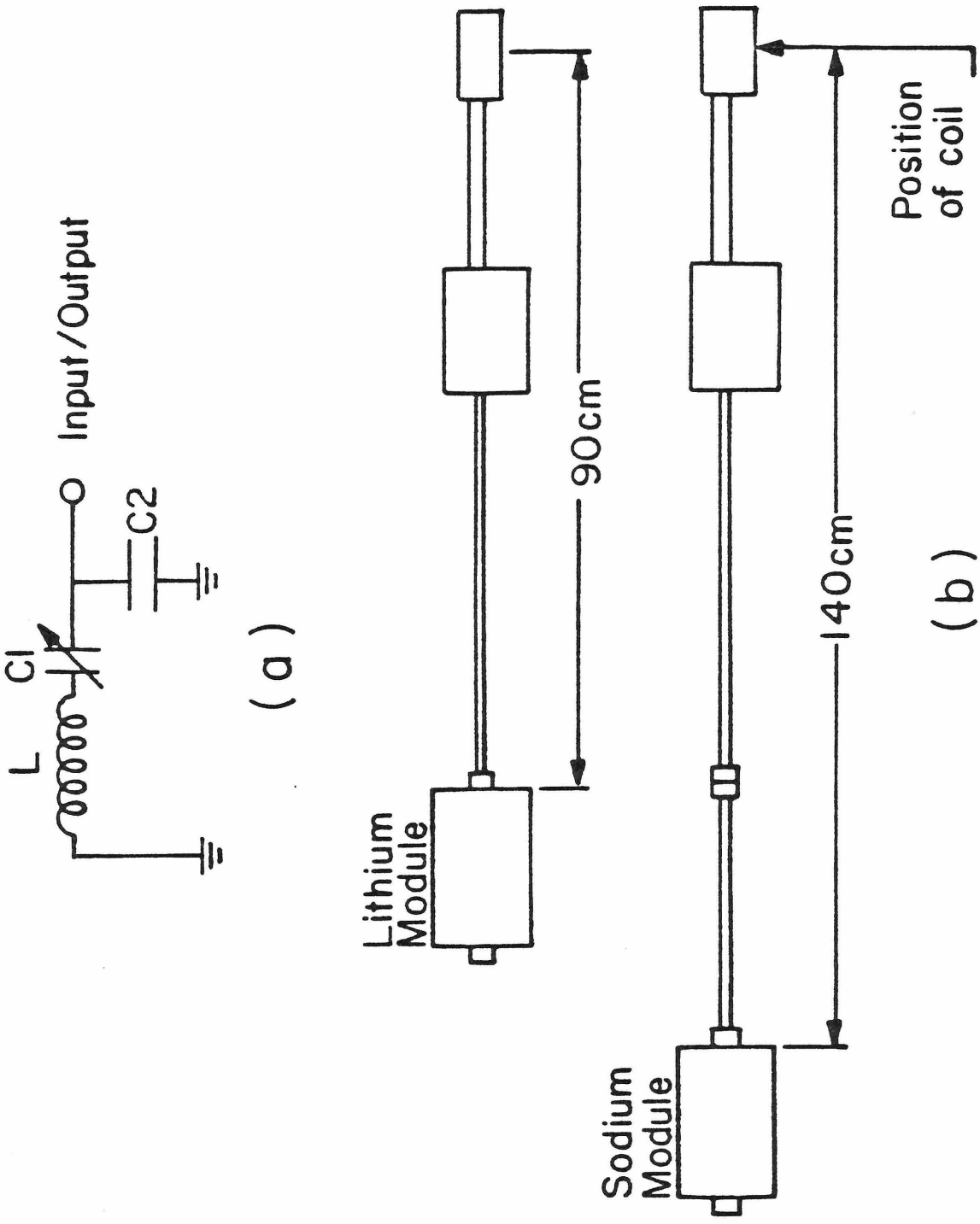
L
C1
C2
Input/Output
(a)
Lithium Module
90cm
Sodium Module
140cm
Position of coil
(b)

4. The Double-Q Probe. The other variation of probe design involves the circuit itself. The double-resonance experiments on sodium place special requirements on the probe response. Typical quality factors (Q) for the previously described probes are approximately 100 - 140. This allows observation of spectra over a frequency range of 700 KHz for sodium and lithium. Unfortunately, the double resonance experiments on sodium require a Q of approximately 30 in order to irradiate portions of the satellite spectrum occuring up to 1 MHz away from the central resonance at which the probe is tuned. Since the ability to detect the NMR signal deteriorates with decreasing Q, lowering the Q of the probe circuit in order to irradiate the satellites makes observation of the central transition more difficult. A probe circuit design which has a low Q during the rf pulse but a high Q for the detection of the central transition magnetization satisfies both of these conditions and is shown in Figure 4.

When the amplifier pulse is turned on, crossed diode pairs D1 through D4 present open circuits and the equivalent circuit "seen" by the amplifier is shown in Figure 4b. The value of the resistor R determines the value of Q of the probe, and the tuning and matching capacitors, C1 and C2, can be selected to tune to the desired frequency. The parallel circuit is tuned with capacitor C5 such that it provides a high impedence point at C and prevents current from flowing to the receiver. When the pulse is off, crossed diodes D1 through D4 provide an open circuit and the equivalent circuit

FIGURE 4

Double Q-probe operation. a) Schematic of double-Q probe showing amplifier input at point A and receiver output at point B. L1 is the probe coil and D1 through D4 are crossed-diode pairs. b) Equivalent amplifier-probe circuit when pulse is on. Capacitors C1 and C2 are tuning and matching capacitors, respectively, and resistor R lowers the probe Q. c) Equivalent receiver-probe circuit when pulse is off. Capacitors C3 and C4 are tuning and matching capacitors, respectively.

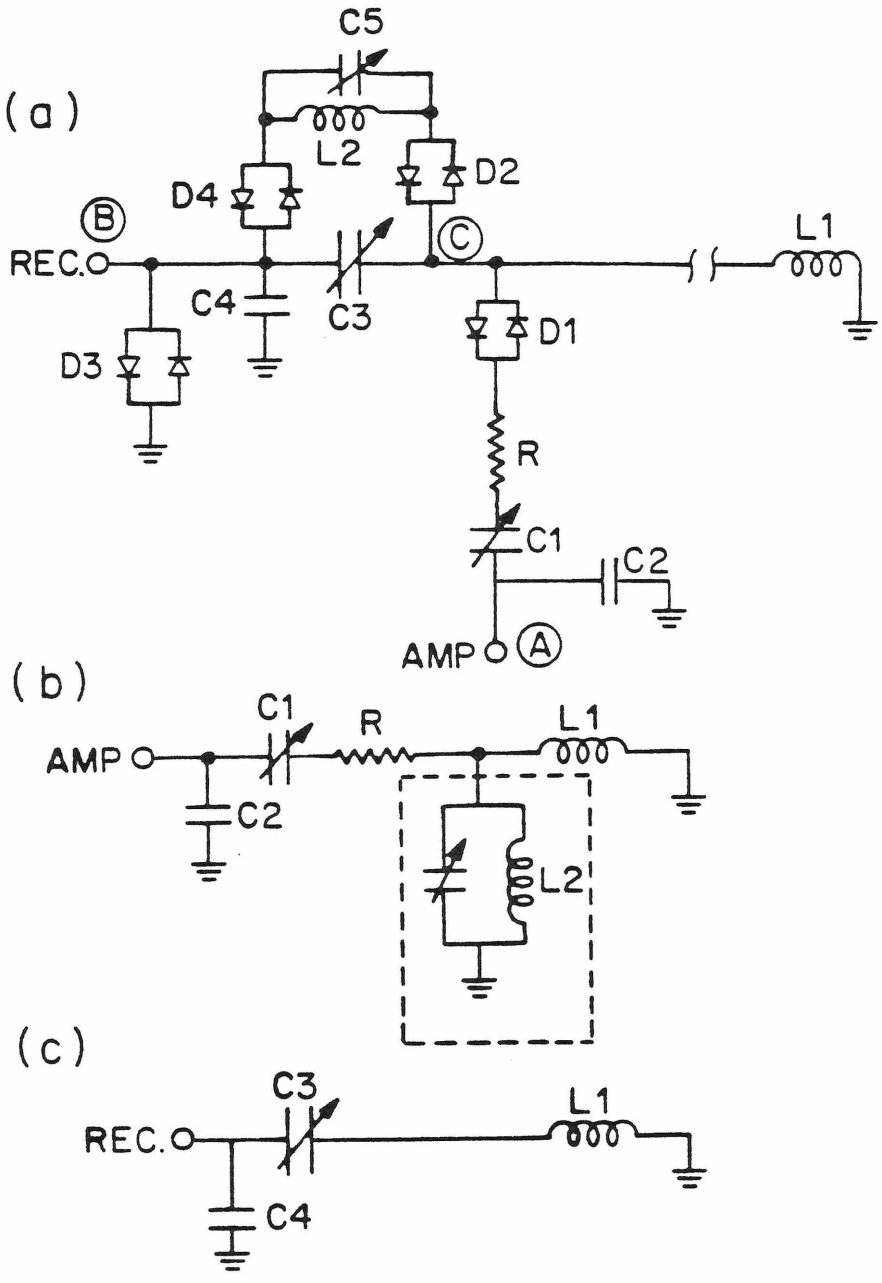
(a)
C5
L2
D4
D2
B
REC.
C
L1
C4
C3
D1
D3
R
C1
C2
AMP
A
(b)
C1
R
L1
AMP
C2
L2
(c)
C3
L1
REC.
C4

for the returning low-voltage NMR signal is shown in Figure 4c. This is exactly the same circuit as in the basic design and its Q and tuning are essentially independent of the pulsing circuit. With this arrangement, the experimental tuning frequency is 71.5 MHz and the Q's are 35 and 110 for amplifier and receiver segments, respectively. With an input voltage at point A of 400 V, the leakage voltage appearing at point B is 8 V, which is a loss of 2% and is easily handled by a conventional crossed diode-$\lambda/4$ protection circuit.

C. NMR THEORY AND EXPERIMENT

Both ^{23}Na and ^{7}Li are sensitive NMR nuclei possessing nuclear spins of 3/2. For these nuclei, the NMR spectral features are dominated by the interaction of the nuclear magnetic moment with the applied magnetic field and the electrostatic interaction of the nuclear quadrupole moment (possessed by nuclei with spins greater than or equal to one) with the electric field gradient (EFG) present at the nucleus. The first interaction (Zeeman) can be made the larger of the two in an appropriately large magnetic field. Consequently, the high-field approximation[3] can be used to compute the effect of the quadrupole interaction. Within this approximation, the spin system is quantized along the magnetic field with $2I + 1$ nuclear states. The magnetic interaction produces four equally-spaced energy levels with the three transitions having a common resonance frequency (Figure 5a). The result of the quadrupolar interaction, which is a perturbation arising from the competing tendency for the spin to align with

FIGURE 5

High field Zeeman and quadrupole interactions. a) Zeeman splitting of $2I + 1$ levels for spin 3/2. Exaggerated shifts due to b) first-order and c) second-order quadrupolar interactions. d) Diagram showing angles, θ and ϕ, the applied field, H, makes with the EFG principal axis system.

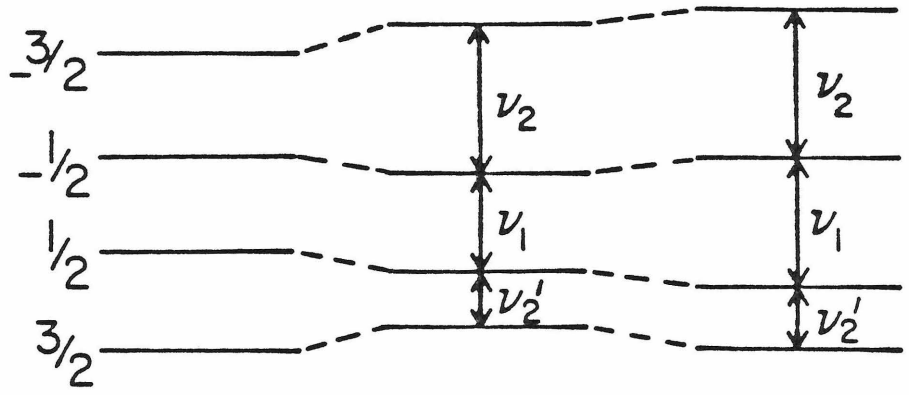
-3/2
-1/2
1/2
3/2
ν2
ν1
ν2'
ν2
ν1
ν2'

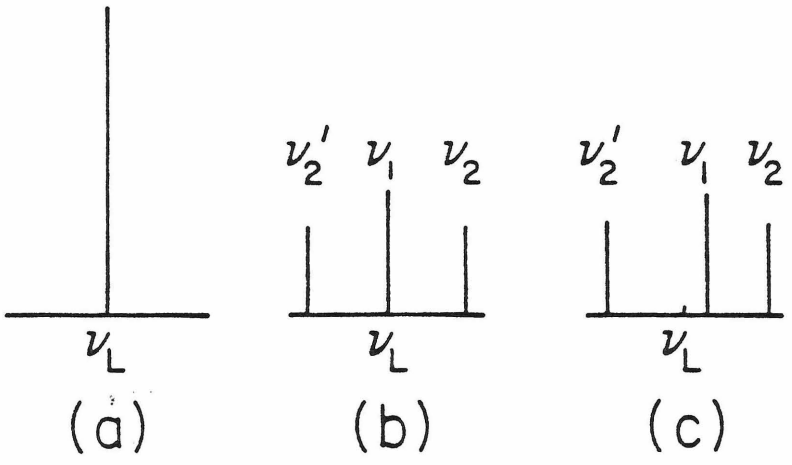
ν2' ν1 ν2
ν2' ν1 ν2
νL
νL
νL
(a)
(b)
(c)

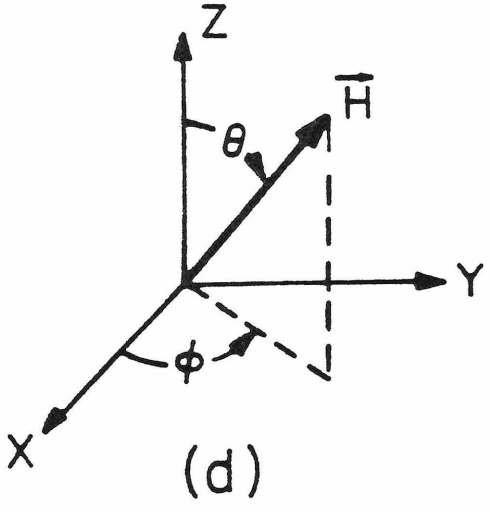
Z
H
θ
Y
φ
X
(d)

the EFG, is to modify the energy level pattern and transitions as follows. To first order the $\pm 3/2 \longleftrightarrow \pm 1/2$ transitions experience equal but opposite shifts so that they occur as satellites symmetrically disposed about the central transition ($+1/2 \longleftrightarrow -1/2$). (See Figure 5b). To second order, however, even the central transition is shifted as shown in Figure 5c.

The EFG is a tensor determined by the charge distribution surrounding the nucleus and the tendency for the spin to align along its axes results in the magnitude of the quadrupole interaction being dependent upon the relative orientation of the applied magnetic field. The expressions for the first- and second-order shifts for the satellite and central transitions arise from the application of second-order perturbation theory and are given below.[4,5]

$+3/2 \longleftrightarrow \pm 1/2$ First order

$$\Delta\nu^{(1)} = \pm 1/2\nu_Q\{3\cos^2\theta - 1 + \eta\cos 2\phi \sin^2\theta\} \qquad (1)$$

$+1/2 \longleftrightarrow -1/2$ Second order

$$\Delta\nu^{(2)} = -\frac{\nu_Q^2}{48\nu_L}\left\{A\cos^4\theta + B\cos^2\theta + C\right\} \qquad (2)$$

$$A = -81 + 54\eta\cos 2\phi - 9\eta^2\cos^2 2\phi$$

$$B = 90 - 48\eta\cos 2\phi - 12\eta^2 + 18\eta^2\cos^2 2\phi$$

$$C = -9 - 6\eta\cos 2\phi + 8\eta^2 - 9\eta^2\cos^2 2\phi$$

The EFG is fully characterized by its magnitude, eq, its asymmetry parameter, η, and the angles, θ and ϕ, that the applied magnetic field makes with its principal axes (Figure

5d). The constant, ν_L, is the resonant frequency of the unperturbed transition, and ν_Q is defined by

$$\nu_Q = \frac{e^2qQ}{2h} \tag{3}$$

where Q is the nuclear quadrupole moment.

The interpretation of spectra taken on single crystals at various orientations relative to the applied magnetic field enables individual EFG's to be characterized. With the aid of the crystal symmetry properties and lattice sum calculations for the EFG, these EFG's can be associated with distinct structural sites. However, when motion is present, the NMR spectra reflect the averaged EFG experienced by the nucleus. A NMR study of the quadrupole interactions versus temperature can determine among which sites motion is occurring and allow calculation of the corresponding activation energy barriers.

In the presence of a quadrupole interaction which produces distinct central and satellite transitions, there exists the possibility of selectively irradiating individual transitions and in the case of a large quadrupole interaction, it may be experimentally impossible to irradiate all transitions with a single pulse. Whether the transitions are irradiated singly or collectively is an important distinction since the duration of the rf pulse necessary to produce a 90° tilt of the magnetization not only differs for these two cases but also differs depending on which transition is irradiated. The duration of a 90° pulse which irradiates all three levels must be halved in order to be a 90° pulse for the central transition and

divided by $\sqrt{3}$ in order to be a 90^{o} pulse for the satellite transitions. In future reference to pulses applied to selectively irradiated transitions, pulse lengths are adjusted to include these factors.

In NMR spectra of the lithium nucleus, the largest observed first-order satellite shifts are usually less than 100 kHz and with typical pulse magnitude values of approximately 100 kHz a single 90^{o} pulse scheme can be employed (Figure 6a). Transition frequencies are measured directly from the absorption spectra obtained by Fourier transforming the FID occurring after the pulse. On the other hand, second-order shifts are undetectable due to the high magnetic field used for these experiments.

The quadrupole moment for the sodium nucleus is larger than for lithium and both first- and second-order quadrupolar shifts are observable. However, this larger interaction places the satellites approximately 1 MHz from the central transition, too large a spread to be irradiated with a single pulse. Selective irradiation of the central transition can measure the second-order shift. However, the distribution of EFG's in β-alumina causes a broadening of the satellites which makes them difficult if not impossible to detect directly. The satellites may, instead, be detected indirectly with a method known as spin interferometry[6] which relies on measuring changes induced in the observable central transition magnetization after a satellite is irradiated. Briefly, the method relies on selective excitation of two adjacent transitions

FIGURE 6

a) Single 90^{o} pulse scheme for direct observation of ^{7}Li. FID after the pulse is Fourier-transformed. b) Two pulse scheme for indirect observation of ^{23}Na satellite spectra. A 90^{o} pulse is applied to the central transition and is immediately followed by a 360^{o} search pulse which is stepped in frequency through the satellite region. Absorption spectra obtained by Fourier-transforming FID's collected after the second pulse are subtracted from the Fourier-transformed spectrum of an FID obtained without the 360^{o} pulse.

(a) Direct Observation

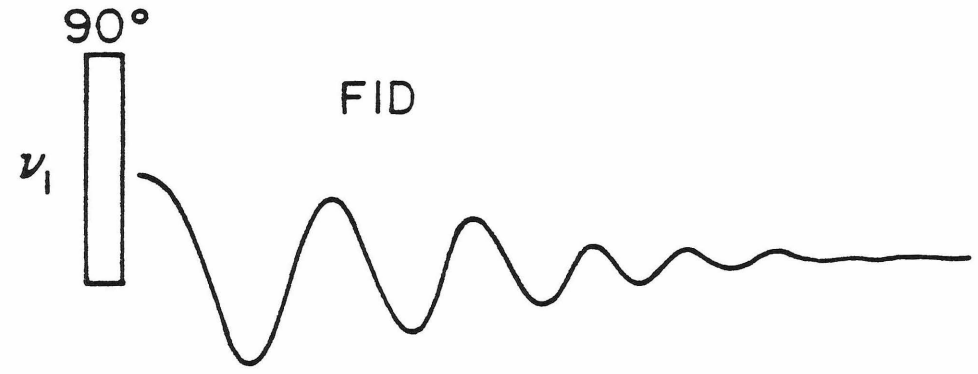

(b) Indirect Observation

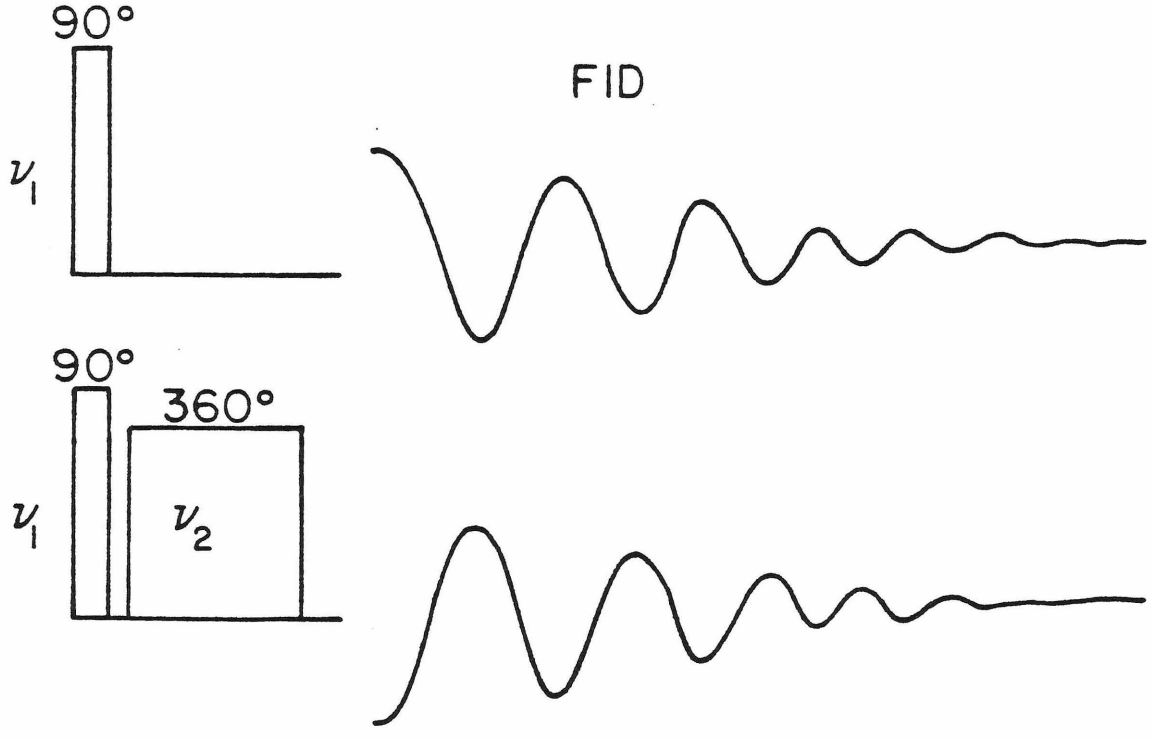

which share a common level. A selective 90^{o} pulse is first applied to the central transition, creating phase coherence between the +1/2 and -1/2 states and establishing an observable magnetization. Immediately thereafter, a selective 360^{o} pulse is applied to a satellite transition. Because the pulse is selective, the satellite transition is treated as a pseudo two-level system and application of the 360^{o} pulse changes the phase factor of the common state which the irradiated satellite transition shares with the central transition by 180^{o}. The phase of the unperturbed central transition state is unchanged and the result is an inversion of the observable magnetization (Figure 6b). However, when a satellite is broad, a selective pulse irradiates less than the full width and only a fraction of the central transition magnetization is inverted. The sum of unperturbed and inverted magnetizations in the central transition results in an overall reduction in the signal magnitude. Therefore, a pulse scheme which applies a 90^{o} pulse to the central transition immediately followed by a 360^{o} search pulse which is stepped in frequency through the satellite region results in a collection of FID's with varying magnitudes. The absorption spectra obtained by Fourier-transforming these FID's are subtracted from the Fourier-tranformed spectrum of a FID obtained without the 360^{o} search pulse. The results are spectral differences which, when plotted versus the irradiation frequency of the search pulse, enable the location and line shape of the satellite to be determined.

References

1. Yao, Y.F.Y. and Kummer, J.T. (1967), J. Inorg. Nucl. Chem. 29, 2453.

2. For a discussion of basic probe design, see, for example, Gilbert, W. and McNeil, J.A. (1973), Rev. Sci. Instrum. 44, 844.

3. Cohen, M.H. and Reif, F. (1957), in "Solid State Physics", Academic Press, N.Y., 4, 321.

4. Abragam, A. (1961), "Principles of Nuclear Magnetism", Oxford University Press, Chap. VII.

5. Narita, K., Umeda, J. and Kusumoto, H. (1966), J. Chem. Phys. 44, 2719.

6. Polak, M. and Vaughan, R.W. (1978), J. Chem. Phys. 69, 3232.

CHAPTER III: SODIUM β-ALUMINA

A. INTRODUCTION

Considerable effort has been expended over the past few years to characterize the structure and complex ionic motional processes responsible for the high ionic mobility of sodium ions in β-alumina.[1] Tracer diffusion[2,3] and ionic conductivity[4-6] measurements indicate that sodium ions participate in long-range diffusive motions in the two-dimensional conduction layer. However, attempts to understand the detailed mechanisms responsible for ionic motion have been limited by techniques which only measure average motional properties. On the other hand, nuclear magnetic resonance has proven to be a most useful experimental technique for supplying details of motion in solids. Earlier ^{23}Na NMR studies are concerned primarily with analyses of the shifts and relaxation rates observed in the central transition[7-13]. However, the second-order quadrupole shifts in the central transition are apparently too complex and too small to be sensitive enough to reveal the detailed motion which causes the static EFG's to average. In addition, studies of relaxation rates have been unable to establish a correspondence between the observed activation energies and a detailed motional process. This ^{23}Na NMR study extends the line-shape analysis to include measurements on the satellite transitions whose shifts follow a simpler first-order expression for the quadrupole interaction. The study of the ^{23}Na satellite shifts permits (i) individual sites in β-alumina to be characterized by their different

EFG patterns, (ii) a more sensitive measure of the effects of motion on the EFG's because shifts in satellite spectra are greater than in central transition spectra which causes the effects of motion to be spread out over an expanded temperature (time) scale, and (iii) the calculation of the activation energy barriers for the observed motional processes.

B. EXPERIMENTAL

Measurement of satellite spectra is accomplished with the use of the spin interferometric method described briefly in Chapter II. Specific values for the selective 90° and 360° pulse lengths, (τ), and magnitudes, (H_1), are given in Table 1. The 90° pulse irradiates the central transition approximately 15 kHz off-resonance. The 360° pulse immediately follows the 90° pulse, but it also prevents observation of the FID for 30 μsec. The truncated FID's following repetition of this 90° (ν_1) 360° (ν_2) sequence are added to improve signal-to-noise and are subsequently Fourier-transformed and stored. This process is repeated for various values of the search frequency ν_2. Phase distortions in the Fourier-transformed spectra arising from the truncation of the early part of the FID are corrected by adding the squares of the absorption and dispersion spectra point by point. The areas of the resulting spectra are subtracted from the area of a similar spectrum obtained without satellite irradiation and the differences plotted versus the irradiating frequency, ν_2, outline the satellite spectrum. This process is then repeated for the desired

Table 1: Pulse lengths and magnitudes for the indirect detection method.

Pulse	τ	H_1
90^o	5 μsec	25 kHz ($2H_1$ = 50 kHz)
360^o	30 μsec	20 kHz ($\sqrt{3}H_1$ = 35 kHz)

crystal orientations and selected temperatures.

C. RESULTS AND DISCUSSION

1. Room-temperature Results. In single crystal β-alumina, only one set of symmetrically spaced satellites is observed at room temperature. The positions of these satellites versus crystal orientation are shown in Figure 1 and can be fit to an EFG tensor with a magnitude of e^2qQ/h = 1.99 MHz and an asymmetry parameter η=0.0. The existence of only one pair of satellites which additionally follow an axially symmetric (η=0.0) pattern, is a manifestation of sodium ions undergoing rapid motion. Long-range diffusive motion through the two-dimensional conduction layer, which is known to occur, predicts this behavior. However, a more restrictive motion where sodium ions are allowed to jump rapidly among sites which are related by a threefold or higher symmetry axis is also sufficient to produce this pattern. Therefore, the pattern itself is not conclusive evidence for long-range motion and other motional processes important to the conduction mechanism may be present. This distinction can be resolved by observing spectra at lower temperatures where motion is retarded. Such temperature dependent studies should establish what exchange processes between which sites become important at what temperature.

2. The Static EFG's. The low temperature single crystal rotation data (77 K - 85 K) for two samples, one rotated about the $[10\bar{1}0]$ axis and the other about the $[11\bar{2}0]$ axis, are shown in Figures 2 and 3, respectively. Plotted are the

Figure 1

Room-temperature rotation pattern for the indirectly detected ^{23}Na satellites obtained for a single crystal β-alumina sample by rotation about the $[11\bar{2}0]$ axis. Plotted are the shifts measured relative to the central transition for the symmetrically placed satellites as a function of crystal orientation. The angle of rotation is the angle between the external magnetic field and the crystal c axis.

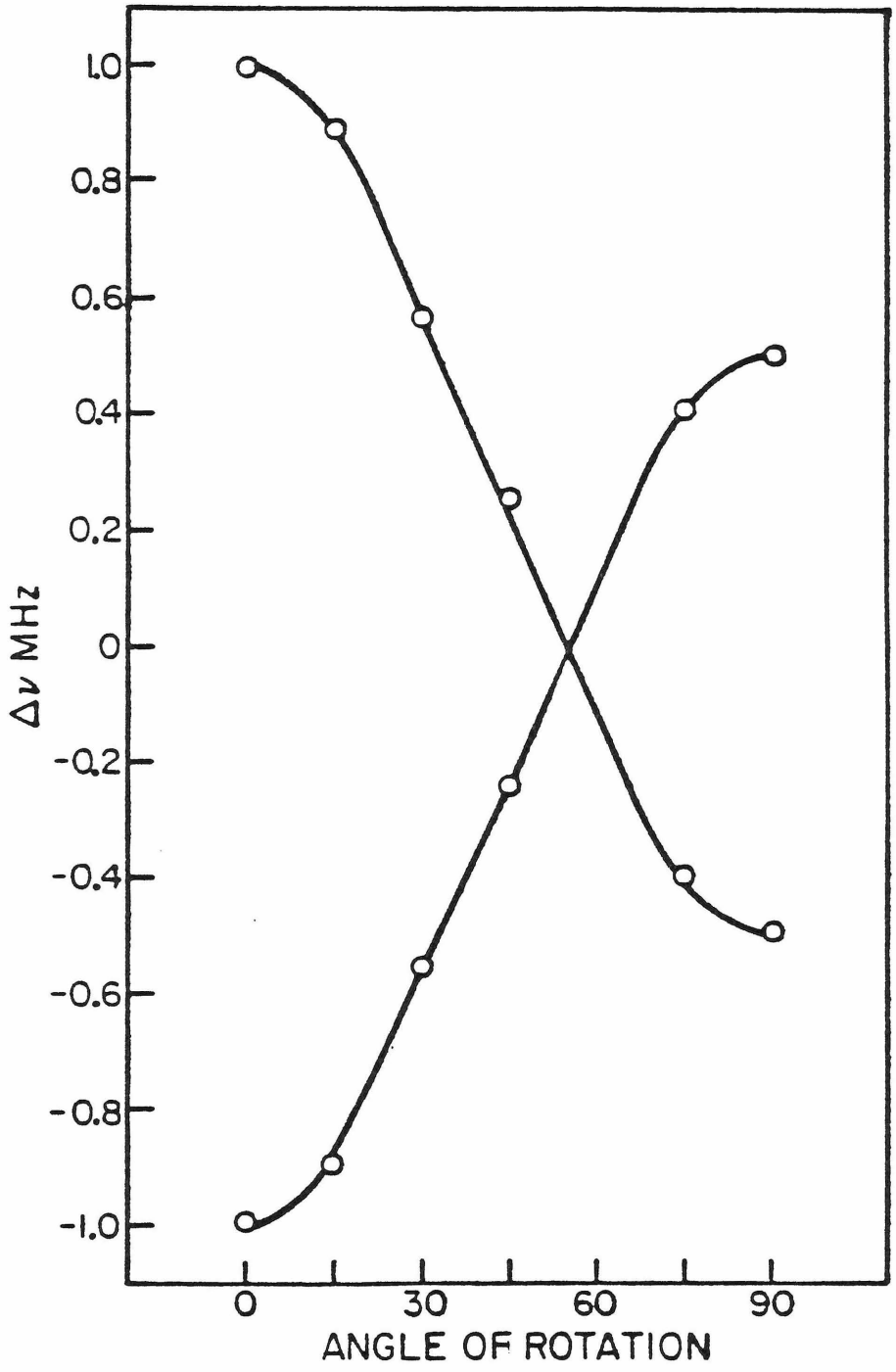
1.0
0.8
0.6
0.4
0.2
0
-0.2
-0.4
-0.6
-0.8
-1.0
Δν MHz
0
30
60
90
ANGLE OF ROTATION

Figure 2

Low-temperature (77 K - 85 K) rotation pattern for the indirectly detected ^{23}Na satellites obtained for a single crystal β-alumina sample rotation about the $[10\bar{1}0]$ axis. Plotted are the shifts measured relative to the central transition for the symmetrically placed satellites as a function of crystal orientation. The angle of rotation is the angle between the external magnetic field and the crystal c axis. A and B refer to the two fitted tensors mentioned in the text and are assigned to the BR and MO sites, respectively.

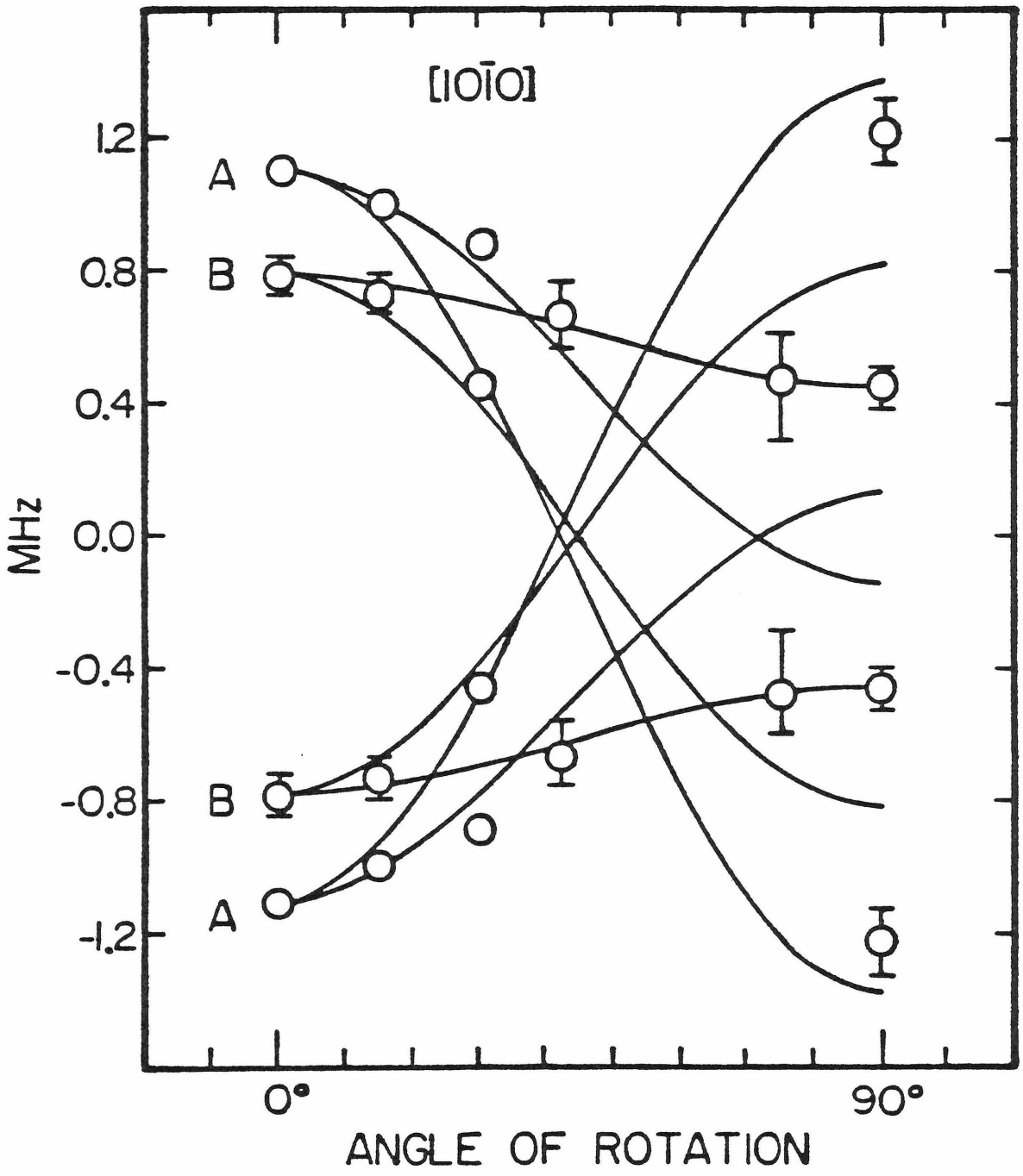
[10$\bar{1}$0]
1.2
0.8
0.4
0.0
-0.4
-0.8
-1.2
MHz
A
B
B
A
0°
90°
ANGLE OF ROTATION

Figure 3

Low-temperature (77 K - 85 K) rotation pattern for the indirectly detected ^{23}Na satellites obtained for a single crystal β-alumina sample rotation about the $[11\bar{2}0]$ axis. Plotted are the shifts measured relative to the central transition for the symmetrically placed satellites as a function of crystal orientation. The angle of rotation is the angle between the external magnetic field and the crystal c axis. A and B refer to the two fitted tensors mentioned in the text and are assigned to the BR and MO sites, respectively.

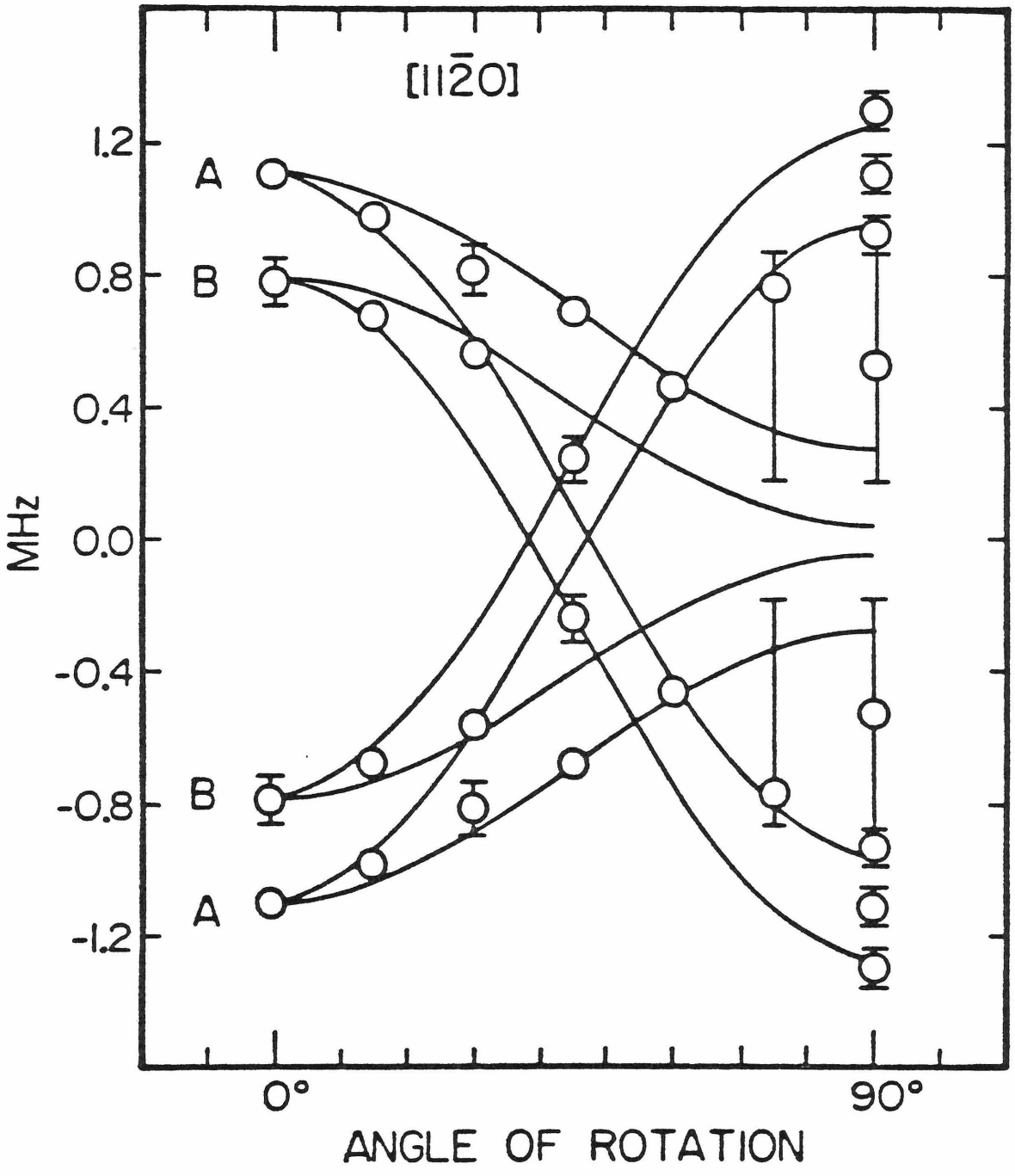
[11$\bar{2}$0]
1.2
0.8
0.4
0.0
-0.4
-0.8
-1.2
MHz
A
B
B
A
0°
90°
ANGLE OF ROTATION

shifts measured relative to the central transition for the symmetrically placed satellites as a function of crystal orientation. The angle of rotation is the angle between the external magnetic field and the crystal c axis. In both figures, the magnitudes of the largest satellite splittings are larger than the room temperature averaged values and more than one line is observed for most orientations.

Determining the positions of these individual lines, however, is not without some difficulty. Figure 4 displays a representative indirectly detected satellite spectrum obtained for the 0^{o} orientation at 85 K. (Central transition resonance is 71.42 MHz). The position and shape of the dominant resonance at 72.52 MHz is relatively easily determined, but the position and shape of the weaker resonance at 72.20 MHz is obscured. Notice that the frequency scale of the indirectly detected spectrum spans more than a megahertz and that the width of the satellite lines is approximately 300 kHz. Although a difference in resonance frequency of 320 kHz separates the two satellite lines, the broadening produced by inhomogeneities due to in-plane defects and static disorder make it difficult to accurately determine line positions. Therefore, the peak positions for the weaker resonances generally have a greater uncertainty which is indicated in Figures 2 and 3 by the presence of error bars. However, the appearance of an unusually large error bar indicates that the observed satellite spectrum is exceptionally broad and oftentimes featureless, the result of overlap of many broad satellite lines.

Figure 4

Representative indirectly detected ^{23}Na satellite spectrum obtained for a single crystal sample of β-alumina at the 0^{o} orientation at 85 K. Central transition resonance is located at 71.42 MHz.

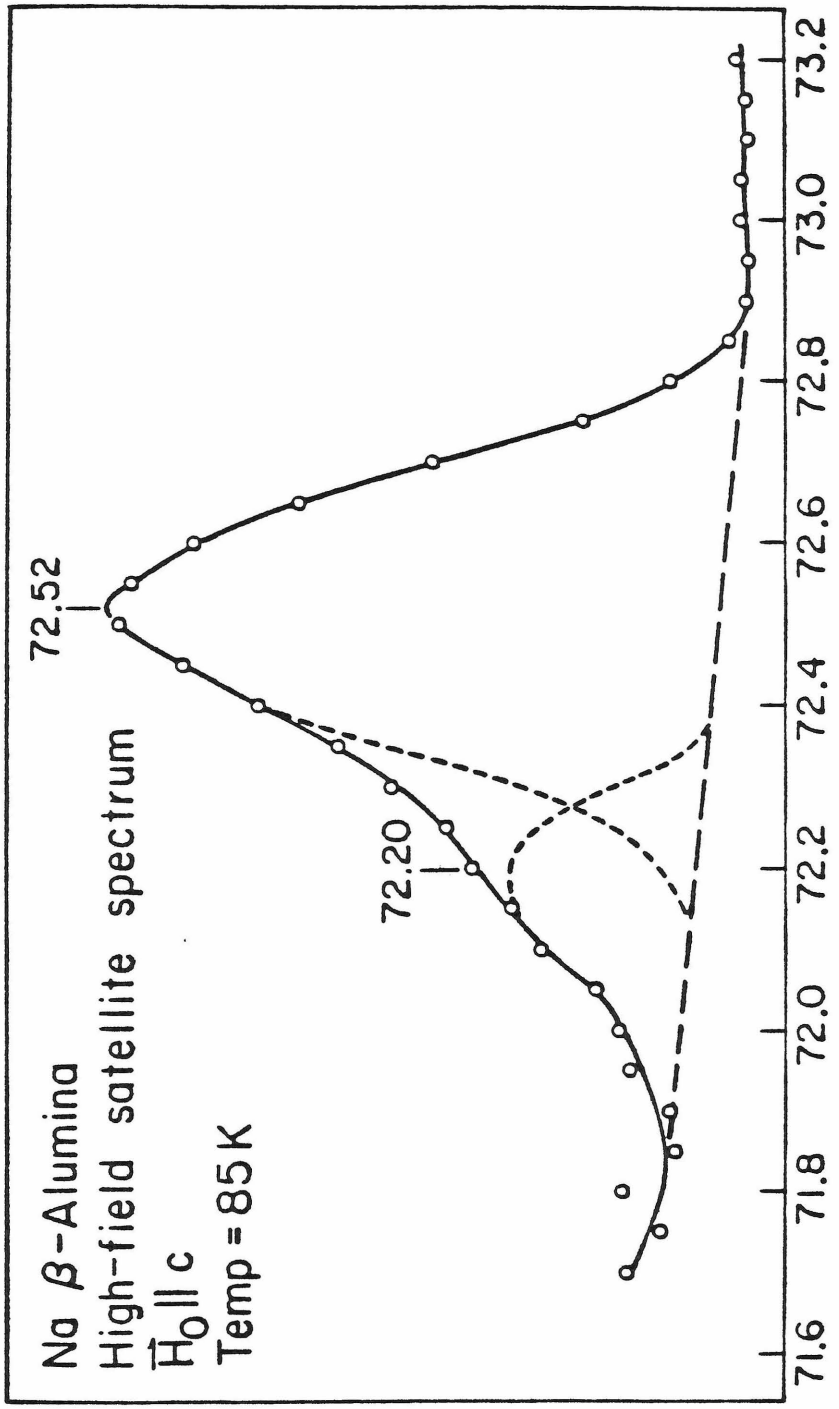
Na β-Alumina
High-field satellite spectrum
$\vec{H}_0 \| c$
Temp = 85 K
72.52
72.20
71.6
71.8
72.0
72.2
72.4
72.6
72.8
73.0
73.2
MHz

The EFG tensor can be specified by its magnitude, e^2qQ/h, its asymmetry parameter, η, and the angles, θ and ϕ, used to locate the principal axes in the crystallographic frame. Equation 1 in Chapter II relates these parameters to the peak-to-peak satellite splitting $\Delta\nu$. It is reasonable to fit the data with as few EFG tensors as possible, considering the relatively few possible sites in β-alumina. The data can reasonably be fit with a minimum of two tensors. The peak positions corresponding to the major resonance are relatively well-defined and hence its tensor is relatively well-characterized. The difficulty in reliably determining peak positions for the weaker resonance introduces greater uncertainty in the values obtained for its tensor. The values of e^2qQ/h, η, and the directions of the principal axes for the best fits are summarized in Table 2. The directions c, a and a* refer to the standard crystallographic unit cell axes. The theoretical patterns generated by these tensors are shown as lines A and B through the data in Figures 2 and 3. Because the rotation axes are symmetry axes in the crystal, two of the three symmetry related components of the tensor produce the same pattern and only two independent components are observed for each tensor.

Assignment of these two tensors to specific sites is straightforward. Low-temperature neutron diffraction data[14] indicates that sodium predominantly occupies two sites, the BR and MO, with a ratio of BR:MO of approximately 2:1. From the intensity of spectra collected at the 0^o orientation alone,

Table 2: Details of and assignments for the observed tensors in sodium β-alumina.

e^2qQ/h	η	V_{zz}	V_{yy}	V_{xx}	Assignment
2.75 ± 0.05 MHz	0.6 ± 0.1	a + 2a*	c	a	BR
2.5 ± 0.1 MHz	0.25 ± 0.1	a	c	a + 2a*	MO

it is reasonable to assign the tensor whose pattern includes the most intense peak as arising from the BR site, and the remaining tensor to the MO site. It is seemingly contradictory that the BR site has its principal V_{zz} axis in the conduction plane since, as pointed out in Chapter I, the BR site is expected to have three-fold symmetry, with the principal V_{zz} axis pointing along the crystallographic c axis, perpendicular to the conduction plane. This apparent contradiction is resolved upon further consideration of existing low-temperature neutron diffraction data. Reidinger's thesis[15], for example, quite clearly points out (Figure 5) that the sodium atoms do not sit in the three-fold site, but are, instead, displaced along the (a + 2a*) direction by approximately 0.5 Å. This displacement apparently is enough to redefine the principal V_{zz} axis along the (a + 2a*) direction, in agreement with the data. Satellites which do not belong to the BR tensor most likely correspond to the MO tensor by elimination. However, the weaker intensities of satellites associated with the MO site are obscured by overlap with the broad, more intense peaks due to the BR site. Even though this makes the fit more subject to error, the reported principal axes of the tensor do, nonetheless, coincide with the normals to symmetry planes at the MO site.

Another approach to obtaining these static EFG's in β-alumina is to observe the second-order shifts in the central transition at low temperatures. Bailey et al.[10] use this approach and observe several lines for a rotation about the

Figure 5

Partial Fourier synthesis of sodium at (a) 80 K and (b) 300 K. This figure is from reference 15.

(a)

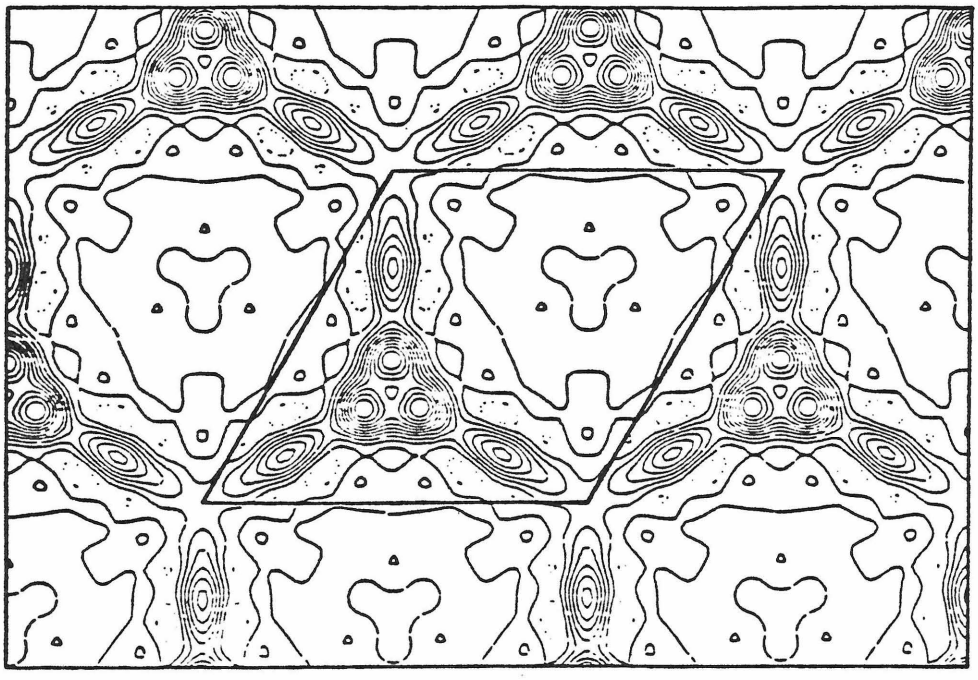

(b)

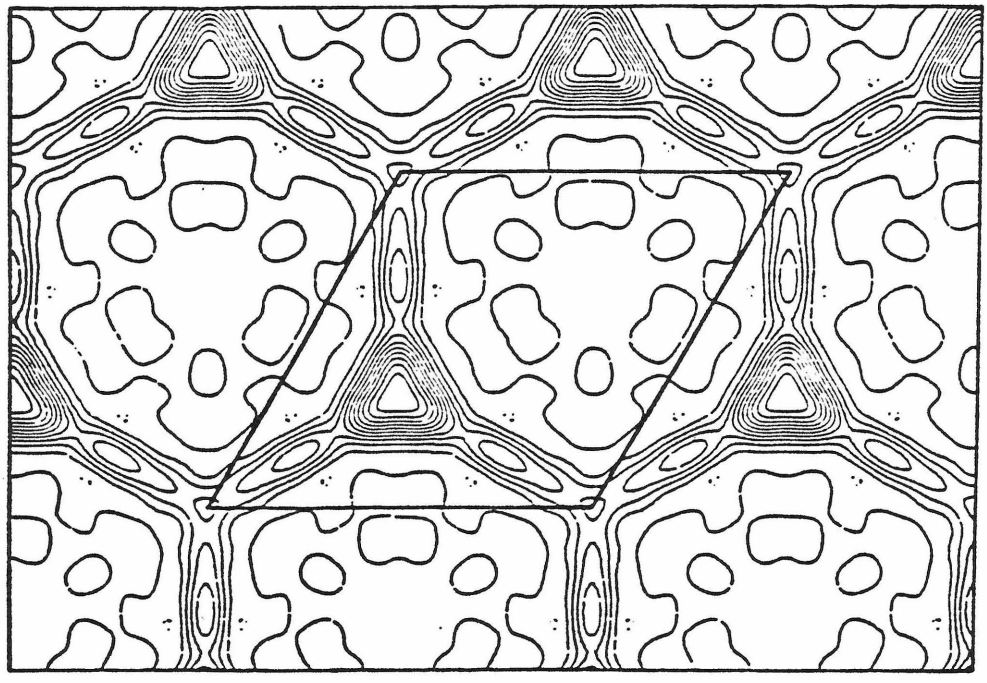

[10$\bar{1}$0] axis. Their best fit to the spectra also consists of two tensors. Although their method for describing the tensors differs from standard practice, values for e^2qQ/h and η converted to conventional definitions are listed in Table 3. A comparison of the tensor values from Tables 2 and 3 shows the larger tensors to be in reasonable agreement. The smaller tensors, however, have approximately the same magnitudes, but the details are in complete disagreement. There are a number of possible reasons for this discrepancy. First of all, if the agreement of the larger tensors is not fortuitous, their second tensor should correspond to the MO site. Consequently, the lower occupation of the MO site should make the intensity of the line corresponding to this site difficult to observe. Secondly, the tensors selected by Bailey et al. generate theoretical patterns which do not account for all of their observed lines. It is possible that other tensors would produce reasonable fits to their data as well, and/or include more of their data in the fit. For example, the tensors obtained here from fits to the satellite rotation patterns are not inconsistent with their reported data. Finally, the onset of motional exchange and collapse of regions in the central transition could produce weak lines which interfere with what are expected to be low temperature static EFG fits. However, for the ensuing motional analysis, exact characterization of the tensors is not necessary. Only the correspondence between the observed satellite peaks and

Table 3: Details of the tensors reported for sodium β-alumina (See ref. 10).

e^2qQ/h	η	V_{zz}	V_{yy}	V_{xx}
2.68 MHz	0.90	a + 2a*	c	a
2.20 MHz	0.86	a + 2a*	c	a

their respective sites is needed.

3. Motional Processes. Details of the sodium ion motion in β-alumina can be obtained by observing changes in the structure of satellite spectra as a function of temperature. As an example, Figure 6 displays representative spectra obtained at various temperatures for a single crystal β-alumina sample rotated about the $[10\bar{1}0]$ axis to an orientation where the applied magnetic field makes an angle of 30^{o} with the crystallographic c axis. A cursory examination of these spectra reveals the presence of two separate motional processes. The first process involves the disappearance of intensity at 72.3 MHz and 71.7 MHz from the low temperature spectrum and the subsequent appearance of a new peak at 72.1 MHz. A second process beginning at a higher temperature appears to involve the already averaged peak at 72.1 MHz and a peak originally at 71.9 MHz. The peak positions of the large spectral areas participating in the first average, as can be seen in Figure 2, have been assigned to the BR tensor components. Therefore, the first process is attributed to a motion of sodium ions among only the displaced BR sites. It appears that the second process averages the already averaged BR components with components assigned to MO sites. Consequently, the second process is an indication that motion is occurring between BR and MO sites.

The above interpretation of the averaging processes is reinforced by the agreement between the experimentally determined coalescence frequencies and those predicted by

Figure 6

Representative indirectly detected ^{23}Na satellite spectra obtained at various temperatures for a single crystal β-alumina sample rotated about the $[10\bar{1}0]$ axis to an orientation where the applied magnetic field makes an angle of 30^{o} with the crystal c axis. The central transition is located at 71.42 MHz.

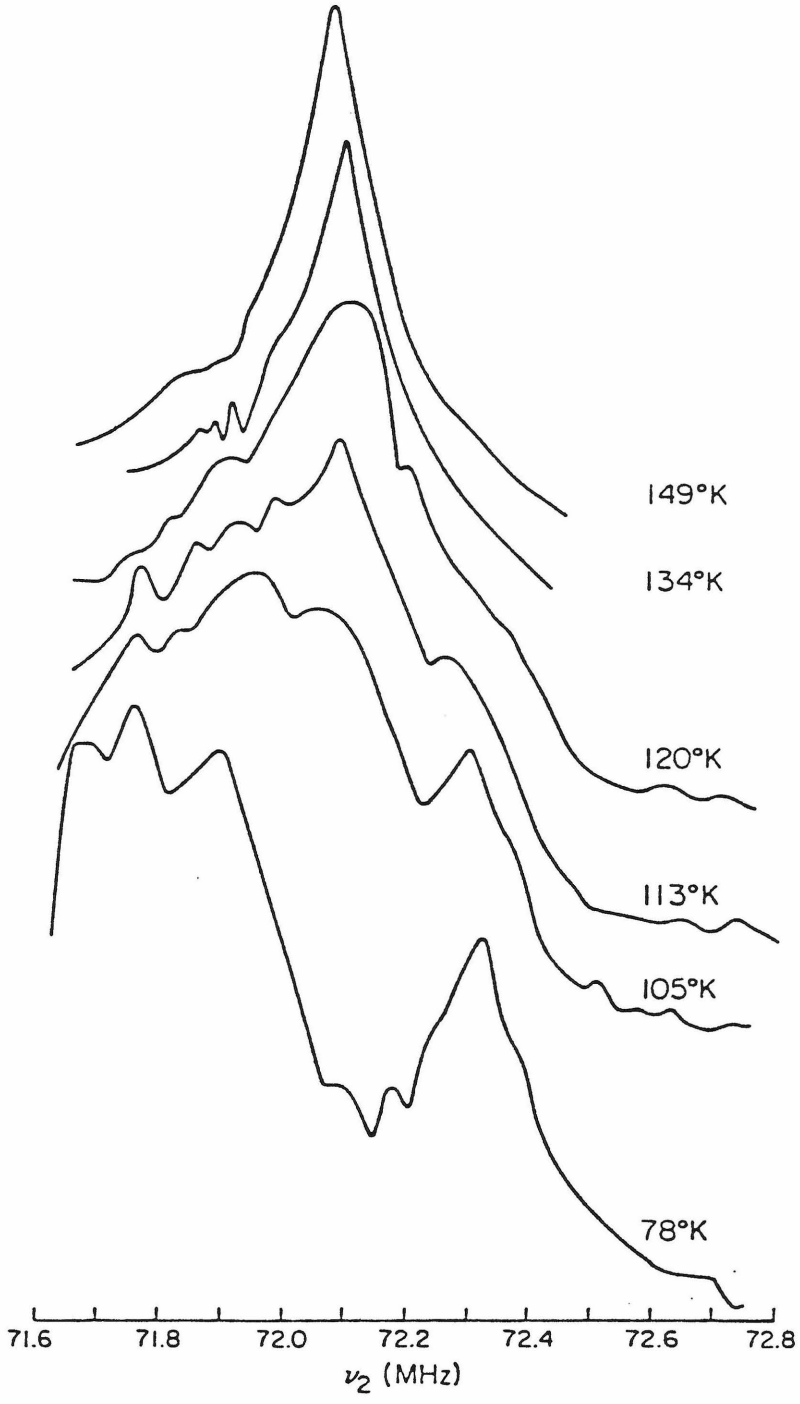
149°K
134°K
120°K
113°K
105°K
78°K
71.6
71.8
72.0
72.2
72.4
72.6
72.8
ν_2 (MHz)

performing the average of the original frequencies weighted by the known relative site populations. The final frequency resulting from the first averaging process indicates that the intensity of the original peaks is 2:1. This is consistent with the motion of sodium ions among the three displaced sites, where two of the three components of the tensor produce identical shifts. The second process indicates that averaging of two populations in the ratio of approximately 3 or 4 to 1 is occurring. The second process is slightly more complicated in that the BR components are averaging with an observable peak which consists of only two components of the MO tensor. The third MO tensor component is not observable since its predicted frequency lies near the frequency of the BR average, but it serves to weight the population of the BR site. Using the population ratio obtained from the neutron diffraction for BR:MO of 2:1, the predicted average occurs at 3.5:1, in agreement with the observed final average.

In theory, such motional information as outlined above is available from spectra obtained at all orientations. In practice, resolution of the individual satellites remains the predominant limitation. However, plots of satellite positions versus temperature for a few favorable orientations of the two samples appear in Figures 7 and 8.

The coalescence of individual satellites due to exchange between sites occurs when the rate of motion of sodium between such sites is equal to the inverse of the separation

Figure 7

Plotted are the indirectly detected ^{23}Na satellite shifts measured relative to the central transition versus temperature for the 0^{o} (circles), 30^{o} (triangles), and 90^{o} (squares) orientations of a single crystal β-alumina sample rotated about the $[10\bar{1}0]$ axis.

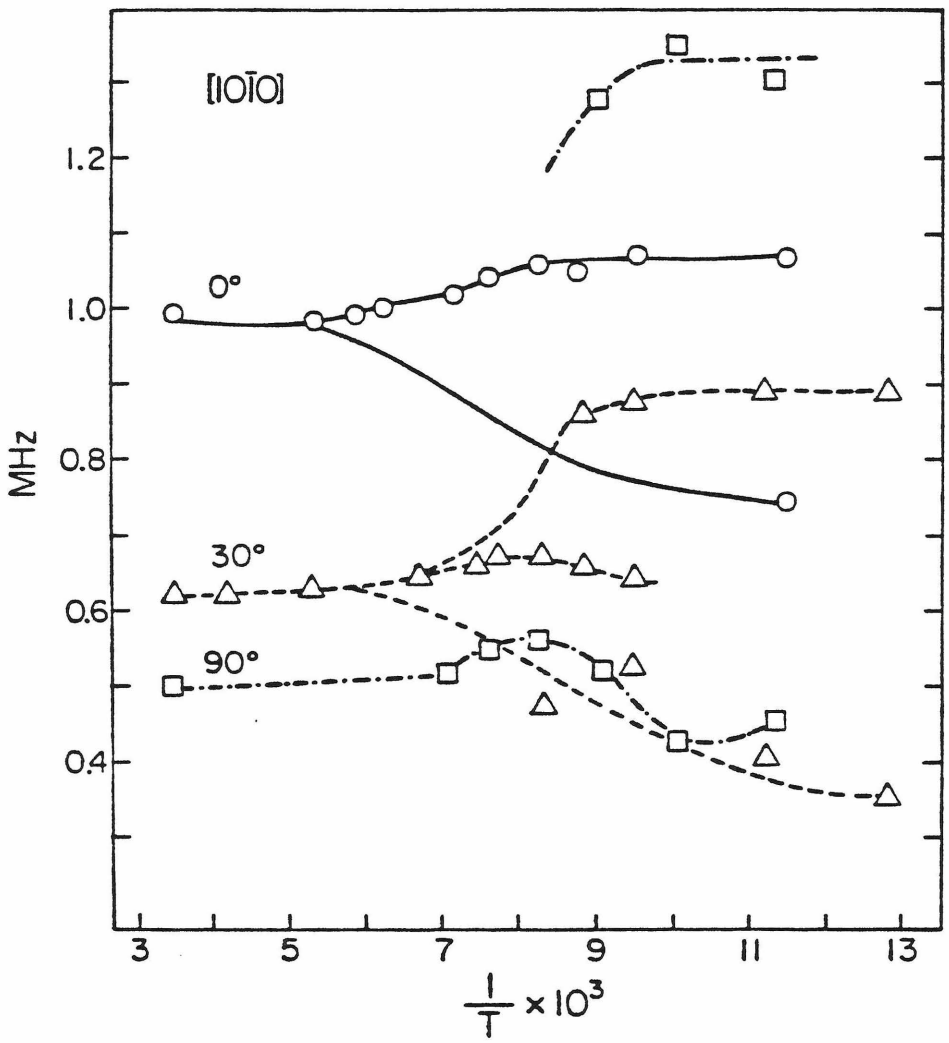
[10$\bar{1}$0]
0°
30°
90°
MHz
1.2
1.0
0.8
0.6
0.4
3
5
7
9
11
13
$\frac{1}{T} \times 10^3$

Figure 8

Plotted are the indirectly detected ^{23}Na satellite shifts measured relative to the central transition versus inverse temperature for the 0^{o} (circles) and 30^{o} (triangles) orientations of a single crystal β-alumina sample rotated about the $[11\bar{2}0]$ axis. Notice that data for the 0^{o} orientation are plotted using the scale at the left of the figure and data for the 30^{o} orientation plotted using the scale at the right of the figure.

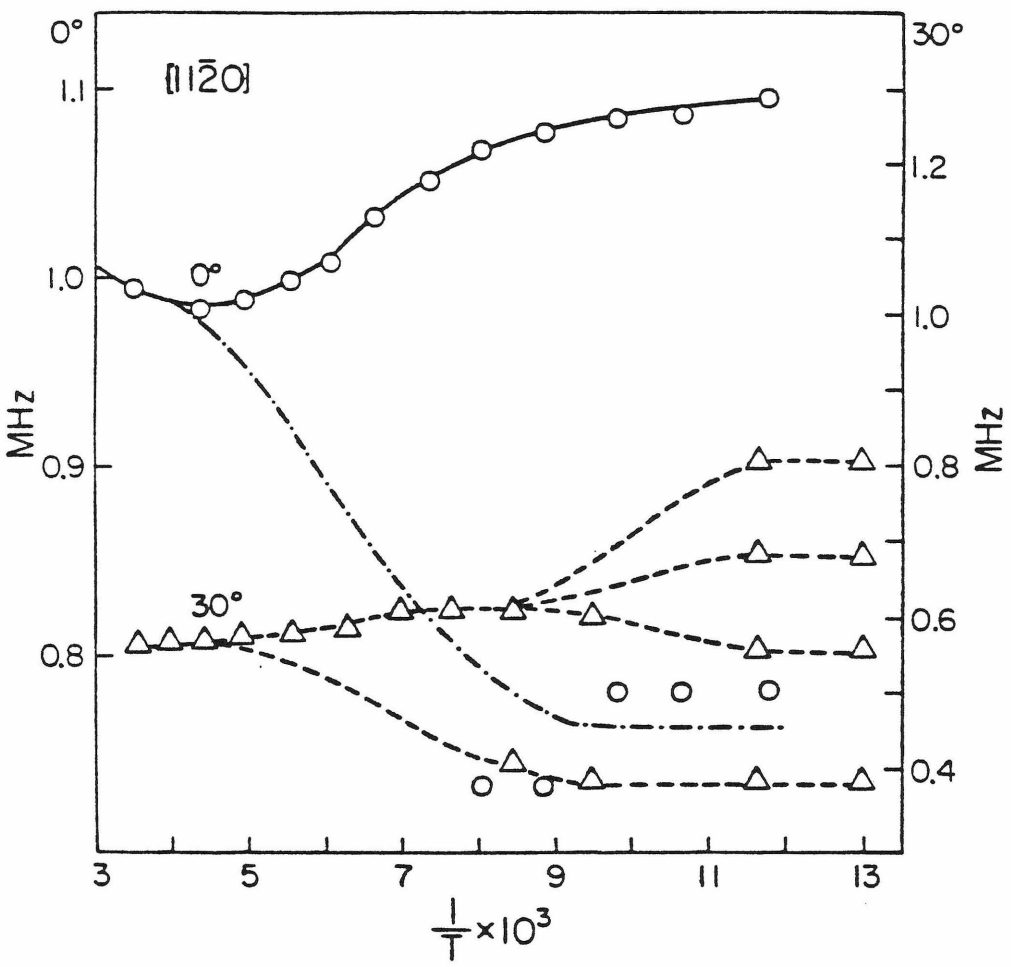
0°
[11$\bar{2}$0]
30°
1.1
1.2
1.0
1.0
0°
MHz
0.9
0.8
MHz
30°
0.8
0.6
0.4
3
5
7
9
11
13
$\frac{1}{T}\times10^3$

between the corresponding satellite frequencies[16]. For the two processes already outlined, these rates and their respective temperatures are 2.3×10^6 sec^{-1} at 120 K and 1.6×10^6 sec^{-1} at 146 K. Observation of the coalescence at other crystal orientations allows the determination of hopping rates at various temperatures. For an activated process, the logarithm of the rate plotted versus the inverse temperature will give a line whose slope is the activation energy barrier for the observed motion. The activation energy barrier associated with the localized BR motion is determined in Figure 9, where $\ln\tau$ (τ = $rate^{-1}$) is plotted versus the inverse temperature. The very low value of 0.04 eV for the activation energy is considerably smaller than that observed for diffusion of sodium ions in β-alumina (0.17 eV), confirming that the process which averages the displaced BR sites is associated with a local motion. This process, then, provides the first explicit demonstration that local motions exist in β-alumina.

Similarly, the activation energy for the barrier between BR and MO sites can be obtained. However, the necessary variation of τ's needed to obtain an activation energy plot is restricted by the degree of satellite broadening and overlap. The maximum τ observable, determined by the maximum difference between the BR and MO quadrupole splittings, is also the lower limit due to the experimental resolution. Therefore, the available τ's for the BR-MO motion are approximately all of the same value. However, the averaged satellite width will undergo exchange narrowing when the rate of motion of the sodium ions is fast compared to the

Figure 9

Activation energy (0.04 eV) for the barrier to sodium motion among the three symmetry-related displaced BR sites. Plotted are $\ln(\tau)$ values versus inverse temperature. The parameter τ (equal to the inverse rate of sodium motion between sites) is obtained from interpretation of the collapse of satellite structure with increasing temperature as shown in Figures 7 and 8.

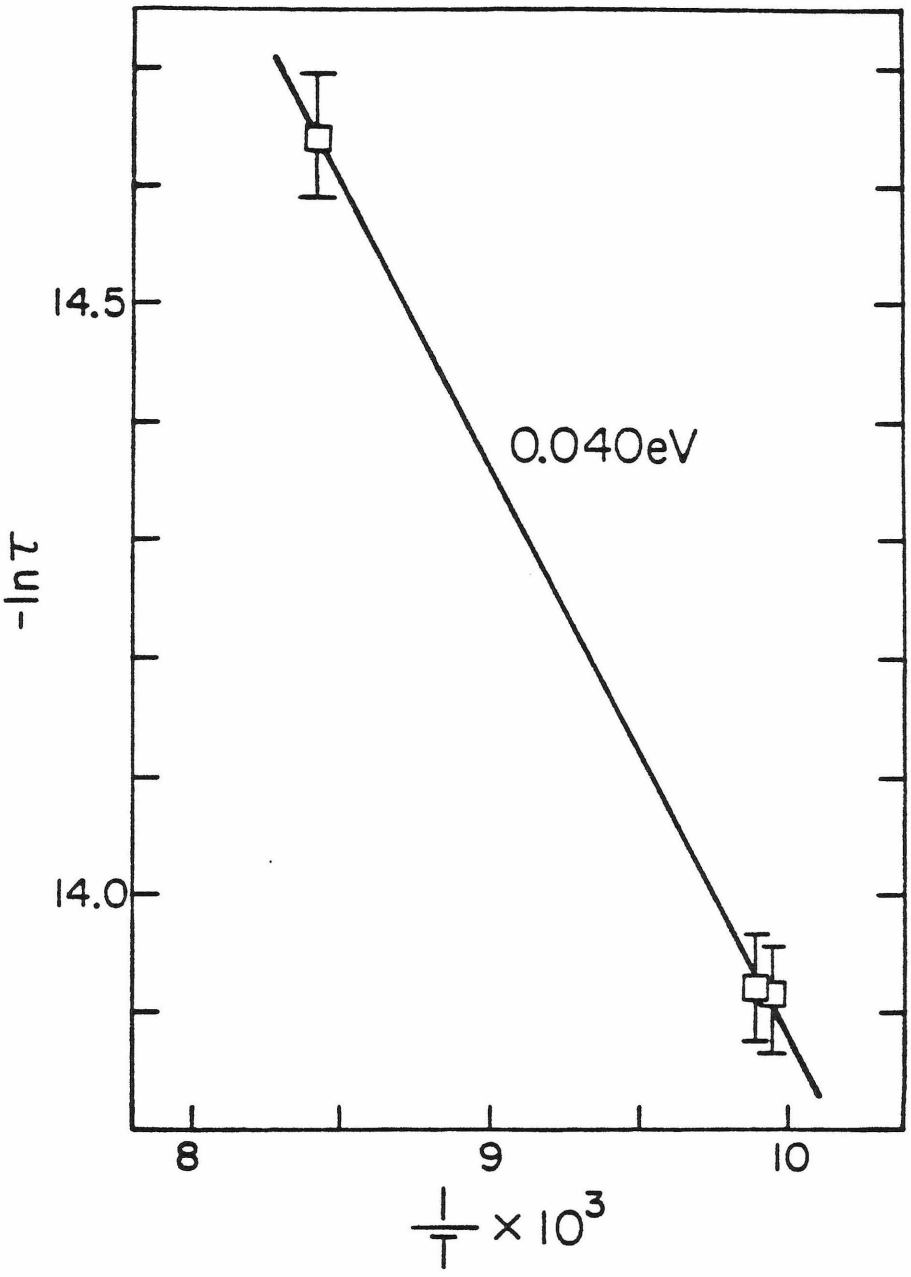
14.5
14.0
-ln τ
0.040eV
8
9
10
1/T × 10³

inverse satellite linewidth. Presumably, averaging of the distribution of EFG's arising from the distribution of BR and MO environments will occur by the same process which allows for the rapid interchange of sodium ions on BR and MO sites. A plot of $\ln\Delta\nu_{1/2}$, where $\Delta\nu_{1/2}$ is the full width at half maximum intensity of the satellite linewidth, versus inverse temperature (Figure 10), gives an activation energy for the process which narrows the satellite of 0.078 eV. Notice that this value for the activation energy is still too low to be the one which limits the diffusion process, although it might be expected that a process which allows sodium ions on BR and MO sites to interchange would be linked to the diffusion mechanism.

Evidence of yet another activated process which might be attributed to long-range diffusion can be seen in Figure 8. The frequency of the narrowed satellite at the 0^{o} orientation is seen to increase slightly at the highest temperature. This is possibly due to sodium ions encountering a higher EFG as they pass through the crystal. This is likely if the sodium ion diffuses past the charge-compensating oxygen defect in the conduction plane, which would be expected to present a large EFG. Unfortunately, the data do not extend up beyond room temperature where this process could be observed in greater detail.

4. Comparisons with Other NMR Data and a Theory of Motion. The majority of the published NMR results on β-alumina[7-10,12,13] involve the measurement of the relaxa-

Figure 10

Activation energy (0.08 eV) for the barrier to sodium motion among BR and MO sites. Plotted is $\ln\Delta\nu_{1/2}$ versus inverse temperature where $\Delta\nu_{1/2}$ is the full width at half maximum intensity of the satellite linewidth in a β-alumina single crystal oriented at 0^{o} (applied magnetic field is parallel to crystal c axis).

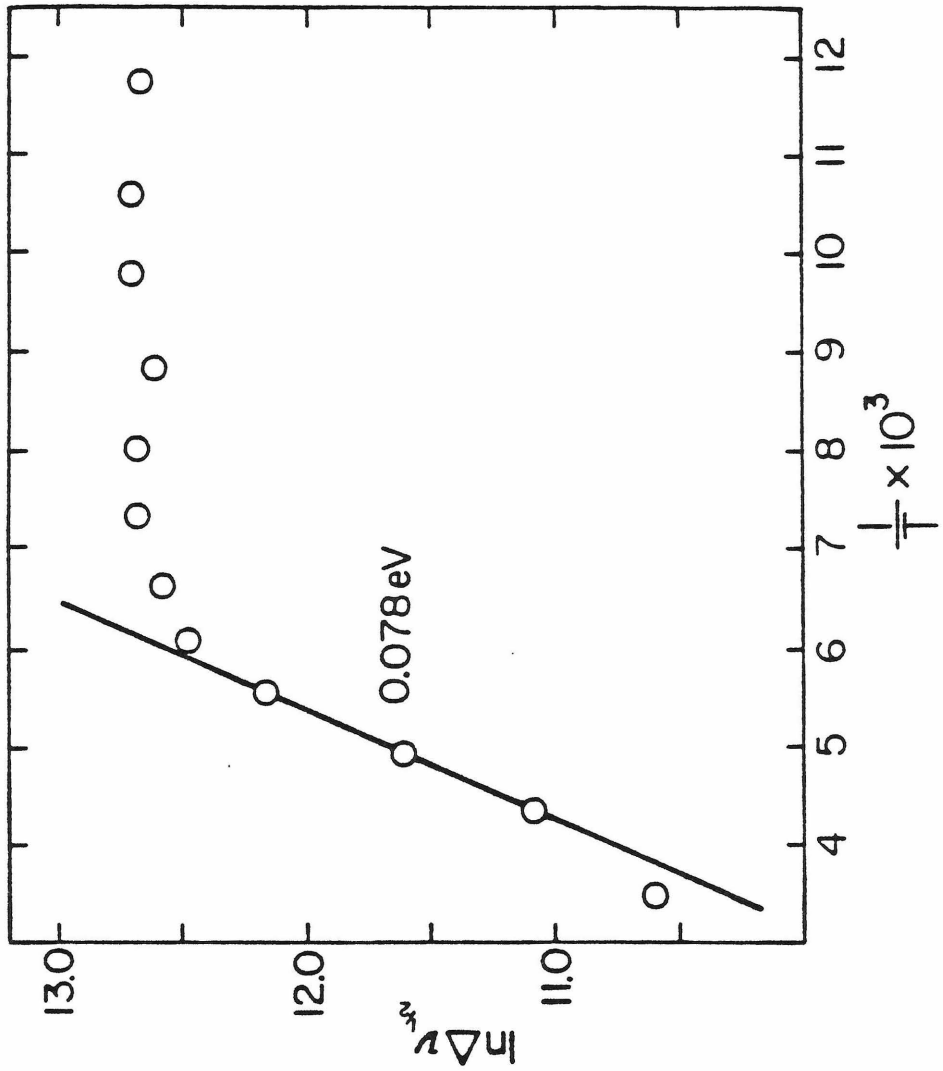
13.0
12.0
11.0
$\ln \Delta \nu_{\frac{1}{2}}$
0.078eV
4
5
6
7
8
9
10
11
12
$\frac{1}{T} \times 10^3$

tion times T_1 (spin-lattice) and T_2 (inverse line width) which provide information on the frequency distribution of motional correlation times.[17] Table 4 summarizes some of the values reported for observed activation energies. The T_1 data of Jerome and Boilot[12] and Walstedt et al.[13] have values which correspond to the measured activation energy obtained by conductivity (0.164 eV)[4] or tracer diffusion (0.165 eV)[3]. What is believed by Chung et al.[8] to be a line-narrowing mechanism is argued by Bailey et al.[10] to be a result of lifetime-broadening effects on the linewidth and is therefore a measurement of T_1, but this also agrees with the accepted value of the activation energy for the diffusion of sodium in β-alumina. Bailey et al. observe a true motional narrowing of the central transition which provides a measured activation energy of 0.08 eV, which is approximately the smaller value obtained by Jerome and Boilot from measurements of T_1. Although none of these reported activation energies is close to the 0.04 eV value observed in this study, the 0.1 eV of Jerome and Boilot and the 0.08 eV of Bailey et al. are close to the 0.078 eV value observed for the motional narrowing of the satellite line. Apparently, then, the results on the satellite line shapes of this work which have allowed the details of a local motion to be determined complement the relaxation results which appear to be more sensitive to processes which involve intermediate and long range motions.

Table 4: Reported values for the activation energies in sodium β-alumina obtained by NMR relaxation studies.

Reference	Activation Energy (eV)		Source
Jerome and Boilot[12]	0.1, 0.2		T_1
Chung et al.[8]	0.17		T_2 (T_1)
Bailey et al.[10]	0.08		T_2
Walstedt et al.[13]	Distribution:		
	Mean	Width	
	0.134	0.045	T_1
	0.150	0.064	

However, neither this work nor the NMR relaxation studies have been able to uncover the details of motion responsible for the two observed activation energies which are approximately 0.08 eV and 0.17 eV. The hope of relating the nature of additional motional processes to these activation energies may come from a better understanding of the interactions which govern relaxation. As it stands now, a rather phenomenological theory introduced by Bloembergen, Purcell and Pound (BPP)[18] is used to explain the relaxation data. Although this theory is generally successful in describing relaxation behavior due to motion, it does not account for all the features observed for relaxation in β-alumina. Briefly, the BPP theory predicts a V-shaped curve for the plot of ln T_1 versus the inverse temperature. The slopes of the sides of this curve give the activation energy associated with the motion and should be equal. Additionally, the minimum of this curve provides the correlation time for motion. In contrast to this prediction, all T_1 curves obtained for β-alumina are characterized by unequal slopes for the high- and low-temperature sides, and these slopes are used to obtain activation energies. Walstedt et al. recognize this problem and attempt to reconcile the observed T_1 behavior within the BPP model by introducing a distribution of barrier heights and report their calculated values for the mean and width for the distribution. The two sets of values listed in Table 4 are the distributions obtained by fitting the T_1 data for two

different samples. Although the idea of a distribution of activation energy barriers is attractive because of the great deal of disorder present in β-alumina, until a less phenomenological theory is developed, this approach may also indicate the degree of latitude available in interpreting T_1 relaxation data in β-alumina.

The combined NMR results indicate the presence of three activation energies which are 0.04 eV, 0.08 eV and 0.17 eV. The 0.04 eV activation energy has been shown in this work to correspond to the local motion around the BR site. However, no explanation has been given for why the displacement of sodium ions should occur and what process causes them to average with the same energy of activation. An interesting theory of the motion of sodium in β-alumina by Wolf[19] may not only provide an explanation for the BR motional process, but provide an explanation for the remaining activation energies as well.

The theory of Wolf proposes the existence of "associated" regions in β-alumina which result from the tendency of the excess sodium ions to cluster about the counter-charge oxygen defects located in the conduction plane. At sufficiently low temperatures, all excess sodium ions are located in the associated regions as MO-MO pairs, but as the temperature is raised, the size of these associated regions decreases with an ever-increasing number of sodium ions participating in the conduction process. This model explains the temperature dependence of the Haven ratio

measurements[20] which indicate that the number of charge carriers (sodium ions) increases with increasing temperature. Fitting this model to the Haven ratio data, Wolf predicts the existence of several activated processes, two of which are important for the interpretation of the NMR results of this work.

The occurrence of the excess sodium ions as MO-MO pairs is generally accepted[1]. Figure 11a displays how the electrostatic repulsions between the MO-MO pair and nearby sodium ions centered on BR sites causes the four nearest-neighbor BR sodium ions to be displaced away from the MO-MO pair. Wolf's model assumes that for motion to occur, the first process must involve creation of a mobile "interstitial" (aBR) from the MO-MO pair. This is shown in Figure 11b as the MO-MO pair becomes an interstitialcy BR-aBR pair. The interstitial may proceed to another MO site and become a MO-MO pair along the directions marked 1,2, or 3 or return to its orignal position along 4. Notice that this motion causes the sodium BR sites to be displaced depending on the position of the MO-MO pair. The creation of the interstitialcy pair (MO-MO $\longrightarrow$ BR-aBR) allows for the motion of sodium around the displaced sites and the averaging of this site should be dependent on the formation energy of interstitials. Wolf defines this activation energy as the enthalpy of interstitial formation and calculates a value between 0.04 eV and 0.05 eV which agrees well with the activation energy for motion found for the BR site

Figure 11

Displaced BR positions and interstitial formation. (a) A pair of sodium ions are located in a MO-MO configuration and local displacement occurs for two sets of sodium ions in the nearest-neighbor BR positions. (b) Interstitialcy pair (BR-aBR) formation from the MO-MO configuration in (a). Arrows labeled 1-4 indicate the possible jump paths back to a MO-MO configuration. (c) A new MO-MO pair is formed from (b) and local displacement occurs for two other sets of sodium ions in the nearest-neighbor BR positions.

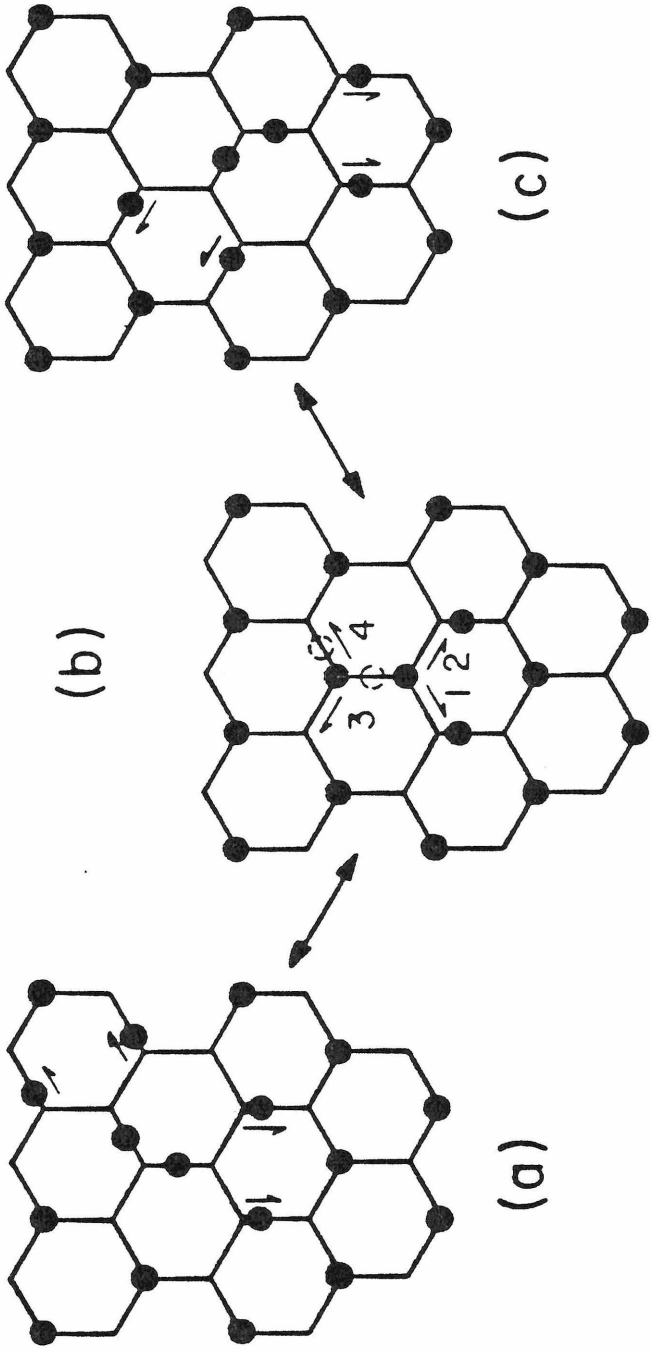
(a)
(b)
(c)
1
2
3
4

averaging process in this work (0.04 eV). It is also necessary that most of the sodium ions should be similarly displaced. Since there are approximately four sodium atoms in BR positions for every MO-MO pair, there are, indeed, enough MO-MO pairs to displace all sodium ions occupying BR positions.

Another major assumption of Wolf's theory is that the size of the associated regions is temperature dependent. Diffuse x-ray scattering[21] supports this assumption and shows temperature-dependent local ordering of sodium ions at low temperatures. Wolf's predicted value for the enthalpy of migration out of these associated regions is 0.07 eV to 0.10 eV. It is quite remarkable that the activation energy observed for the motion necessary to average the MO and BR sites (0.08 eV) falls in this range, in agreement with Wolf's model. Finally, at higher temperatures, where T_1 relaxation data measure an activation energy of 0.17 eV, the sodium ions are no longer bound to the associated regions and the same barriers to long range motion responsible for the observed activation energy in the conductivity data should influence the T_1 relaxation rate.

References

1. (a) Van Gool, W., Ed. (1973), "Fast Ion Transport in Solids", Plenum Press, New York. (b) Mahan, G.D. and Roth, W.L., Eds. (1976), "Superionic Conductors", Plenum Press, New York. (c) Geller, S., Ed. (1977), "Solid Electrolytes", Top. Appl. Phys., V. 21, Springer-Verlag, Berlin, Heidelberg, New York. (d) Salamon, M.B., Ed. (1979), "Physics of Superionic Conductors", Top. Current Phys., V. 15, Springer-Verlag, Berlin, Heidelberg, New York. (e) Vashishta, P., Mundy, J.N. and Shenoy, G.K., Eds. (1979), "Fast Ion Transport in Solids-Electrodes and Electrolytes", North-Holland, New York, Amsterdam, Oxford.
2. Kummer, J.T. (1972), Progr. Solid State Chem. 7, 141.
3. Yao, Y.-F.Y. and Kummer, J.T. (1967), J. Inorg. Nucl. Chem. 29, 2453.
4. Whittingham, M.S. and Huggins, R.A. (1971), J. Chem. Phys. 54, 414.
5. Whittingham, M.S. and Huggins, R.A. (1971), J. Electrochem. Soc. 118, 1.
6. Strom, U., Taylor, P.C. and Bishop, S.G. (1975), Bull. Am. Phys. Soc. 20, 330.
7. Kline, D., Story, H.S. and Roth, W.L. (1972), J. Chem. Phys. 57, 5180.
8. Chung, I., Story, H.S. and Roth, W.L. (1975), J. Chem. Phys. 63, 4903.
9. Boilot, J.P., Zuppiroli, L., Delplanque, G. and Jerome,

L. (1975), Philos. Mag. 32, 343.

10. Bailey, W., Glowinkowski, S., Story, H.S. and Roth, W.L. (1976), J. Chem. Phys. 64, 4126.
11. West, L.C., Cole, T. and Vaughan, R.W. (1978), J. Chem. Phys. 68, 2710.
12. Jerome, D. and Boilot, J. P. (1974), J. Phys. Lett. (Paris) 35, L-129.
13. Walstedt, R.E., Dupree, R., Remeika, J.P. and Rodriguez, A. (1977), Phys. Rev. B 15, 3442.
14. Roth, W.L., Reidinger, F. and La Placa, S. in ref. 1(b), p. 223.
15. Reidinger, F. (1979), Ph.D. thesis, State Univ. of New York at Albany.
16. For a general discussion of motional-narrowing, see, for example: Pople, J.A., Schneider, W.G. and Bernstein, H.J. (1959), "High-Resolution Nuclear Magnetic Resonance", McGraw-Hill, New York, Toronto, London, Chap. 10.
17. For a general discussion of NMR concepts, see, for example: Abragam, A. (1961), "The Principles of Nuclear Magnetism", Oxford University Press, London.
18. Bloembergen, N., Purcell, E.M. and Pound, R.V. (1948), Phys. Rev. 73, 679.
19. Wolf, D. (1979), J. Phys. & Chem. Solids (GB), 40, 757.
20. Kim, K.K., Chen, W.K. and Mundy, J.N. (1979), J. Phys. & Chem. Solids (GB) 40, 743.
21. Boilot, J.P., Collin, G., Comes, R., Thery, J., Collongues, R. and Guinier, A., in ref. 1(b), p.243.

CHAPTER IV: LITHIUM AND MIXED LITHIUM-SODIUM β-ALUMINA

A. INTRODUCTION

It has long been known that various alkali cations can be readily exchanged for the sodium ions in β-alumina.[1] However, despite the attractiveness of using lithium in an electrochemical cell, interest in the lithium substituted β-alumina has been limited. In large measure, the neglect of lithium β-alumina has been because its ionic conductivity was generally believed to be considerbly lower than that of sodium β-alumina.[2,3] A surge of interest in lithium-exchanged β-alumina developed when Roth and Farrington[4,5] observed that the conductivity in a β-alumina sample where the sodium/lithium ratio was approximately 1:1 was higher than had been reported for the pure lithium β-alumina. They proposed the existence of "coionic conduction" where the mobility of the lithium ions was greatly enhanced by the presence of sodium. The coionic effect is now known not to occur. Conductivity measurements on carefully dried lithium-exchanged β-alumina samples have established that the pure lithium β-alumina has the highest conductivity and that the earliest measurements were in error.[6] However, studies on mixed-alkali β-aluminas are revealing new features about the interactions among the mobile cations and the host structure.[7]

This work presents results for the NMR investigation of (i) the character and occupation of sites (structure) of pure lithium β-alumina, (ii) the site occupation of cations versus the degree of lithium exchange, and (iii) the mobility

of the lithium of the ions versus the degree of lithium exchange. In addition, the results of the investigations (ii) and (iii) are interpreted with the aid of a theory developed for explaining the "mixed-alkali effect" observed in glasses.[8]

B. EXPERIMENTAL

1. NMR Parameters. Direct observation of the entire ^{7}Li spectrum (central and satellite transitions) is possible in lithium β-alumina. All spectra are referenced to a standard LiCl aqueous solution for which the 90° pulse length is 4.5 μsec with a pulse magnitude (H_1) of approximately 55 kHz (33 Gauss). The FID's immediately following a succession of 2 μsec pulses are coadded to improve the ratio of signal-to-noise and the result is Fourier-transformed to produce the absorption spectrum from which peak positions and widths are obtained.

2. Presence and Influence of H_2O. Yao and Kummer[1] were the first investigators to report that lithium-exchanged β-alumina is hydroscopic even in single crystal form. However, it is now recognized that as-exchanged samples of lithium β-alumina contain H_2O which enters the crystal during the exchange process itself.[9] Presumably, H_2O is strongly coordinated with the molten salt even at temperatures greater than 350°C and accompanies lithium as it diffuses into the β-alumina structure. Figures 1a and 1b show the IR region between 2500 cm^{-1} and 4000 cm^{-1} for an 80% lithium-exchanged β-alumina taken with a conventional Perkin-Elmer #257 Grating Infrared Spectrophotometer. The broad peak at

Figure 1

Infrared transmission spectra at room temperature of an 80% lithium-exchanged β-alumina single crystal. (a) Spectrum taken on the as-exchanged sample. (b) Spectrum taken on the same sample heated at 500°C for 11 hours.

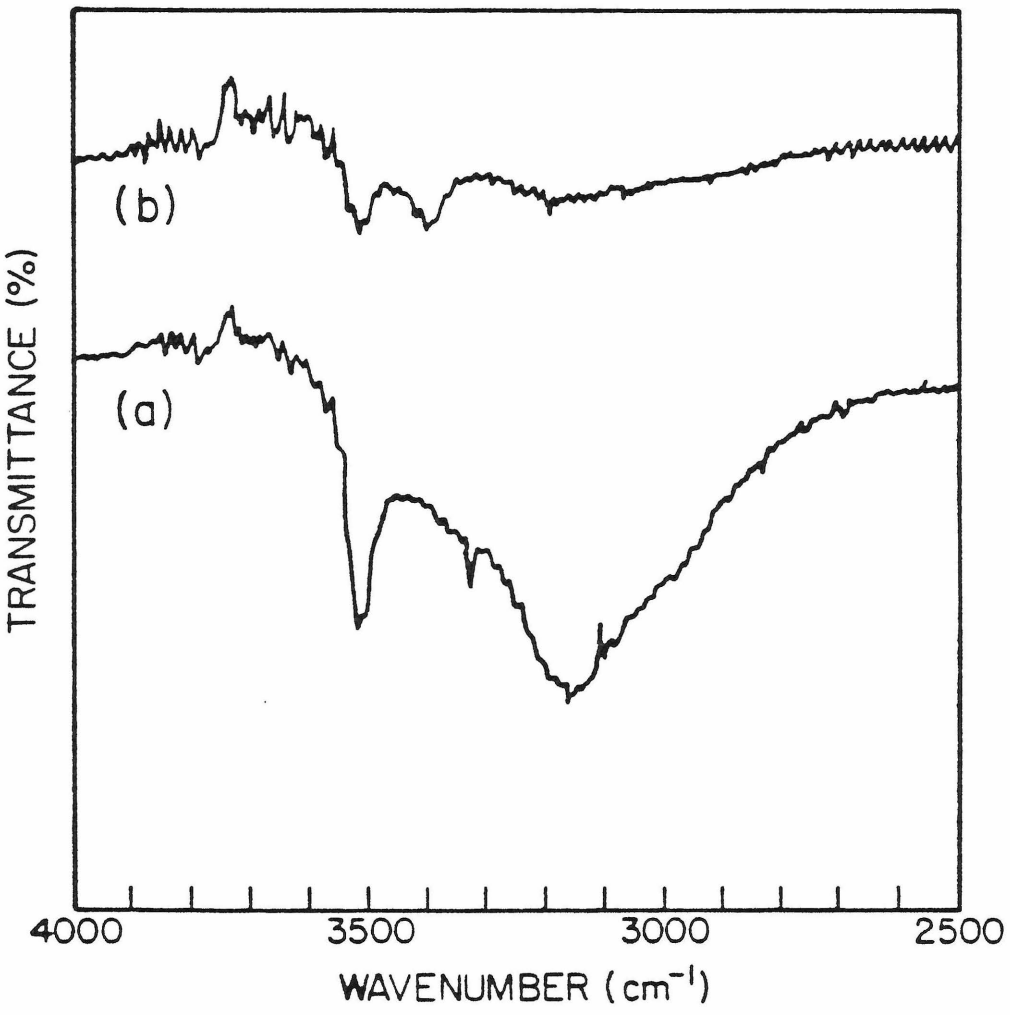
(b)
(a)
TRANSMITTANCE (%)
4000
3500
3000
2500
WAVENUMBER (cm⁻¹)

3150 cm^{-1} and the sharp peaks at 3510 cm^{-1} and 3400 cm^{-1} are attributed to stretches of H_2O molecules in the β-alumina material, as confirmed by the reduction of intensity observed in the IR spectrum taken on the sample heated at 500°C for 11 hours. (Shown in Figure 1b). With further heating, all of the peaks due to water can be made to disappear. The amount of water present, determined by the weight difference between the as-exchanged sample and the thoroughly dried sample, is less than 0.1 weight percent.

A study of the presence of H_2O in lithium-exchanged β-aluminas by Bates et al.[9] reports the observation of a broad peak at 3194 cm^{-1}, and sharp peaks at 3406 cm^{-1} and 3518 cm^{-1} in IR spectra of as-exchanged lithium β-alumina samples, which are close to the peak positions observed in this study. Bates et al. assign these peaks to the anti-symmetric (ν_3) stretching mode of the H_2O molecule in the conduction plane of β-alumina. From their analysis of the intensity and shape of the IR bands, they conclude that the H_2O is coordinated with the alkali-metal cations. In addition, they observe that the intensities of the three IR components show independent variations versus the degree of lithium exchange and heat treatment and conclude that the three peaks arise from H_2O occupying three different sites. The model of Bates et al. for the location of the H_2O molecule in β-alumina places it in an unoccupied MO position. The H_2O molecule may be coordinated with a pair of lithium ions which occupy the two closest MO positions

or, alternatively, a triangle of H_2O molecules in MO positions may surround a lithium ion which occupies a BR position. In both of these configurations, it is proposed that the hydrogen atoms are directed away from the BR site toward the aBR site and that hydrogen bonding with the close-packed oxygen atoms above and below the conduction plane occurs.

The presence of a small amount of water has been shown to have a pronounced effect on the measured conductivity of lithium-exchanged β-alumina samples and has been used to explain the discrepancies between values measured by different investigators.[6] Carefully dried samples of lithium-exchanged β-aluminas exhibit a higher conductivity than those with small amounts of water present.

The presence of water also has a pronounced effect on NMR spectra. For example, a plot of the measured central transition linewidths versus temperature for an as-exchanged sample of β-alumina (50% lithium-exchanged) and for the same sample after it has been dried for several hours at 650°C is shown in Figure 2. Motional narrowing of the central transition in the as-exchanged sample occurs at a higher temperature. This increase in the line-narrowing temperature is not likely the result of an additional broadening mechanism due to the dipolar coupling of lithium and hydrogen nuclei since the amount of water present indicates that there are more than 20 lithium atoms for every hydrogen atom. The reason for the increase in the line-

Figure 2

Measured ^{7}Li central transition linewidths ($\Delta\nu_{1/2}$ = full width at half maximum intensity) versus temperature for a 50% lithium-exchanged β-alumina single crystal oriented with the magnetic field parallel to the crystal c axis. Circles are for the as-exchanged sample and squares are for the same sample heated at 650°C for several hours.

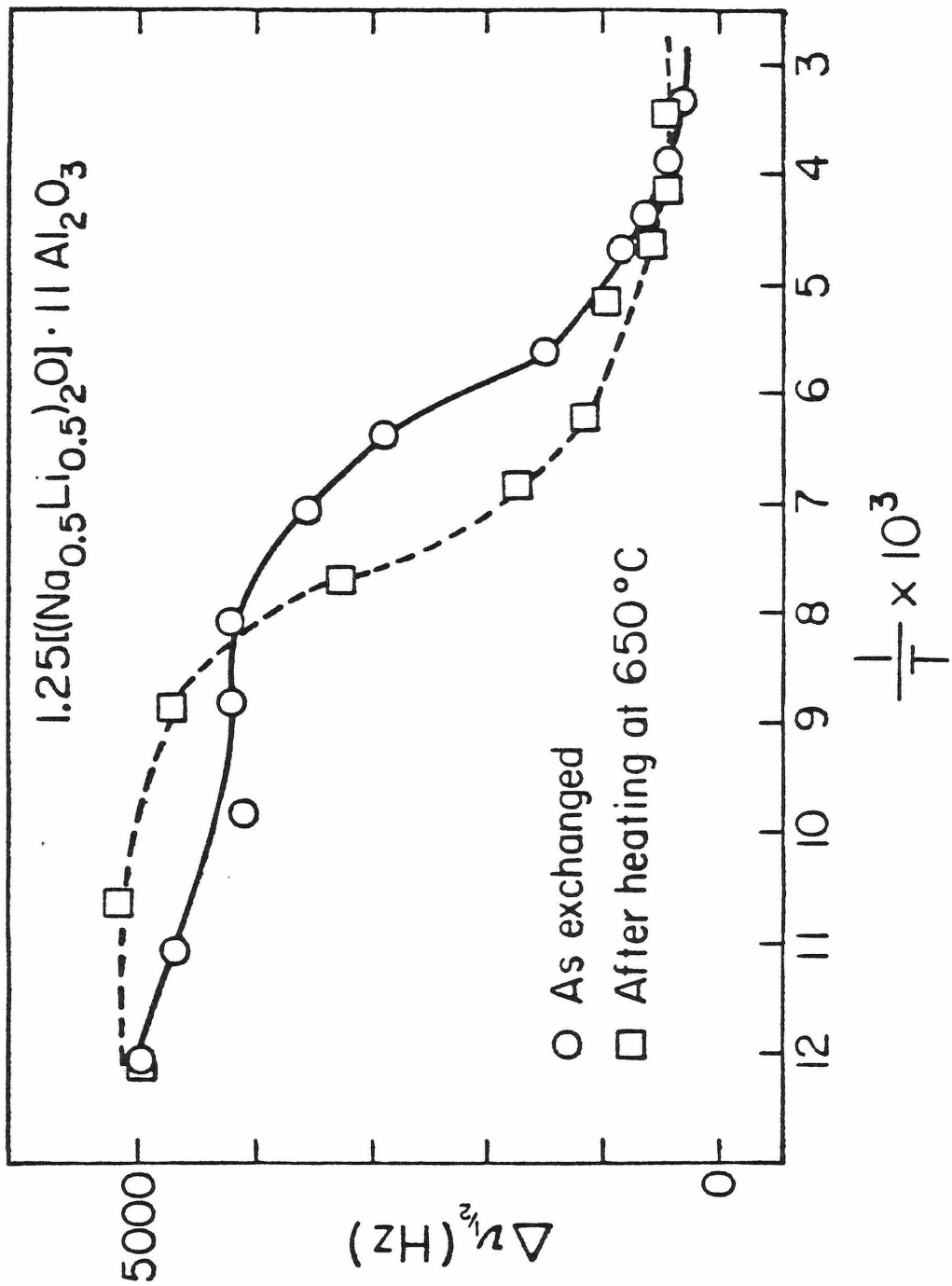
1.25[(Na0.5Li0.5)2O]·11 Al2O3
5000
0
Δν1/2 (Hz)
O As exchanged
□ After heating at 650°C
12 11 10 9 8 7 6 5 4 3
1/T × 10³

narrowing temperature must be that water is severely restricting lithium ion motion. Additionally, the presence of small amounts of water greatly influences the distribution of lithium ions among the BR and MO sites at both low and high temperatures. It may be that the water molecules behave much like the oxygen defects in the conduction plane and contribute to blockage of conduction pathways and create additional associated regions.

The fact that such a small amount of water drastically affects the distribution of lithium ions among the BR and MO sites raises the question of whether small differences in the oxygen defect distribution in different samples similarly affects the distribution of lithium ions among the BR and MO sites. Carefully dried samples with the same degree of lithium exchange do show variations in the lithium ion occupancies of BR and MO sites. Therefore, measurements which seek to reveal trends versus the degree of lithium exchange must use the same sample, continually re-exchanged, throughout. Consequently, results presented in subsequent sections which report values versus the degree of lithium exchange are obtained from measurements on a carefully dried sample which is re-exchanged and re-dried for each measurement at a different lithium exchange concentration.

C. RESULTS AND DISCUSSION

1. Room Temperature Results. The peak-to-peak satellite splittings for all lithium-exchanged β-alumina samples follow a single axially symmetric single-crystal rotation pattern

at room temperature, regardless of the degree of lithium exchange. The presence of only one set of satellites indicates that the lithium ions are undergoing rapid enough motion to average any site variations. Additionally, sodium spectra in the same samples indicate that the sodium ions are undergoing rapid motion as well. However, there is a clear dependence of the magnitude of the lithium satellite splittings versus the lithium exchange concentration. Since the rotation patterns are axially symmetric ($\eta=0$), the peak-to-peak satellite splittings observed when the applied magnetic field is parallel to the crystallographic c axis are exactly equal to the value of e^2qQ/h. The room-temperature values of e^2qQ/h versus lithium exchange content in β-alumina are plotted in Figure 3. The values of e^2qQ/h increase with increasing lithium content. In addition, however, even the largest of these values is far smaller than is expected considering the relative sizes of the quadrupole moments for sodium and lithium. The discrepancy between the expected and measured values indicates that the sites occupied by lithium ions are different from those occupied by sodium ions, and/or the relative occupations of the sites during the motional process vary as a function of lithium content.

2. The Static EFG's. To determine whether lithium occupies the same sites as sodium in β-alumina, low-temperature single crystal rotation data are used to observe and characterize the EFG's present. The following results

Figure 3

Room-temperature values of e^2qQ/h ($e^2qQ/h = \Delta\nu$ when magnetic field is parallel to crystal c axis) plotted versus lithium exchange content in β-alumina.

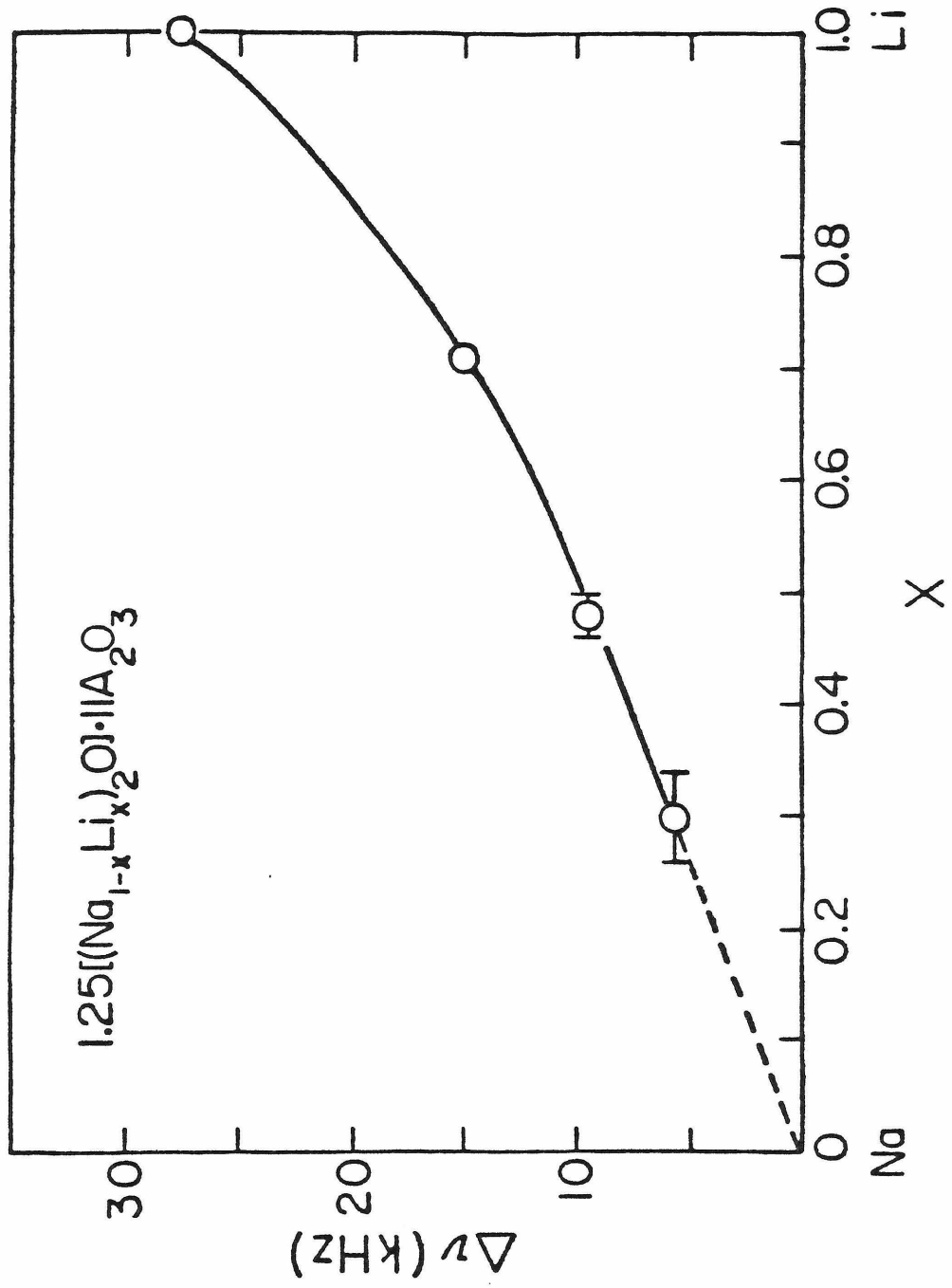
1.25[(Na1-xLix)2O]·11A2O3
Δν (kHz)
30
20
10
0
0.2
0.4
0.6
0.8
1.0
Na
Li
X

identify two dominant lithium sites, both of which (i) exhibit EFG's which are independent of lithium exchange concentration, (ii) show varying site occupations as a function of lithium exchange, and (iii) are different from those occupied by sodium in β-alumina.

Low temperature single crystal rotation data (at 85 K) for two samples, with 45% and 91% lithium exchange content, rotated about the $[10\bar{1}0]$ axis, are shown in Figure 4. Plotted are the shifts measured relative to the central transition for the symmetrically placed satellites as a function of orientation. The angle of rotation is the angle between the external magnetic field and the crystal c axis. Data for the two samples are superimposed in this figure to illustrate the similarities in their rotation patterns. Figure 5 displays the data for a 76% lithium-exchanged sample rotated about the $[11\bar{2}0]$ axis. In both figures, more than one line is observed for most orientations and the magnitudes of the splittings are considerably larger than the room temperature averaged values and are now consistent with expected values for lithium. Additionally, the fact that the data from the 45% and 91% lithium-exchanged samples exhibit splittings which, within experimental error, follow the same pattern, indicates that the nature of the lithium sites is independent of exchange concentration. This result follows without the need of fitting the data theoretically or assignment of specific sites.

The EFG tensor is specified by its magnitude, e^2qQ/h, its

Figure 4

Low temperature (85 K) single crystal rotation pattern for the ^{7}Li satellites in β-alumina obtained by rotation about the $[10\bar{1}0]$ axis. Plotted are the shifts measured relative to the central transition for the symmetrically placed satellites as a function of crystal orientation. The angle of rotation is the angle between the external magnetic field and the crystal c axis. Circles and squares correspond to a 45% and 91% lithium-exchanged β-alumina sample, respectively. A, B and C refer to the three tensors mentioned in the text.

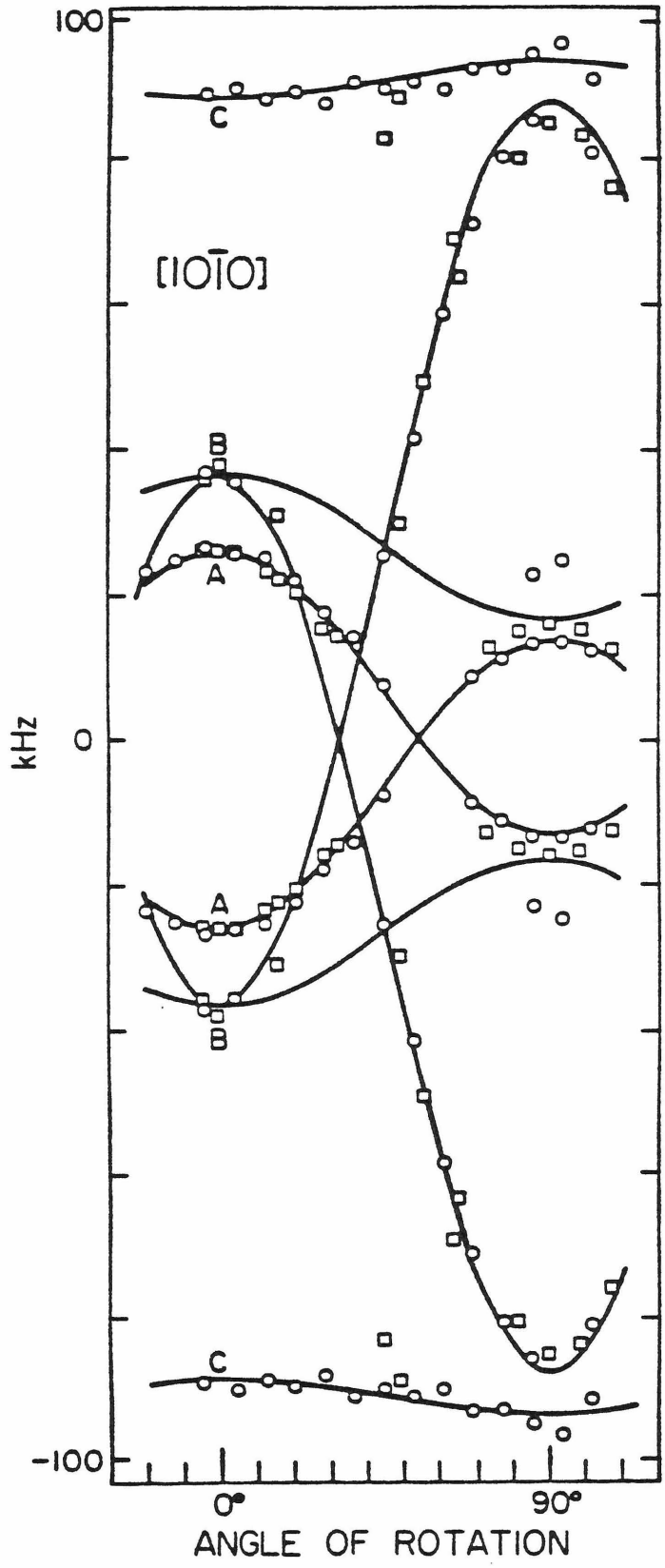
100
C
[10$\bar{1}$0]
B
A
kHz
0
A
B
C
-100
0°
90°
ANGLE OF ROTATION

Figure 5

Low temperature (85 K) single crystal rotation pattern for the ^{7}Li satellites in a 76% lithium-exchanged β-alumina sample obtained by rotation about the $[11\bar{2}0]$ axis. Plotted are the shifts measured relative to the central transition for the symmetrically placed satellites as a function of crystal orientation. The angle of rotation is the angle between the external magnetic field and the crystal c axis. A and B refer to the tensors mentioned in the text.

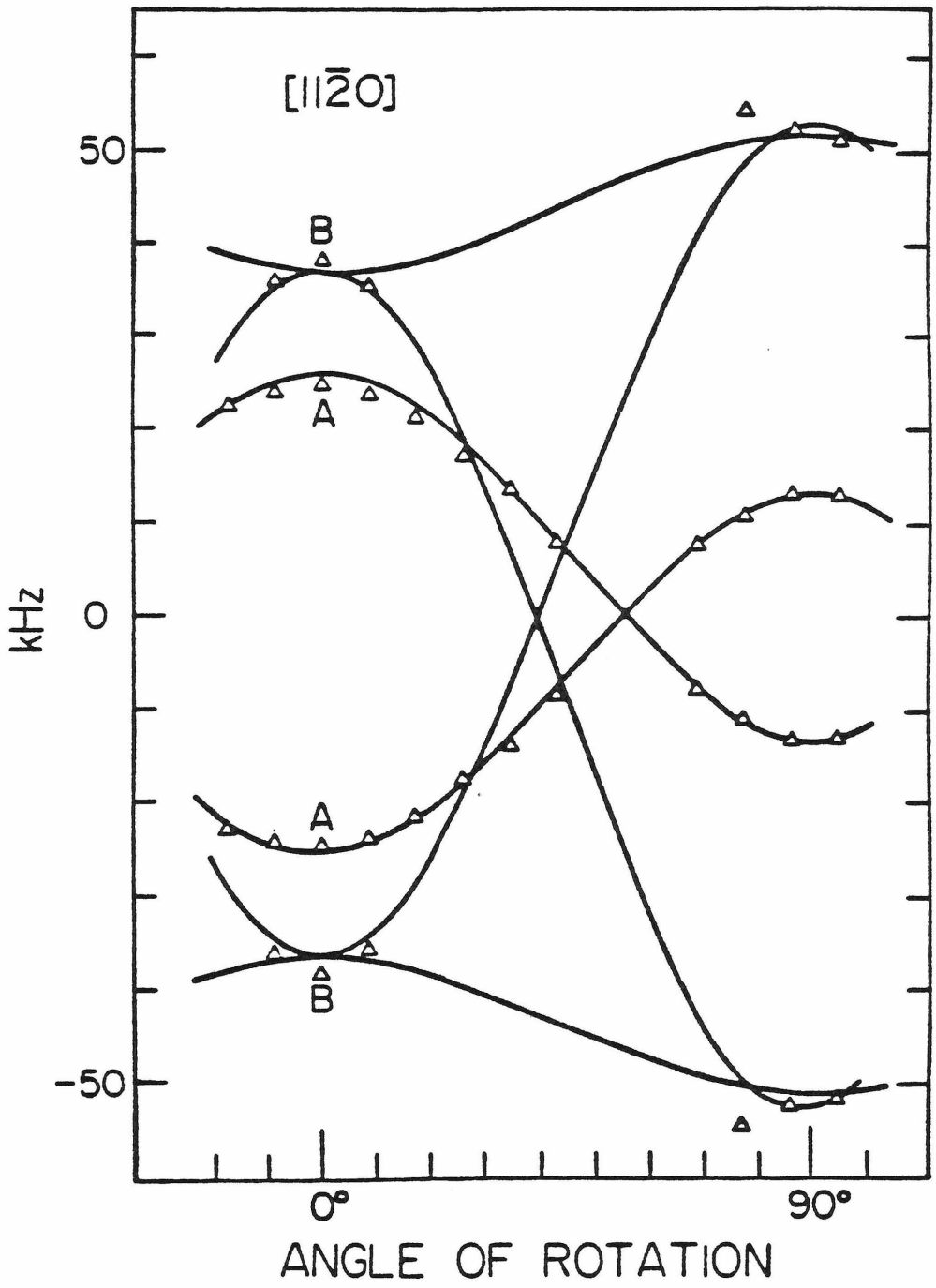
[11$\bar{2}$0]
50
0
-50
kHz
B
A
A
B
0°
90°
ANGLE OF ROTATION

asymmetry parameter, η, and the angles used to locate the principal axes in the crystallographic frame. Equation 1 in Chapter II relates these parameters to the peak-to-peak satellite splitting $\Delta\nu$. It is reasonable to attempt to fit the data with as few EFG tensors as possible, considering the relatively few possible sites in β-alumina. The majority of the data for both rotation axes can be fit with a minimum of two tensors, and a very weak line with little intensity is attributed to a third tensor. The values of e^2qQ/h, η, and the principal axes directions for the best fit are summarized in Table 1. The patterns generated by these tensors are shown as the lines A, B and C through the data in Figures 4 and 5.

The observed tensors can be compared with the characteristic tensors for the possible sites in β-alumina calculated using the following simple point-charge model. The components of the electric field ($F_{x,y,z}$) at a point (x_o,y_o,z_o) due to a point charge at (x,y,z) are given by the equations[10]

$$F_x = e(x-x_o)/r^3 \quad , \quad F_y = e(y-y_o)/r^3 \quad , \quad F_z = e(z-z_o)/r^3 \qquad (1)$$

where $r = \left[(x-x_o)^2 + (y-y_o)^2 + (z-z_o)^2\right]^{1/2}$. The components of the gradient of the electric field (Q_{xx}, Q_{yy}, Q_{zz}, Q_{xy}, etc.) are subsequently obtained by differentiation of Equation 1. For example,

$$Q_{xx} = \frac{-\delta F_x}{\delta x} \quad , \quad Q_{xy} = \frac{-\delta F_y}{\delta x} \quad , \quad \text{etc.} \qquad (2)$$

Table 1: Details of and assignments for the lithium tensors observed in β-alumina.

e^2qQ/h	η	V_{zz}	V_{yy}	V_{xx}	Assignment
53 ± 1 kHz	0.04 ± .07	c	a + 2a*	a	BR
178 ± 2 kHz	0.17 ± .02	a	a + 2a*	c	MO
367 ± 3 kHz	0.03 ± .01	a + 2a*	a	c	(?) Defect associated

are used to obtain the following relationships:

$$Q_{xx} = \frac{e}{r^3}\left\{\frac{3(x-x_o)^2}{r^2} - 1\right\}$$

$$Q_{yy} = \frac{e}{r^3}\left\{\frac{3(y-y_o)^2}{r^2} - 1\right\}$$

$$Q_{zz} = \frac{e}{r^3}\left\{\frac{3(z-z_o)^2}{r^2} - 1\right\} \qquad (3)$$

$$Q_{xy} = \frac{3e}{r^5}(x-x_o)(y-y_o)$$

$$Q_{xz} = \frac{3e}{r^5}(x-x_o)(z-z_o)$$

$$Q_{yz} = \frac{3e}{r^5}(y-y_o)(z-z_o)$$

The EFG components at a particular site (x_o,y_o,z_o) are then computed by performing a lattice sum over an extended volume until the sum converges. The EFG calculation for the various sites in β-alumina uses the atomic positions obtained by Peters et al.[11] and includes contributions from atoms within a sphere of 50 Å radius to ensure convergence. However, no corrections are made for electron polarizability, lattice relaxation, or long-range cation disorder. As such, the calculation is not expected to yield accurate values for the EFG tensors, but is rather used in a correlative fashion in identifying sites. The results of this calculation for selected sites is given in Table 2.

Table 2: Components of the electric field gradient tensor for selected sites in β-alumina.

Site[a]	Q_{zz}[b]	Q_{yy}	Q_{xx}	Q_{xy}	Q_{xz}	Q_{yz}
BR1 (Li)	-0.0779	0.0392	0.0392	0	0	0
BR2 (Na)	-0.0763	0.0696	0.0067	0	0	0
MO1 (Na)	-0.0360	0.0416	-0.0048	-0.0594	0	0
MO2 (Li)	0.2119	-0.2026	-0.0092	0	0	-0.0152

[a]BR1 is the centered BR position occupied by lithium.

BR2 is one of the three displaced BR positions occupied by sodium.

MO1 is one of the three centered MO positions occupied by sodium. The contribution from the other sodium ion in the MO pair is included.

MO2 is one of the two MO positions occupied by lithium which are displaced off the conduction plane by almost 1 Å.

[b]Q_{zz}, Q_{yy}, and Q_{xx} are the tensor components along the directions of the c, a + 2a*, and a axes, respectively.

One of the tensors (A) observed in lithium β-alumina is very nearly axially symmetric (η=0) and has its principal V_{zz} axis colinear with the crystal c axis. It is assigned to the BR position which has local axial symmetry based upon the EFG calculation (BR1). The other major tensor (B) observed in lithium β-alumina is highly asymmetric with its principal V_{zz} axis in the conduction plane and it is assigned to the MO site. The EFG calculation for the lithium site (MO2) indicates that the principal V_{zz} axis is in the conduction plane, but it is not in the same direction as observed. This could possibly result from polarization or other effects which have not been taken into account. The final tensor (C) observed in lithium β-alumina has a principal V_{zz} component which is quite high for lithium and is directed in the conduction plane. Considering the weak intensity and large magnitude associated with this tensor, it is possibly caused by lithium ions close to a charge-compensating defect which could exhibit a large electric field gradient.

Details of both the lithium and sodium EFG tensors are shown in Table 3. A comparison of these tensors indicates that lithium and sodium ions do occupy different environments at low temperatures. The BR site occupied by lithium ions has three-fold symmetry whereas sodium ions have been shown to occupy one of three sites slightly displaced from the centered BR position. The principal axes directions for the MO site for these nuclei also differ, but more importantly, the EFG components in the c direction for the BR and MO

Table 3: A comparison of the details of and assignment for the tensors of sodium and lithium in β-alumina

	e^2qQ/h	η	V_{zz}	V_{yy}	V_{xx}	Assignment
Na						
	2.75 MHz	0.60	a + 2a*	c	a	BR
	2.5 MHz	0.25	a	c	a + 2a*	MO
Li						
	53 kHz	0.04	c	a + 2a*	a	BR
	178kHz	0.17	a	a + 2a*	c	MO

sites in lithium β-alumina are of opposite sign whereas the same components for sodium β-alumina are of the same sign. This difference in sign can be seen in Table 2, but its consequence will be discussed in the next section.

3. Lithium Site Occupation Versus Exchange. The most populated sites are those assigned as BR and MO sites. Assuming only these two sites participate in the motional exchange at higher temperatures and that the time spent in transit between sites is small, the room-temperature satellite splitting can be used to calculate the relative occupation of the two sites. For example, the EFG components directed along the c axis participate in the averaging of the static splittings measured at the 0^{o} orientation. If the signs of the EFG components are the same, the average splitting must lie somewhere between the static values. If the EFG components are of opposite signs, the average value will be smaller than the value of the largest static splitting, and the final sign of the EFG can be the same as either static component depending on the relative amount of time spent in the two sites. Since the averaged room-temperature splitting for lithium is much smaller than the static values, the EFG components directed along the c axis must be of opposite signs. Furthermore, this sign difference is consistent with the EFG calculation and recent neutron diffraction data by Tofield and Farrington.[12] The normal sodium positions in the BR (BR2) and MO (MO1) sites have c axis components which are calculated to be of the same sign

and is consistent with the results of Chapter III. The neutron diffraction work of Tofield and Farrington indicates that the lithium is positioned at the MO site but is displaced off the conduction plane by almost 1 Å. The calculated EFG component in the c axis direction changes sign for this displaced site (MO2), creating the necessary situation for the indicated averaging to take place.

The population ratio BR:MO at low temperatures is obtained directly from the ratio of the satellite peak areas (See Figure 6). The BR:MO ratio at low temperatures versus lithium content is plotted in Figure 7 as the solid line. The calculated population ratio BR:MO at room temperature plotted versus lithium exchange content in β-alumina is shown as the dashed line in Figure 7. There is only a weak dependence of the calculated population ratios versus lithium content at room temperature. However, at low temperature the lithium site occupation shows considerable variance versus the degree of lithium exchange. There appears to be a maximum in the BR site preference when approximately 70% to 80% of the sodium is replaced by lithium. However, in sharp contrast to the site preference observed in pure sodium β-alumina, lithium ions in the 100% lithium β-alumina show a very strong preference for the MO positons.

The strong preference for the MO sites shown by the lithium ions indicates that the BR and MO sites have the same energy or that the MO site is lower in energy. If this latter case is true, an ordered arrangement of the lithium

Figure 6

Population ratios (BR:MO) obtained from the peak areas of the low temperature (85 K) ^{7}Li NMR spectra of lithium substituted single crystal β-alumina samples oriented with the magnetic field parallel to the crystal c axis. Spectra are for a) 30%, b) 48%, c)71% and d) 100% lithium-exchanged β-alumina samples, and are magnified to better display the satellite transitions (central transition peaks are off-scale).

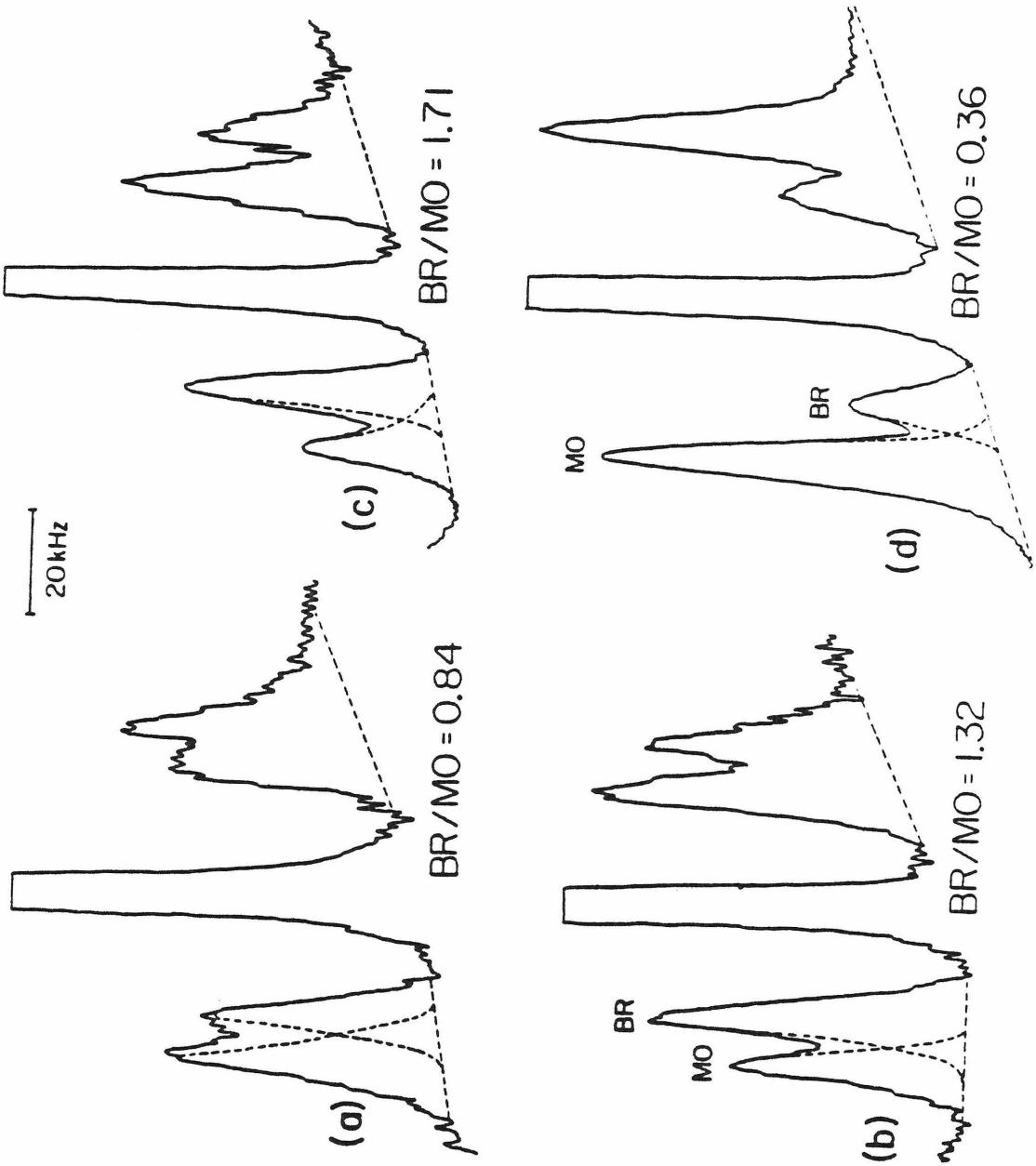
20kHz
(a)
BR/MO=0.84
(c)
BR/MO=1.71
BR
MO
(b)
BR/MO=1.32
MO
BR
(d)
BR/MO=0.36

Figure 7

The distribution of lithium ions given by the population ratio BR:MO versus the extent of lithium exchange. Circles and squares indicate ratios observed at room temperature and 80 K, respectively.

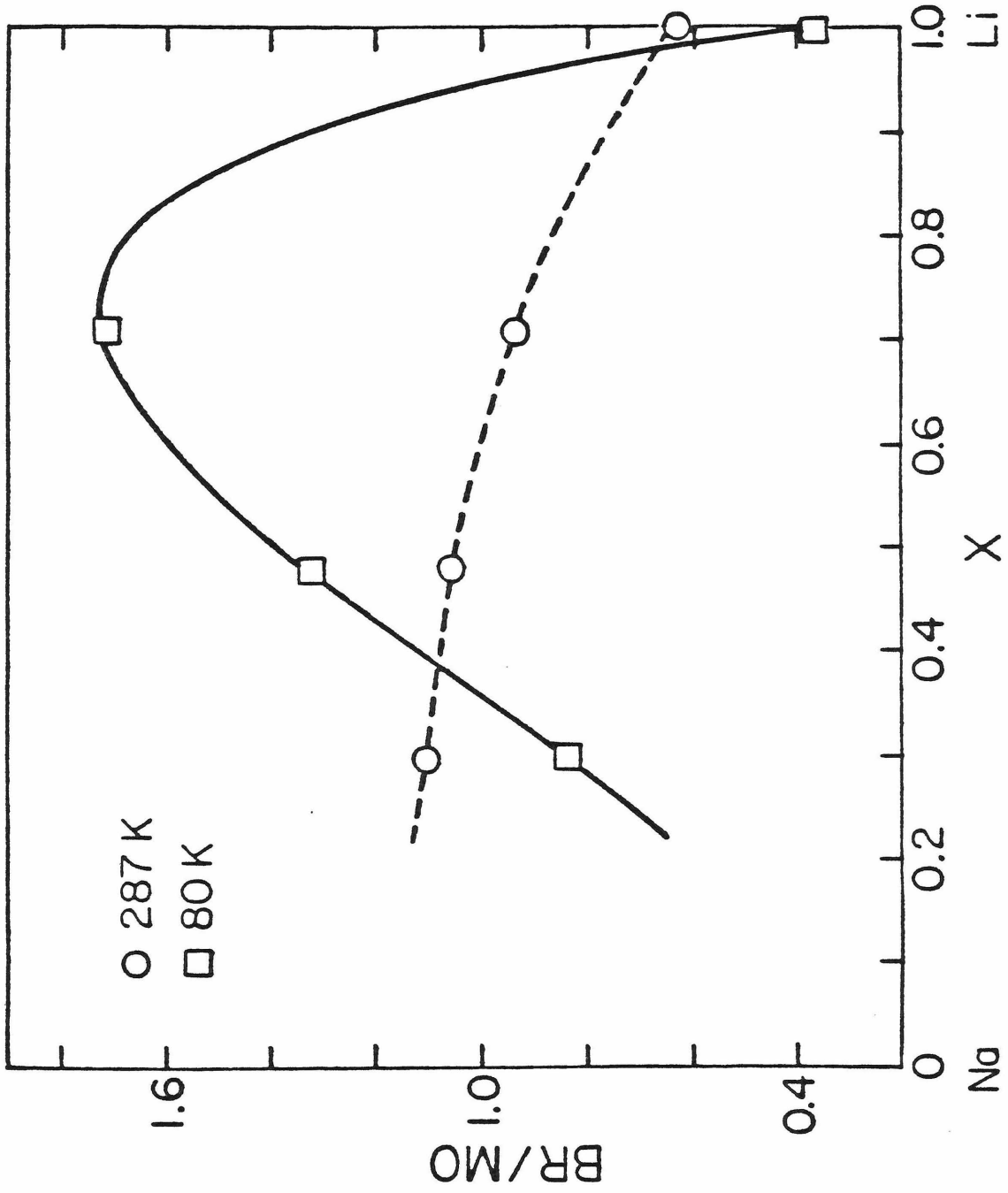
BR/MO
1.6
1.0
0.4
O 287 K
□ 80 K
0
0.2
0.4
0.6
0.8
1.0
Na
X
Li

ions in a stoichiometric β-alumina would conceivably look like the arrangement of the darkened circles in Figure 8a. With the introduction of 25% excess of the cation, the additional lithium would form MO pairs as shown in Figure 8b. However, three lithium ions are then in close proximity and it is likely that one of these would be displaced to occupy a BR site due to electrostatic repulsion between the ions. Therefore, for every excess ion introduced, one MO-MO pair is formed and one BR site is occupied. For a cation excess of 25%, the predicted ratio BR:MO is 0.25. In the case where the BR and MO lithium sites have the same energy the distribution is governed largely by the ratio of the availability of sites. If a "cell" is defined by the dotted line shown in Figure 8a, there will be a number of doubly-occupied cells equal to the number of excess cations which will contain a MO-MO pair, and the remainder of the cells will contain a single lithium ion in either a BR or MO position. If there is an equal distribution of BR and MO lithium-occupied sites in the singly-occupied cells, the resulting ratio BR:MO is 0.43. In addition, the presence of electrostatic repulsions between lithium ions in MO sites of adjacent cells could give rise to a displacement of some ions to BR sites. Also, factors such as the influence of the oxygen defect in the conduction plane on site distribution and the contribution of configurational entropy from the availability of three MO sites per cell must be included in analyses of both cases to determine which comes closer

Figure 8

(a) Ordered arrangement of lithium ions on MO sites (darkened circles) indicating the vacancy of BR sites (open circles). (b) Introduction of an excess lithium ion to produce a doubly-occupied cell which is outlined by the dashed line. Electrostatic repulsions force the nearby lithium ion in a MO site to be displaced to a BR site.

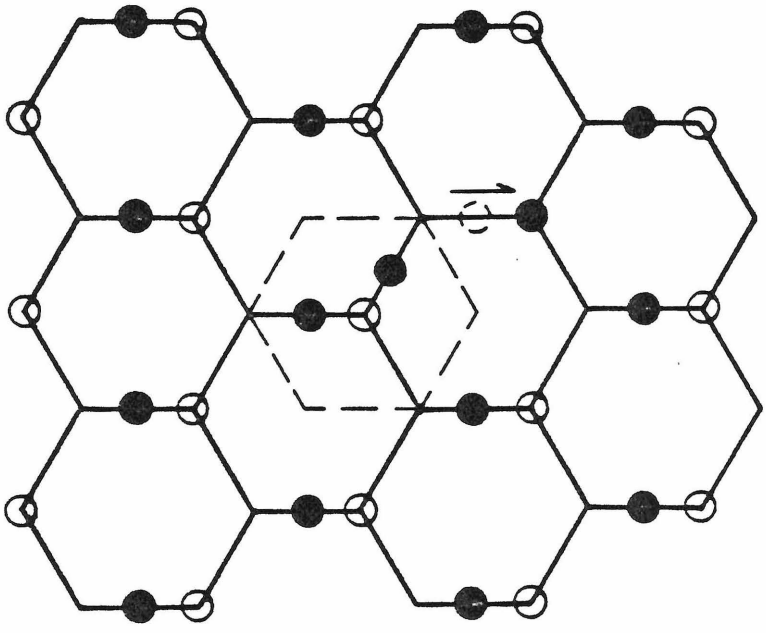

(b)

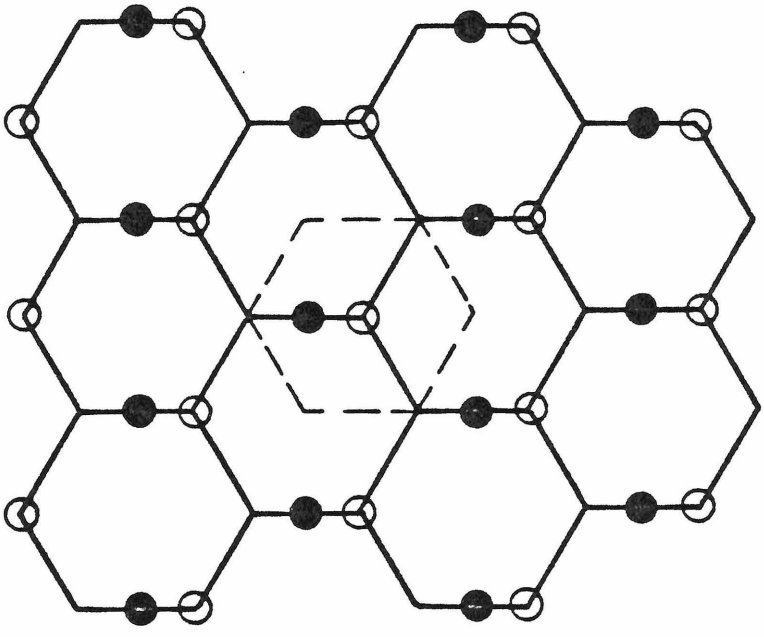

(a)

to predicting the observed BR:MO ratio of 0.36 in lithium β-alumina.

However, there is an experimental method for determining whether the BR or the MO site is lower in energy. The peak-to-peak satellite splitting is a sensitive measure of the relative population of lithium ions in BR and MO sites. Since the energies of the BR and MO sites are different, their populations will be governed by a Boltzmann distribution, $\exp(-\Delta E/kT)$, and will vary with temperature. Consequently, a plot of $\ln\Delta\nu$, where $\Delta\nu$ is the peak-to-peak satellite splitting, versus inverse temperature is a line whose slope is the energy difference between the BR and MO sites (Figure 9). The direction of the shift in the satellite splittings also indicates which of the two sites is lower. A value of 0.01 eV is obtained for the energy difference between the BR and MO sites in the 100% lithium β-alumina, and the MO site has the lower energy. In contrast, in all other samples of β-alumina which have at least a 10% sodium content the BR site is observed to be lower in energy. Apparently, there is a delicate balance among interactions (i) between sodium ions and the lattice, (ii) between lithium ions and the lattice, and (iii) between sodium ions and lithium ions. The presence of even a small amount of sodium ions, which strongly favor the BR position in lithium β-alumina introduces repulsive interactions between the sodium ions in BR sites and lithium ions in MO sites which tip the balance toward both cations preferring BR sites.

Figure 9

The observed slope (0.01 eV) from a plot of the logarithm of the peak-to-peak satellite splittings ($\ln\Delta\nu$) versus inverse temperature gives the energy difference between the BR and MO sites.

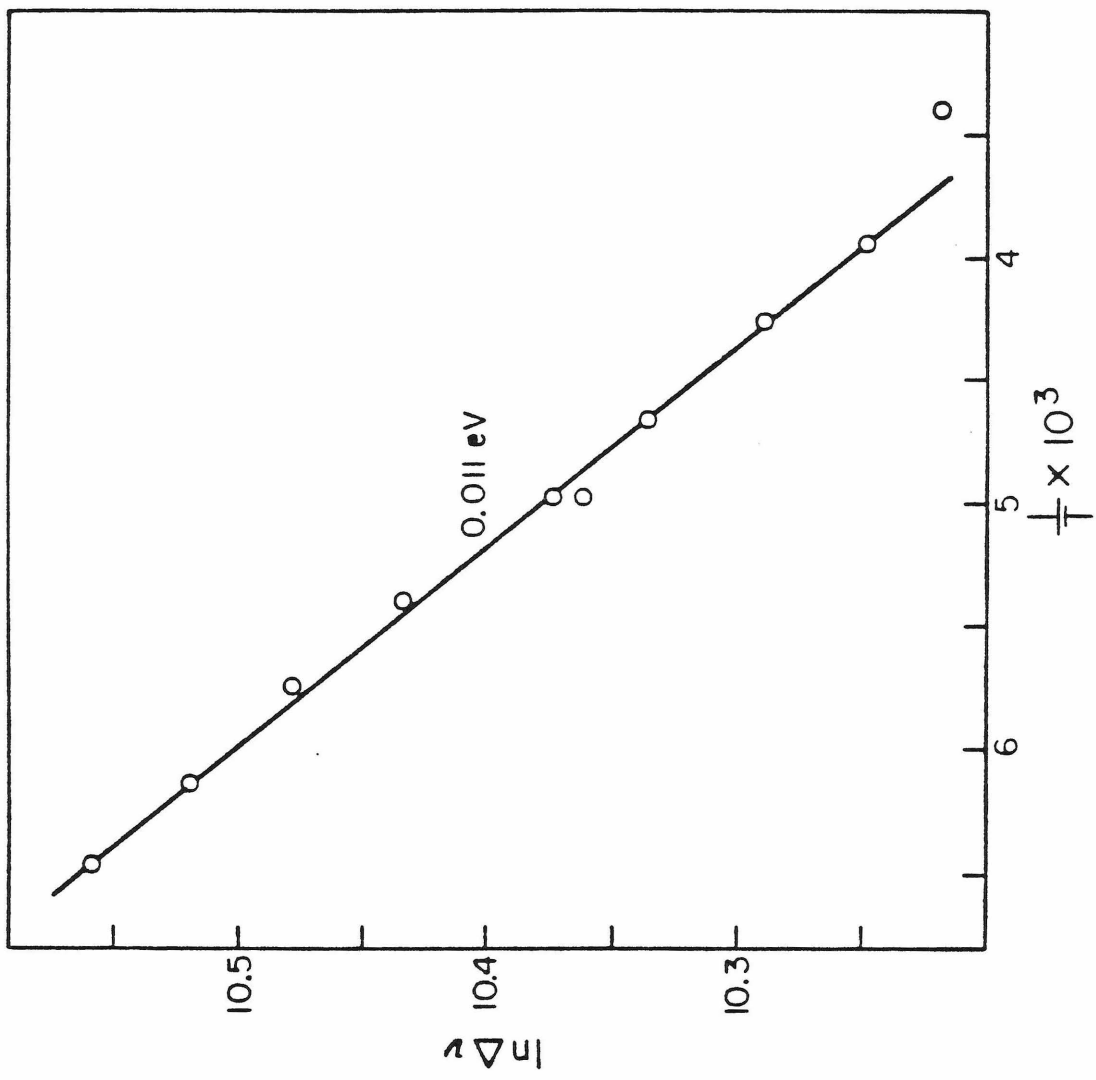
0.011 eV
10.5
10.4
10.3
ln Δν
4
5
6
1/T × 10³

The variation of the BR:MO ratio with lithium exchange content is undoubtably linked to the presence of and interaction between the two different cations. It has been demonstrated that the BR site is preferred by both lithium and sodium for all compositions except for those near 100% lithium content. Therefore, the major difference in the mixed conductors is the presence of like and unlike MO-MO pairs (Na-Na, Li-Li, Na-Li). Hendrickson and Bray[13] consider the interactions for these pairs of different alkali ions in order to explain the "mixed-alkali effect" observed in mixed-alkali glasses. Briefly, the term mixed-alkali effect is applied to any of the observed large deviations from linearity of many physical properties when one alkali is progressively substituted for another. For example, values for the measured electrical conductivity, which is due to cation motion, show a definite minimum. The theory of Hendrickson and Bray involves the calculation of an electrodynamic interaction between the electric dipoles created by the oscillating alkali ions. Briefly, an oscillating dipole with a field of $\vec{E}_1 \sin\omega_1 t$ will interact with a second ionic dipole nearby which will respond with an induced dipole moment $p_2(t)$ parallel to $\vec{E}_1(t)$. The interaction energy is given by

$$W = - p_2(t)E_1 \sin\omega_1 t \qquad (4)$$

Using the theory of forced damped oscillators, the time-average for the interaction is calculated. The energy of interaction is zero for like ions but is shown to be negative

for unlike ions in mixed-alkali glasses. Therefore, the activation barrier for motion of an unlike pair is higher than for a like pair, and the increased activation barrier accounts for the observed conductivity behavior versus mixed-alkali ratio. The consequences of the theory for the MO-MO pairs in β-alumina are that i) the energy of the Na-Li pair is lower than either the Na-Na pair or the Li-Li pair and ii) the activation energy barrier for motion of the Na-Li pair is higher. The first effect should be reflected in the equilibrium site occupation of like and unlike pairs versus lithium exchange content and the second should cause the activation energy for conductivity versus lithium exchange content to exhibit a maximum over the composition range. To simplify the theory, it is assumed since they are of lower energy, that Na-Li MO-MO pairs form at the expense of all other pairs. The expected BR:MO ratio for this assumption is shown as the solid line in Figure 10a. In contrast, the constant ratio of 1.5 is predicted by a random distribution of like and unlike pairs. Although the assumption is rather crude, the low temperature data generally follow the features corresponding to the preferential occupation of MO-MO pairs by unlike ions. At room temperature, the cations are in rapid motion and the BR:MO ratio indicates that the distribution among like and unlike MO-MO pairs is closer to random. The tendency of both sets of data toward lower BR:MO ratios may be an indication of the increasing lithium ion preference for the BR:MO site with increasing lithium content.

Figure 10

(a) Comparison of observed and predicted BR:MO ratios versus lithium exchange. Circles and squares are data from Figure 7. The solid line is predicted by a model which assumes that Na-Li MO-MO pairs form at the expense of all other pairs. The dash-dotted line is predicted by a random distribution of like and unlike pairs. (b) Activation energy for conductivity versus degree of lithium exchange (from Ref. 6).

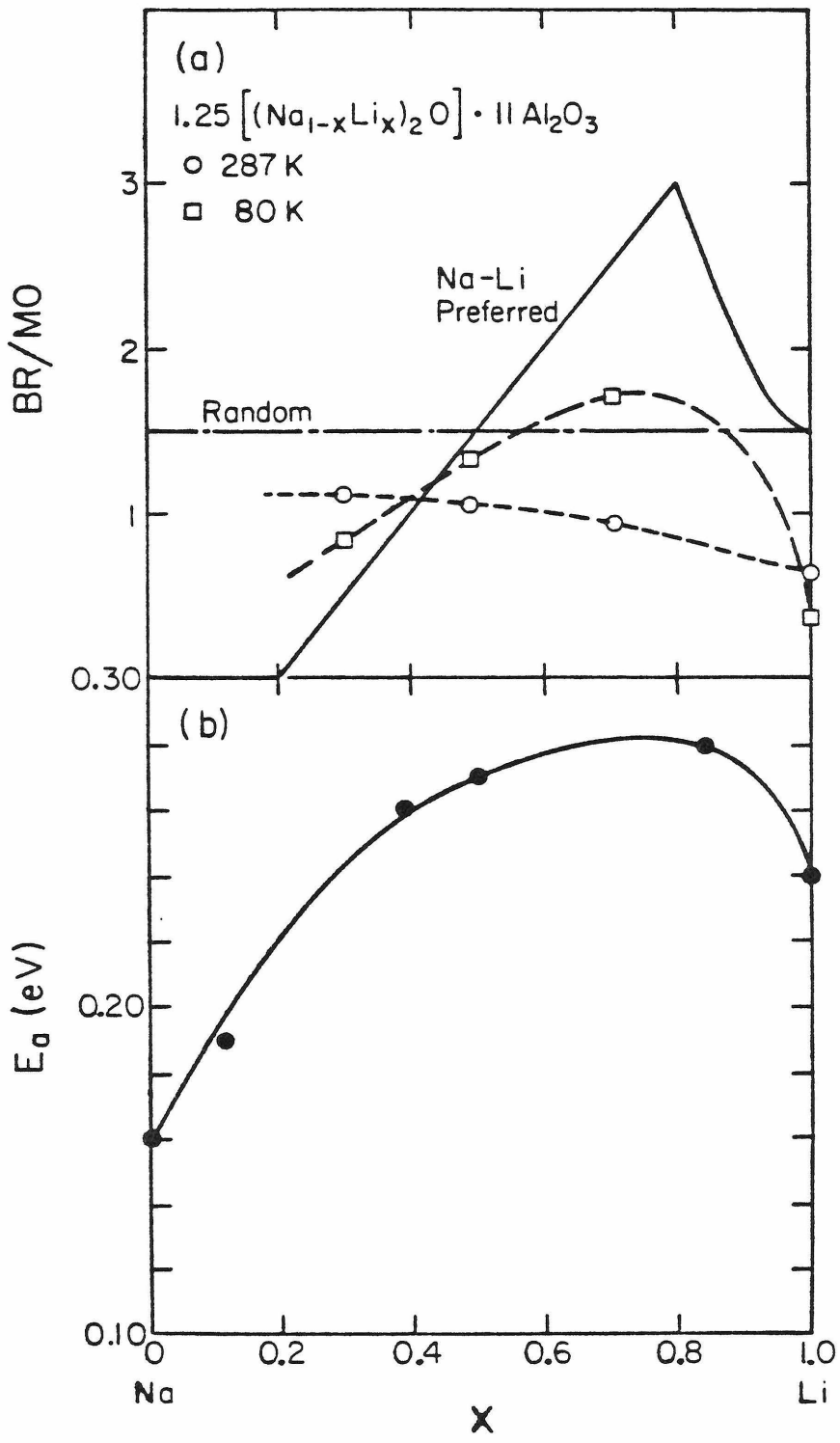
(a)
1.25 [(Na1-xLix)2O] · 11 Al2O3
o 287 K
□ 80 K
Na-Li
Preferred
Random
BR/MO
3
2
1
0.30
(b)
Ea (eV)
0.20
0.10
0
0.2
0.4
0.6
0.8
1.0
Na
Li
X

Since the low temperature NMR data indicate that the interaction energy between pairs does lower the overall energy of the unlike pairs relative to the like pairs, the second consequence of the interaction, which predicts a maximum in the activation energy for conduction, should also be observed. Recent conductivity data obtained by Briant and Farrington[6] on mixed Li/Na β-alumina is shown in Figure 10b where the activation energy for conduction is plotted versus the degree of lithium exchange. Indeed, the activation energy does go through a maximum and at approximately the same composition the maximum in the BR:MO ratio is observed.

4. Lithium Motion in β-alumina. Details of lithium ion motion in β-alumina can be, in principle, obtained from the collapse of the satellite spectra versus temperature. For example, the collapse of the pair of satellites shown in Figure 11 for two single crystal samples of lithium-exchanged β-alumina (76% and 91% Li) oriented with the c axis parallel to the magnetic field give a correlation time of motion (τ) of 3.6×10^{-6} sec for a temperature of approximately 160 K. However, the temperature at which the collapse occurs is frequently difficult to determine at other orientations because the averaged satellite positions are very close to the central transition. Therefore, in practice, correlation times for motion are difficult to obtain. However, the width of the satellites after collapse still contains important information. The satellite line-

Figure 11

Collapse of ^{7}Li satellite structure (positions of satellites measured relative to the central transition) versus inverse temperature for two single crystals of lithium-exchanged β-alumina oriented with the c axis parallel to the magnetic field. Circles and squares are for 76% and 91% lithium-exchanged samples, respectively.

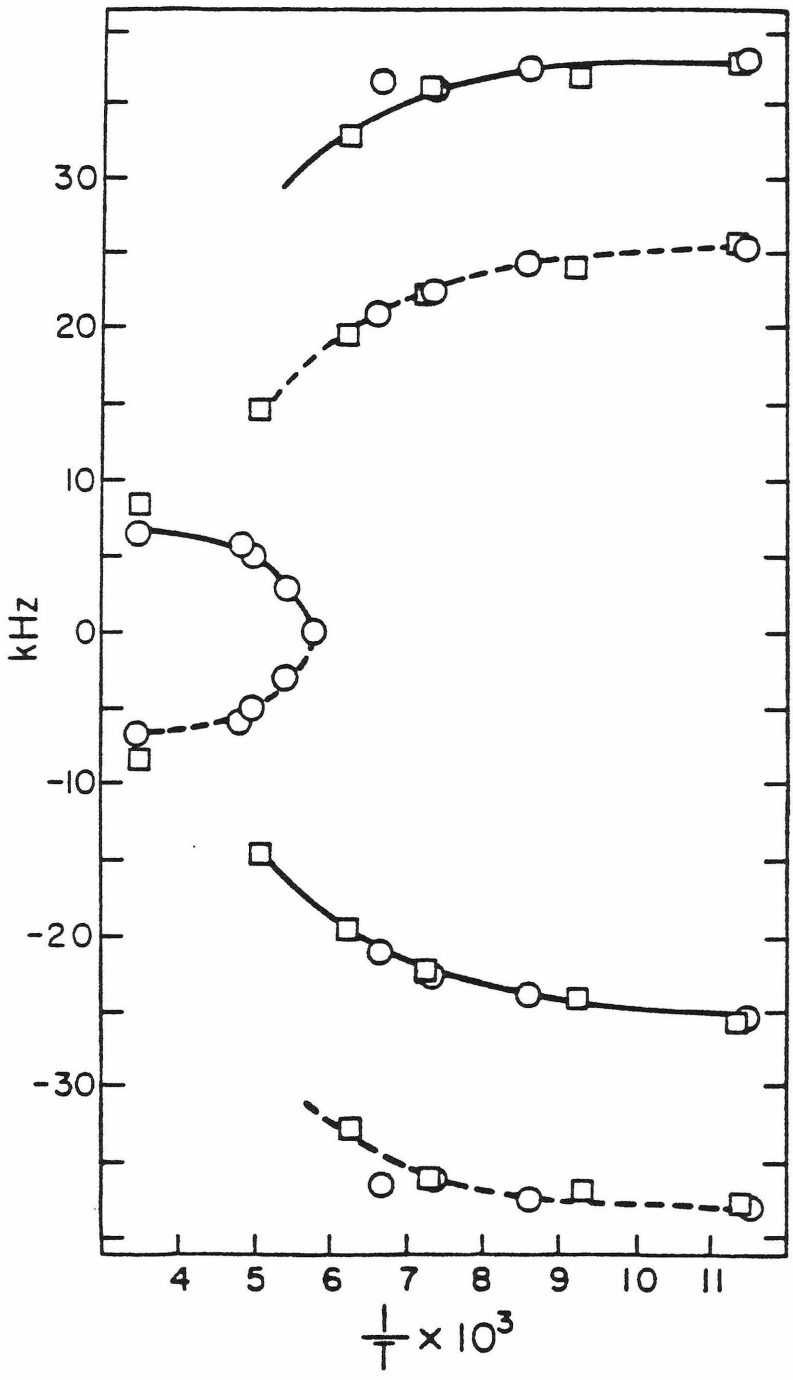
30
20
10
0
-10
-20
-30
kHz
4
5
6
7
8
9
10
11
1/T x 10^3

width is a measure of the distribution of EFG's arising from the distribution of BR and MO environments, and exchange narrowing will occur when lithium ions are rapidly interchanging among BR and MO sites. A plot of $\ln\Delta\nu_{1/2}$ where $\Delta\nu_{1/2}$ is the full width at half maximum intensity of the satellite linewidth, versus inverse temperature (Figure 12) gives an activation energy for the interchange among BR and MO sites in the 100% lithium β-alumina of 0.08 eV.

Unfortunately, there is not a great deal of NMR relaxation data on lithium in β-alumina. However, one study[14] has reported two activation energies from the low- (0.067 eV) and high-temperature slopes (0.168 eV) of the T_1 relaxation data on a 71% lithium-exchanged β-alumina.

Information on lithium motion in β-alumina can also be obtained from the narrowing of the central transition with temperature. Unlike the central transition for sodium, where the predominant interaction contributing to the observed linewidth is the quadrupole interaction, the predominant interaction contributing to the observed line broadening of 5 kHz in the lithium central transition is the heteronuclear dipole-dipole coupling between lithium and aluminum nuclei. The line broadening contribution from the quadrupole interaction in lithium is calculated to be less than 40 Hz for the static EFG and less than 1 Hz for the averaged EFG. The dipolar interaction is modulated by the motion of lithium ions which causes the observed linewidth to narrow as the correlation time for motion approaches the inverse of

Figure 12

Activation energy (0.08 eV) for the barrier to lithium motion among BR and MO sites. Plotted in $\ln\Delta\nu_{1/2}$ versus inverse temperature where $\Delta\nu_{1/2}$ is the full width at half maximum intensity of the satellite linewidth in a 100% lithium-exchanged β-alumina single crystal oriented with the c axis parallel to the applied magnetic field.

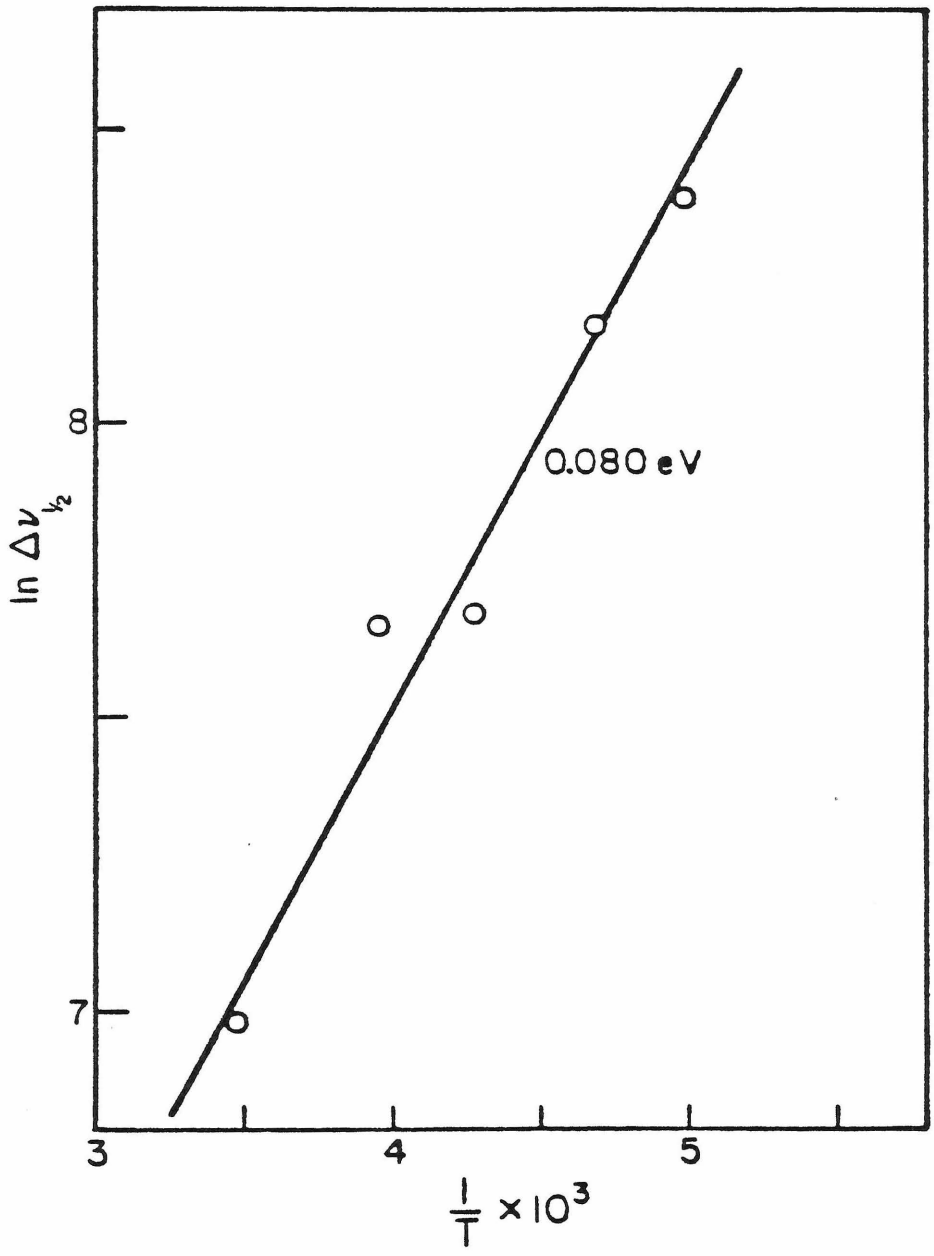
8
7
0.080 eV
ln Δν½
3
4
5
1/T × 10³

the static line width.[15] In Figure 13, the observed linewidths for four different compositions of mixed-alkali β-alumina are shown plotted versus the inverse temperature. The temperature at which motional narrowing occurs increases with decreasing lithium content, indicating that the most mobile lithium ions are in the pure lithium β-alumina.

The mobility of the lithium ions versus the degree of lithium exchange in mixed-alkali β-alumina can be compared with the mobilities of cations in mixed-alkali glasses. The diffusion coefficients (and mobilities) of cations in single alkali glasses are always observed to be higher than for any composition of a mixed-alkali glass. The introduction of any second cation into a single alkali glass always results in the lowering of the diffusion coefficient of the original cation, and for low concentrations the diffusion coefficient of the second cation is also always lower than the original cation. As a consequence, diffusion coefficient versus composition curves for the two alkali ions intersect at some intermediate composition where the diffusion coefficients are equal, and the overall conductivity, which is governed by the diffusion of the fastest diffusing ion, will go through a minimum. The lithium data in the previous section were shown to be consistent with a theory which explains the mixed-alkali effect in glasses. In addition, the NMR linewidth versus lithium exchange data indicate that the lithium diffusion coefficient increases with lithium content, analogous to what is observed in mixed-alkali

Figure 13

Motional narrowing of the central transition linewidth versus the degree of lithium exchange. Plotted are the central transition linewidths ($\Delta\nu_{1/2}$) versus the inverse temperature for four degrees of lithium exchange (30%, 48%, 71%, 100%) in single crystal samples of β-alumina.

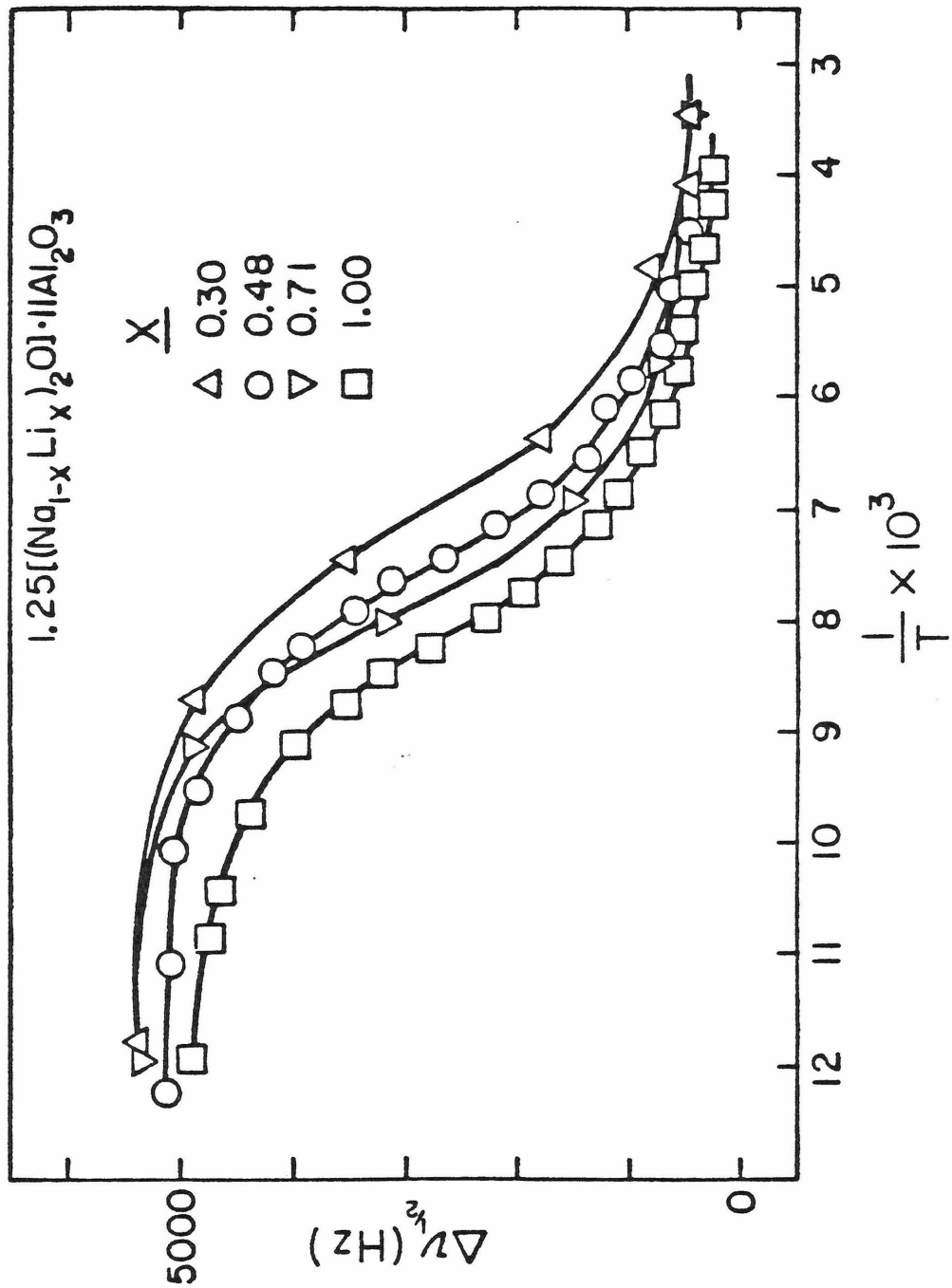
1.25[(Na1-xLix)2O]·11Al2O3
X
0.30
0.48
0.71
1.00
Δν½ (Hz)
5000
0
1/T × 10³
3
4
5
6
7
8
9
10
11
12

glasses. Therefore, the proposed "co-ionic effect" in mixtures of lithium and sodium in β-alumina is not observed.

Values for the activation energies for motion in lithium-exchanged β-alumina can be obtained from the central transition line-narrowing data and compared to the variations observed in the activation energy with lithium exchange from conductivity data. A plot of $\ln T_2$ (T_2 is proportional to the inverse linewidth) versus inverse temperature for β-alumina samples which are 50% and 100% lithium-exchanged are shown in Figure 14. As expected from the conductivity data and the comparison with theory, the activation energy for the 100% lithium-exchanged sample (0.060 eV) is lower than that for the 50% lithium-exchanged (0.066 eV) although this is inconclusive since the error in these measurements does overlap.

It is troublesome that the values for the activation energy obtained from the line narrowing of the central transition (0.06 eV) are lower than that obtained from the line narrowing of the satellite transition (0.08 eV), even though the same motional process should be responsible for both. Recent studies have investigated the effect of diffusion in lower than three dimensions on the measured NMR relaxation rates. Richards[16], for example, has derived an expression for the observed inverse dipolar line width (T_2) in the presence of two-dimensional motion (Equation 1).

$$T_2 = \langle \Delta\omega^2 \rangle^{-1} \tau_c^{-1} \left[\ln \left(\frac{1}{\langle \Delta\omega^2 \rangle \tau_c^2} \right) \right]^{-1} \qquad (1)$$

Figure 14

Activation energies (0.066 eV and 0.060 eV) for the barrier to lithium motion among BR and MO sites for 50% (circles) and 100% (squares) lithium-exchanged β-alumina single crystal samples. Plotted is $\ln T_2$ versus the inverse temperature (where $T_2 = (\pi \Delta \nu_{1/2})^{-1}$ and $\Delta \nu_{1/2}$ is the full width at half maximum intensity of the central transition linewidth).

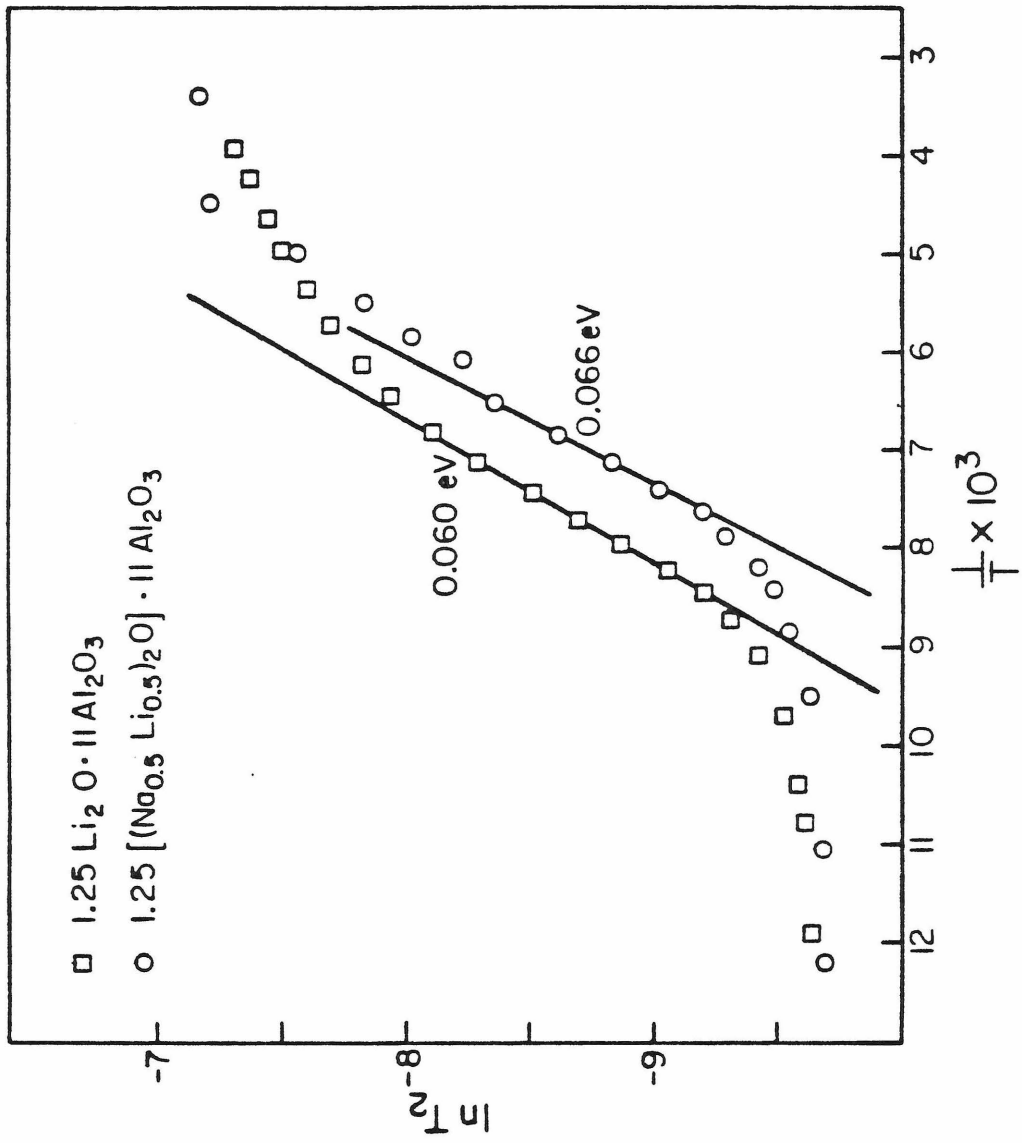
□ 1.25 $Li_2O \cdot 11Al_2O_3$
○ 1.25 $[(Na_{0.5}\ Li_{0.5})_2O] \cdot 11Al_2O_3$
0.060 eV
0.066 eV
$\ln T^2$
$\frac{1}{T} \times 10^3$
-7
-8
-9
3
4
5
6
7
8
9
10
11
12

The parameter τ_c is the correlation time for motion, $\langle \Delta\omega^2 \rangle$ is the dipolar second moment, k is the Boltzmann constant and T is the absolute temperature. For an activated hopping mechanism, τ_c is related to the energy of activation (E) by Equation 2,

$$\tau_c = \tau_o \exp(E/kT) \qquad (2)$$

and the slope of the plot of $\ln T_2$ versus inverse temperature which gives the energy of activation must be corrected to give the true activation energy with the following expression.

$$d(\ln T_2)/d(1/kT) = -E + -2E/\left\{\ln(\langle \Delta\omega^2 \rangle/\tau_o{}^2) + 2E/kT\right\} \qquad (3)$$

The value of τ_o is somewhat difficult to determine, but with an estimate of τ_o to lie between 10^{-12} sec and 10^{-9} sec, the corrected activation energies at 130 K are 0.067 eV and 0.087 eV, respectively, for the 100% lithium-exchanged sample. The correction for the activation energy due to the reduced dimensionality of the diffusion is in the proper direction and the value of 0.08 eV measured from the narrowing of the satellite transiton is within the range of activation energy values calculated for a reasonable range of τ_o values.

Finally, it is interesting to note that the value of 0.08 eV for the activation energy barrier for the motion among the BR and MO sites in lithium β-alumina is the same as the activation energy measured for the same sodium motion in sodium β-alumina. Since the sodium activation energy is

believed to correspond to the enthalpy of ion migration out of the associated regions[17] surrounding the oxygen defect in the conduction plane, it is an attractive possibility that the observed activated process in lithium β-alumina may be due to the same mechanism.

References

1. Yao, Y.-F.Y. and Kummer, J.T. (1967), J. Inorg. Nucl. Chem. 29, 2953.

2. Whittingham, M.S. and Huggins, R.A. (1972), in "Solid State Chemistry", (R.E. Roth and S.J. Schneider, Jr., eds.), Spec. Publ. 364, National Bureau of Standards, Washington, D.C., p. 148.

3. Radzilowski, R.H., Yao, Y.-F.Y. and Kummer, J.T. (1969), J. Appl. Phys. 40, 4716.

4. Roth, W.L. and Farrington, G.C. (1977), Science 196, 1332.

5. Farrington, G.C. and Roth, W.L. (1977), Electrochem. Acta 22, 767.

6. Briant, J.L. and Farrington, G.C. (1980), submitted to J. Electrochem. Soc.

7. See, for example: Vashishta, P., Mundy, J.N. and Shenoy, G.K., eds. (1979), "Fast Ion Transport in Solids-Electrodes and Electrolytes", North-Holland, New York, Amsterdam, Oxford.

8. For review of this subject, see, for example: Day, D.E. (1976), J. Non-Crystalline Solids 21, 343.

9. Bates, J.B., Frech, R., Engstrom, H., Wang, J.C. and Kaneda, T. (1980), Solid State Ionics 1, 15.

10. Bersohn, R. (1958), J. Chem. Phys. 29, 326.

11. Peters, C.R., Bettman, M., Moore, J.W. and Glick, M.D. (1971), Acta. Cryst. B27, 1826.

12. Tofield, B.C. and Farrington, G.C. (1979), Nature 278, 438.

13. a) Hendrickson, J.R. and Bray, P.J. (1972), Phys. and Chem. Glasses 13, 43. b) Hendrickson, J.R. and Bray, P.J. (1972), Phys. and Chem. Glasses 13, 107.

14. Dubin, R.R. and Casabella, P.A. in ref. 7, p. 367.

15. For a discussion of these concepts, see, for example: Abragam, A. (1961), "The Principles of Nuclear Magnetism", Oxford University Press, London.

16. Richards, P.M. (1979) in "Physics of Superionic Conductors", (M.B. Salamon, ed.), Top. Current Phys. 15, 141. (Springer-Verlag, Berlin, Heidelberg, New York)

17. Wolf, D. (1979), J. Phys. & Chem. Solids (GB), 40, 757.

CHAPTER V: SUMMARY

The observation that a number of solids exhibit unusually high ionic conductivities has focused much attention on the role of structure in the conduction process. As a result, the solid electrolytes have been thoroughly investigated by structural techniques.[1] However, it is now clear that one of the hallmarks of solid electrolytes is that the regularity of the crystalline lattice is disrupted by the disorder of the mobile cations. In addition, in β-alumina, for example, the number of current carrying cations is only about 4% of the total number of all atoms. These two factors compound the difficulties which conventional structural techniques encounter in separating contributions arising from in-plane defects, static disorder, anharmonic vibrations, and diffusive motion of the cations. On the other hand, techniques which reflect properties due to long-range motions of the cations, such as ionic conductivity and tracer diffusion, are unable to provide any direct information about the structure. In contrast to these and other techniques, NMR is capable of probing both the structural and dynamical properties of solids.

The solid state NMR techniques described in the present work rely on observing features in NMR spectra which are governed by the structure sensitive quadrupole interaction. The first order quadrupole shifts in the ($\pm 3/2 \longleftrightarrow \pm 1/2$) transitions in the spin 3/2 nuclei sodium and lithium have allowed the electric field gradients (EFG)

for the nominal BR and MO sites to be characterized. The details of the EFG's for, and the distribution of cations among, BR and MO sites indicate that the potentials experienced by sodium and lithium are different for both sites. For example, in sodium β-alumina, the NMR results confirmed that the sodium ion which occupies the BR site is displaced from the three-fold symmetry axis[2] and is of lower energy than the MO site.[3] In lithium β-alumina, the BR site is at the center of the three-fold axis but lithium ions in MO sites, reported to be displaced off the conduction plane by almost 1 Å,[4] are observed to have a lower energy than lithium ions in BR sites which results in a different structural distribution of lithium ions.

In addition to structural information, the study of the temperature (motional) dependence of the quadrupole interaction in sodium β-alumina has revealed a process involving local motion of sodium ions in displaced BR sites, and allows an activation energy for the motion to be determined. This motion can be interpreted using a model of motion in β-alumina developed by Wolf,[5] which proposes that a MO-MO pair must pass through a BR-aBR configuration in order to create the "interstitial" sodium ion at an aBR site necessary for conduction. The enthalpy of interstitial formation for this process is calculated to be between 0.04 eV and 0.05 eV which agrees with the observed activation energy and accounts for the displacement and local motion of sodium ions in BR sites. Further observations

of an interaction energy of 0.08 eV in both sodium and lithium β-alumina were, however, not equated with details of a particular motional process. It was observed that this activation energy was associated with a motion in which cations were exchanging among BR and MO sites, although this value is considerably lower than the activation energies reported for both lithium and sodium conductivity measurements.[6,7]

The work in this study presents strong evidence for correlated cation motion. An early calculation by Wang et al.[3] predicts that the MO-MO pairs substantially lower the energy of activation for motion relative to the barrier expected for a single particle jump mechanism in β-alumina. The previously mentioned presence of MO-MO pairs which cause the displacement of sodium cations from the centered BR site indicates that not only is there a strong MO-MO pair correlation, but that there are interactions among cations which extend from the MO-MO pair to the cations in nearby BR sites as well. In addition, a study of the interaction of MO-MO pairs was performed by observing the effect of varying the composition of mixed lithium-sodium β-alumina on the distribution of cations among the available sites. The results were interpreted using a theory previously developed to explain the mixed-alkali effect in glasses[8] and indicate that MO-MO pairs made up of unlike cations are lower in energy than those made up of like cations. Furthermore, recent conductivity data on mixed lithium-

sodium β-alumina[6] support this interpretation by observing an increase in the activation energy for conductivity over the same composition range in which the NMR data indicate the presence of unlike MO-MO pairs.

This work, therefore, has accomplished the following. The electric field gradient tensors for mobile cation sites in sodium and lithium β-alumina have been characterized and indicate that unique structural sites can be identified with solid state NMR techniques. In addition, details of local cation motions among the identified sites have been revealed. Finally, it was demonstrated that correlated motion of cations does exist and is important to the ionic conduction process.

References

1. See, for example: Salamon, M.B., Ed. (1979), "Physics of Superionic Conductors", Top. Current Phys., V.15, Springer-Verlag, Berlin, Heidelberg, New York and references therein.

2. Reidinger, F. (1979), Ph.D. thesis, State Univ. of New York.

3. Wang, J.C., Gaffari, M. and Choi, S. (1975), J. Chem. Phys. 63, 792.

4. Tofield, B.C. and Farrington, G.C. (1979), Nature 278, 438.

5. Wolf, D. (1979), J. Phys. & Chem. Solids (GB), 40, 757.

6. Briant, J.L. and Farrington, G.C. (1980), submitted to J. Electrochem. Soc.

7. Kim, K.K., Chen, W.K. and Mundy, J.N. (1979), J. Phys. & Chem. Solids (GB), 40, 743.

8. a) Hendrickson, J.R. and Bray, P.J. (1972), Phys. and Chem. Glasses 13, 43. b) Hendrickson, J.R. and Bray, P.J. (1972), Phys. and Chem. Glasses 13, 107.